Topological Light–Matter Design Simulations in Polariton Profiles and Ultracold Atom Systems

Lancaster University, United Kingdom

Konstantin Rips

2019/2020

Contents

1 Concepts for Simulations in ultra cold atom systems and lattices **1**

1.1 Basics for Topological Phase Engineering 1

1.2 Lattice systems - Elementary concepts 3

1.2.1 Structure of Lattice–Hamiltonian 3

1.2.2 Su Schrieffer Heeger (SSH) Lattice realizations 4

1.2.3 Prominent Lattices and Brillouin Zone–Topology 8

2 Berry Structures **15**

2.1 Numerical Approach 15

2.1.1 Abelian Berry Phase 15

2.1.2 Berry connection and curvature 19

2.1.3 Non–abelian Berry phase and U(n)–fibres 23

2.2 Advanced Methods and Tools 31

2.2.1 Topological Quantities I 31

2.2.2 Topological Quantities II 33

2.3 Two–Level System: Monopole and 'hidden' structures 36

2.3.1 Hamiltonian 36

2.3.2 A topological model and fibre bundle structure 38

2.3.3 Constructions: Linking and Hopf invariant 40

2.3.4 Qubit state geometry and Qubit maps 42

3 Polariton Graphs, Topological Insulators, Fibrations **44**
3.1 Technical Achievements and Prerequisites 44
3.1.1 Derivation - The polaritonic lattice Hamiltonian 45
3.2 Polaritonic Lattices and Topological Band Structures 47
3.2.1 Square Lattice Crystal 48
3.2.2 Kagome Lattice – Fresh Perspectives of the bulk 50
3.2.3 General Methods for Topological Bands 59
3.2.4 Exploiting Fibrations and Homotopy Sequences 64
3.3 Challenges in Polariton Graphs 69
3.3.1 Discussion - Engineering Chern insulators 69

4 Novel Topological Design in Ultracold Atoms **72**
4.1 Abelian monopoles in spin–1 ultracold atoms 72
4.1.1 Experimental setup scheme 72
4.1.2 Chern numbers, phase transitions, spin textures 76
4.1.3 Discussion of Results 85
4.2 Non–abelian monopole in spin–3/2 cold atoms 86
4.2.1 Experimental setup scheme 86
4.2.2 Approach to a topological bundle model 88
4.2.3 Gauge field(s), Berry curvature, Topological number 91
4.2.4 First Principle Computation - Ground state 2^{nd} Chern number 95
4.2.5 Adiabatic state evolution 96

A Review of Group theory approach to Diagonalization **99**
A.1 Basic Principles 99
A.2 Momentum space Hamiltonian 102

B Geometry and Topology **103**
B.1 Gauge field Geometry 103
B.1.1 Curvature and Wilson loop - A proof 103
B.1.2 Gauge Fields on Manifolds 104

B.2 Results in Algebraic and Differential Topology 106
B.2.1 Basics of Homotopy 106
B.2.2 Homology and Cohomology 107
B.3 Berry Curvature - Merging QM and Topology 108

C Symmetries of Hamiltonians **110**
C.1 Time Reversal Symmetry (TR) 110
C.2 Particle–Hole Symmetry (PH) 111
C.3 Sublattice Symmetry (SL) 112
C.4 Altland– Zirnbauer classification 113

D Representation of spin operators **114**
D.1 Spin 1 Matrices 115

Bibliography **115**

Abstract

This work analyses novel schemes for realizing topological light–matter in ultracold atom and polaritonic systems. The observed phenomena can be formulated in the language of space fibrations, homotopy, homology–cohomology duality, and the geometry of gauge fields. The main aspects of this research work consist of:

1. Polaritonic lattice geometries in dimension $D = 2$ can simulate topological insulators based on symmetry class A Hamiltonians by breaking time–reversal symmetry. The competing transverse electric–transverse magnetic (TE-TM) (δt) and Zeeman splitting term ($\mathcal{B}$) yield gapped phases - these are described by Grassmann manifolds $\mathbb{G}_{2,6}(\mathbb{C})$ and $\mathbb{G}_{3,6}(\mathbb{C})$ with respect to the spectral–flattened Hamiltonian on the proposed lattice geometry. Valence Bloch bundles over the Brillouin zone are illustrated, and corresponding Chern numbers computed. We discover an index formula which relates the sum of valence band Chern numbers to the index of the projector onto the valence band states. This finding sheds new light on the bulk–boundary correspondence in polaritonic lattices, and allows to extrapolate some properties of single sheet 2D Chern insulators. The formulation is supported by careful numerical analysis of the gapped phases in the $(\delta t, \mathcal{B})$–space. Numerical evidence allows us to predict $\mathcal{C} = 2$–Chern insulators, which must be accompanied by topologically protected polaritonic edge mode states.

2. Laser–assisted coupling of hyperfine levels in cold Rubidium atoms provides a platform to simulate spherical spaces which host monopoles and carry a fibre bundle structure. Within the pseudo–spin 1 realization one finds non–

Landau phase transitions between ground states of Chern numbers $\mathcal{C} = 2, 1, 0$ - we compute the corresponding spin texture configurations. An explanation is offered based on a topology change of the total space of the bundle, since no typical symmetry breaking occurs. Via careful combination of numerical and topological analysis we find transitions between spaces $\mathbb{R}P^3$, $\mathbb{S}^3$ and $\mathbb{S}^2 \times U(1)$. Furthermore, I respond to the recent experiment of Sugawa et al. on a pseudo–spin 3/2 system: An alternative analytical derivation of the ground state 2$^{\text{nd}}$ Chern number is provided by exploiting the full symmetry of the artificial non–abelian gauge field geometry. In fact, detailed bundle structure analysis reveals a symplectic geometry with a connection to an instanton type bundle $(\mathbb{S}^7, \mathbb{S}^4, \mathbb{S}^3)$.

Declaration of Authorship

I declare that this dissertation is the final result of my own research work, undertaken in theoretical condensed matter physics at Lancaster University. It has not been previously submitted for the award of a higher degree elsewhere.

Acknowledgement

First of all, I would like to thank my supervisor, Prof Janne Ruostekoski, for guidance and discussions on research topics that combine physical and mathematical aspects of condensed matter science in a way that especially appeals to me. He gave me the necessary freedom to develop my own research methods and work towards becoming an independent scholar. I think this approach is owed to his Scandinavian background and calm personality. May I also take this opportunity to express my gratitude to have been a proud member of Lancaster University (UK), the Physics Department, and the CMT group in particular.

Moreover, I am indebted to my family for the constant support and unconditional love throughout all stages of my life.

Chapter 1

Concepts for Simulations in ultra cold atom systems and lattices

1.1 Basics for Topological Phase Engineering

Optical Lattices and Laser–assisted tunnelling. Optical lattices are at the core of quantum simulations and exploring exotic condensed matter models [34] or even gauge field theory. They consist of a large amount of (micro) dipole traps created by interfering laser fields. The atoms are prepared by laser cooling, magnetic trapping and evaporative cooling techniques in order to get into the appropriate quantum regime. Subsequently, they can be loaded into an optical lattice of a particular geometry. The basic principle behind the optical lattice is the following: a laser field $\mathbf{E}$ induces an atomic dipole moment $\mathbf{p} = \alpha(\omega_L)\mathbf{E}$, where ω_L is the laser frequency and α the atom polarization. In this way the atom acquires a dipole potential $-\mathbf{p}\cdot\mathbf{E}$. Superimposed counter propagating laser beams create a standing wave pattern with a spatially varying $\mathbf{E}$–field. Averaging over time we obtain an effective potential of the form $V = -\frac{1}{2}\alpha(\omega_L)|\mathbf{E}(\mathbf{r})|^2$ which can be used as a periodic trapping potential for atoms [9]. Remarkable features of these artificial light crystals include being free of disorder, defects and unwanted thermal effects.

By activating a resonant laser field we can induce tunnellings between neigh-

bouring sites of the optical lattice. Consider an atom at a specific lattice site with an internal state $|A\rangle$ and a nearest neighbour atom in a state $|B\rangle$. The (effective) hopping amplitude $|A\rangle \leftrightarrow |B\rangle$ between both sites can be shown to be of the mathematical form $\kappa_{AB} = |\kappa_{AB}| \exp(i\mathbf{qx})$, where $\mathbf{q}$ represents the wave vector of the resonantly coupled laser field [46]. This is an analogue of the Peierls phase or Peierls substitution [43]. Instead of static lattices, it is also possible to generate dynamical ones. The scheme is known as *Floquet engineering*, and it is based on a time–periodic modulation of the underlying static optical lattice [10].

Exciton–Polaritons in micro-cavities. *Polaritons* (exciton-polaritons) are bosonic quasi–particles which emerge from photons and quantum well excitons entering the strong coupling regime in semiconductor micro-cavities. As bosons they can undergo a phase transition into a Bose-Einstein condensate (BEC). Furthermore, they exhibit various other collective phenomena, such as lasing and superfluidity [52, 3]. There exist some common aspects to atomic BECs - however, atomic BECs are strongly related to thermodynamic equilibrium whereas polaritons lead to a non-equilibrium setting due to their decay into photons and thus, short lifetime. For the population configuration to be stable, the system must be frequently restocked from a pump source. Our actual interest, however, is in nano-fabricated polaritonic metamaterials which mimic topological insulators; those are materials which behave as insulators inside the bulk, but develop edge states on their surface as a result of the bulk-boundary correspondence. These topologically protected edge modes are insensitive to local perturbations or defects because of the bulk topology. Long range spatial coherence [15] makes polariton condensates attractive candidates for engineering landscapes of topologically non–trivial phases compared to purely electronic systems. Several techniques for creating trapping potentials for polariton condensates (similar to optical lattices for atoms) have been proposed. This paves the way to novel applications in quantum simulations, optimization and quantum devices [8, 49, 17].

In Chapter 3 we demonstrate the following

Claim 1 *The formation of topologically insulating phases in polaritonic simulators stems mainly from the photonic component of these light–matter quasi particles. The contributions are revealed as cross–polarized terms in the effective Hamiltonian due to TE-TM splitting. Another competing term comes from Zeeman–splitting in the exciton component.*

1.2 Lattice systems - Elementary concepts

This section introduces some of the ubiquitous lattice configurations in the broad area of condensed matter science. Firstly, we describe a one–dimensional poly-acetylene lattice type. Secondly, we present 2D lattices, some of which play a major role in the engineering of polaritonic or electronic topological insulators.

1.2.1 Structure of Lattice–Hamiltonian

The general Hamiltonian structure of a lattice system we are studying is given by

Notation 2

$$\hat{H} = \sum_{\langle i,j \rangle} \kappa_{ij} \hat{a}_i^\dagger \hat{a}_j + \sum_{\langle\langle i,j \rangle\rangle} \kappa_{ij} \hat{a}_i^\dagger \hat{a}_j + \cdots , \tag{1.1}$$

$$a_i^\dagger \left|0\right\rangle = \left|_{\textit{particle at site } i}\right\rangle , \tag{1.2}$$

in the second quantization formalism. The sum is assumed to run over *nearest–neighbour* (*nn*) and *next–nearest–neighbour pairs* (*nnn*), denoted by $\langle i,j \rangle$ and $\langle\langle i,j \rangle\rangle$, respectively. $\hat{a}_i^\dagger$ and $\hat{a}_j$ represent the creation and annihilation operators of *particles*[1] at sites i and j, respectively. $|0\rangle$ is a generic vacuum state. Note that in this general notation we suppress other properties of the particles (polarization, spin etc.) which might be present in principle. We refer to the matrix elements κ_{ij}[2]

[1] The formalism applies to various contexts: quasi-particles, atoms, polaritons etc.

[2] It can be written as a space integral of overlapping orbitals for two neighbouring sites i, j. $\kappa_{ij} = \langle i | \hat{V} | j \rangle = \int\int \phi_i^*(\mathbf{x}) V(\mathbf{x},\mathbf{y}) \phi_j(\mathbf{y})\, d\mathbf{x}\, d\mathbf{y}$.

as hopping amplitudes and specify them later on. A plethora of lattice Hamiltonians has been designed for both Bose and Fermi gases in various contexts [34], some even reveal the phenomenon of fermion fractionalization [46]. The above Hamiltonian can be naturally generalized, including on–site terms $U_i\hat{a}_i^\dagger\hat{a}_i$ etc.

1.2.2 Su Schrieffer Heeger (SSH) Lattice realizations

We first review the SSH model and describe some modifications thereof. At the same time we present relevant concepts that form the theoretical basis of topological insulators.

Standard SSH model

Example 3 *(Su-Schrieffer-Heeger (SSH)-Hamiltonian) An example of a one – dimensional lattice system with N unit cells is the SSH model which has the following Hamiltonian*

$$\hat{H}_{SSH} = \sum_{i=1}^{N} v\hat{a}_{i,A}^\dagger\hat{a}_{i,B} + \sum_{i=1}^{N-1} w\hat{a}_{i+1,A}^\dagger\hat{a}_{i,B} + h.c., \quad v, w \in \mathbb{R}, \tag{1.3}$$

where the index i refers to the lattice unit cell and A, B to the sublattices. The model has been proposed to describe the hopping of non-interacting spin-polarized electrons on a one-dimensional lattice, e.g. polyacetylene.

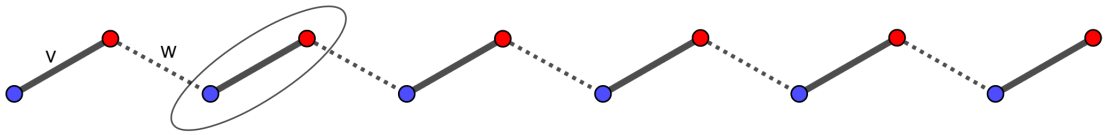

Figure 1.1: SSH lattice with alternating hopping amplitudes v, w (thick, undotted; thin, dotted) and N=6 unit cells (the 2nd unit cell is shown circled). The lattice sites belonging to sublattice A(B) are coloured with blue(red), respectively.

Making use of the (second) quantization formalism we can rewrite the Hamiltonian of the open SSH chain

$$\hat{H}_{\mathsf{SSH,chain}} = v \sum_{i=1}^{N} |i, A\rangle \langle i, B| + w \sum_{i=1}^{N-1} |i+1, A\rangle \langle i, B| + h.c., \tag{1.4}$$

$$|i, A\rangle = |i\rangle \otimes |A\rangle \in \mathfrak{H}_{ext} \otimes \mathfrak{H}_{int}, \tag{1.5}$$

such that the states are elements of the tensor product of two Hilbert spaces (one called external and the other internal). Regarding the dimensions, we see that $\dim \mathfrak{H}_{ext} = N$, $\dim \mathfrak{H}_{int} = 2$ and therefore, $\dim(\mathfrak{H}_{ext} \otimes \mathfrak{H}_{int}) = 2N$.

$$|i, A\rangle \langle i, B| + |i, B\rangle \langle i, A| = |i\rangle \otimes |A\rangle \langle i| \otimes \langle B| + |i\rangle \otimes |B\rangle \langle i| \otimes \langle A| \tag{1.6}$$

$$= |i\rangle \langle i| \otimes \big(|A\rangle \langle B| + |B\rangle \langle A|\big) \tag{1.7}$$

$$= |i\rangle \langle i| \otimes \hat{\sigma}_x \tag{1.8}$$

For the last step we use the algebraic relation

$$|A\rangle \langle B| + |B\rangle \langle A| = \begin{pmatrix} 0 & 1 \\ 1 & 0 \end{pmatrix} = \hat{\sigma}_x. \tag{1.9}$$

$$|i+1, B\rangle \langle i, A| + |i, A\rangle \langle i+1, B| = |i+1\rangle \otimes |B\rangle \langle i| \otimes \langle A| \tag{1.10}$$

$$+ |i\rangle \otimes |A\rangle \langle i+1| \otimes \langle B| \tag{1.11}$$

$$= |i+1\rangle \langle i| \otimes |B\rangle \langle A| + h.c. \tag{1.12}$$

$$= |i+1\rangle \langle i| \otimes \left(\frac{\hat{\sigma}_x - i\hat{\sigma}_y}{2}\right) + h.c. \tag{1.13}$$

Last line follows because we have the representation

$$|B\rangle \langle A| = \begin{pmatrix} 0 & 0 \\ 1 & 0 \end{pmatrix} = \frac{1}{2}(\hat{\sigma}_x - i\hat{\sigma}_y). \tag{1.14}$$

Rewriting the Hamiltonian in this form enables us to read off some relevant properties and proceed with diagonalisation.

$$\hat{H}_{\mathsf{SSH,chain}} = v \sum_{i=1}^{N} |i\rangle \langle i| \otimes \hat{\sigma}_x + w \sum_{i=1}^{N-1} |i+1\rangle \langle i| \otimes \left(\frac{\hat{\sigma}_x - i\hat{\sigma}_y}{2}\right) + h.c. \tag{1.15}$$

There exists an operator $\hat{\Gamma}$ which reflects the sublattice symmetry (SL) or chiral symmetry of the SSH model. It follows from the anticommutation – relation $\{\hat{\sigma}_i, \hat{\sigma}_z\} = 0$ that

$$\hat{\Gamma} = \hat{\mathbb{1}}_N \otimes \hat{\sigma}_z, \quad \{\hat{H}_{\mathsf{SSH,chain}}, \hat{\Gamma}\} = 0. \tag{1.16}$$

Since $\hat{\Gamma}^2 = \hat{\mathbb{1}}_{2N}$ this group can be identified with $\mathbb{Z}_2$ - the operator $\hat{\Gamma}$ is a unitary representation of $\mathbb{Z}_2$.

Modification - SSH ring model

The above system has two open ends since no boundary conditions have been imposed so far. Usually one introduces periodic boundary conditions on theoretical grounds, i.e. one considers the construction in the thermodynamic limit $N \to \infty$. It is mathematically correct to say that in the thermodynamic limit the system will be independent of the definition of the edges, and one is then allowed to impose periodic boundary conditions which are equivalent to a system in a ring form.

Claim 4 *The bulk physics of the open SSH chain in the thermodynamic limit $N \to \infty$ and that of the finite closed SSH ring are equivalent.*

The construction amounts to the following Hamiltonian

$$\hat{H}_{\mathsf{SSH,ring}} = v \sum_{i=1}^{N} |i, A\rangle \langle i, B| + w \sum_{i=1}^{N-1} |i+1, A\rangle \langle i, B| + w\, |1, A\rangle \langle N, B| + h.c. \tag{1.17}$$

This new Hamiltonian 1.17 has a further symmetry:

Proposition 5 *The symmetry group of the realized SSH ring is a direct product of the form*

$$\mathbb{Z}/N\mathbb{Z} \times \mathbb{Z}_2. \tag{1.18}$$

The first factor refers to the external cyclic symmetry and the second factor describes the internal chiral symmetry. The full group is realized through a unitary representation

$$\hat{T} \otimes \hat{\gamma} \colon \mathbb{Z}/N\mathbb{Z} \times \mathbb{Z}_2 \to \mathcal{U}(\mathfrak{H}_{ext} \otimes \mathfrak{H}_{int}), \tag{1.19}$$

$$(\hat{T} \otimes \hat{\gamma})(s, i) = \hat{T}(s) \otimes \hat{\sigma}_z^{i-1} \quad \square \tag{1.20}$$

More information can be found in appendix A of this work.

Momentum Space Hamiltonian

The underlying *external* symmetry group $\mathbb{Z}/N\mathbb{Z}$ allows the Hamiltonian to be Fourier transformed into momentum space. The resulting Hamiltonian $\hat{H}(k)$ for the constructed ring is (see appendix A)

$$\hat{H}(k) = \begin{pmatrix} 0 & v + we^{-ik} \\ v + we^{ik} & 0 \end{pmatrix}. \tag{1.21}$$

The eigenvalues and hence the dispersion relations are given by

$$E_{1/2}(k) = \pm|v + we^{-ik}| = \pm\sqrt{v^2 + w^2 + 2vw\cos(k)}, \quad k \in [-\pi, \pi]. \tag{1.22}$$

For a staggered hopping amplitude configuration ($v \neq w$) the energy gap is $\Delta = |v - w| \neq 0$, and we have the condition for an insulator. Non-staggered hopping ($v = w$) leads to $\Delta = 0$ which describes a metal-like phase. Also note, that on the level of the momentum Hamiltonian we can simply read off several symmetries, next to SLS: for instance, time–reversal symmetry of the SSH model is reflected through $\hat{H}^*(k) = \hat{H}(-k)$.

Main topological properties

The momentum space Hamiltonian of the two–band SSH model is given by

$$\hat{H}(k) = d_0(k)\hat{\mathbb{1}}_2 + \mathbf{d}(k)\sigma \tag{1.23}$$

where $\sigma = (\sigma_1, \sigma_2, \sigma_3)$ consists of Pauli-matrices. For our case we have from Eq. (1.21)

$$d_0(k) = 0, \quad \mathbf{d}(k) = (v + w\cos(k), w\sin(k), 0). \tag{1.24}$$

The condition for an insulator ($v \neq w$) restricts the map to $\mathbf{d}\colon \mathcal{BZ} \to \mathbb{R}^2 - \{0\}$ with the Brillouin zone homeomorphism $\mathcal{BZ} \approx [-\pi, \pi]/R \approx \mathbb{S}^1$. The maps can be classified through homotopy classes

$$\{\mathbb{S}^1, \mathbb{R}^2 - \{0\}\} = \pi_1(\mathbb{R}^2 - \{0\}) = \pi_1(\mathbb{S}^1) = \mathbb{Z}. \tag{1.25}$$

Thus, insulating topological phases will be characterized by integers. In fact, we shall see that just two possible numbers occur - so, we have two topologically distinct phases. The property can be understood in terms of the homology–cohomology duality (see Chapter 2 for details).

Coupled double ring system. Advancing the idea of ring–like SSH models may lead to the following constructions:

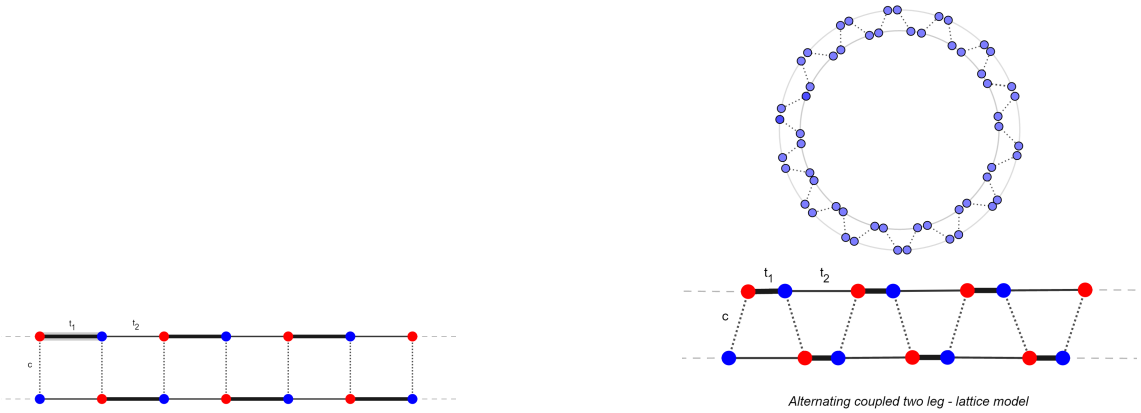

(a) Two coupled alternating SSH legs

(b) Coupled concentric ring (above) and alternating leg geometry (below)

Figure 1.2: Proposals of lattice profiles consisting of two SSH legs. The systems may be realized via utilizing some ultracold atom scheme. Atoms are arranged on lattice sites with alternating tunneling amplitudes t_1, t_2 and inter–leg coupling c.

1.2.3 Prominent Lattices and Brillouin Zone–Topology

Before embarking on the detailed study of topological band structures in Chapter 3, we offer some examples of lattice graphs which go slightly beyond the standard square, triangular or hexagonal configurations in two dimensions. Hamiltonians which are constructed on periodic 2D lattices, as in Figure 1.3, share a crystallographic feature: There exists a 2D Bravais type lattice $\Lambda = \{\mathbf{R}(m,n) := m\mathbf{a}_1 + n\mathbf{a}_2 | (m,n) \in \mathbb{Z}^2\}$ such that unit cells can be translated by elements of Λ while leaving the lattice geometry invariant. In practice (m,n) denotes the unit

cells and $\mathbf{a}_1/\mathbf{a}_2$ are the primitive lattice vectors generating Λ. These crystallographic concepts can be extended to higher dimensions.

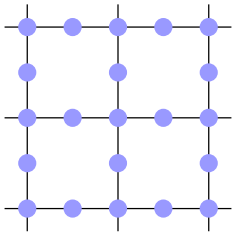

(a) Lieb Lattice

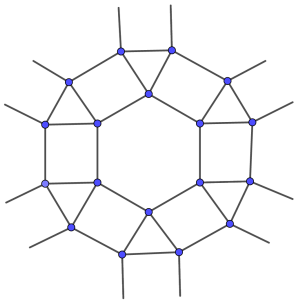

(b) Ruby Lattice

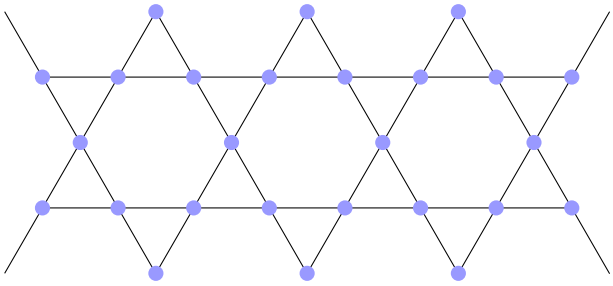

(c) Kagome Lattice

Figure 1.3: Snapshots of prominent lattice structures hosting topological features. Lattice sites are depicted by blue dots and the links between them indicate non–vanishing hopping amplitudes. In all three cases, one can define a non–trivial unit cell which consists of multiple levels. Consequently, this property creates a multiple band structure over the momentum space.

Methods - Fourier Spectroscopy. Let $\hat{H}$ be a Hamiltonian (1.1) which is based on a periodic 2D lattice, e.g. as in Figure 1.3. It acts on the Hilbert space $\mathfrak{H}_{ext} \otimes \mathfrak{H}_{int}$, where $\mathfrak{H}_{ext}$ refers to the external space of the underlying lattice structure and $\mathfrak{H}_{int}$ is the space of internal degrees of freedom (spin, polarization), respectively. Translational invariance allows for a Fourier transformation $|\mathbf{k}\rangle = \frac{1}{\sqrt{N}} \sum_{(m,n)\in\mathbb{Z}^2} e^{i\mathbf{k}\cdot\mathbf{R}(m,n)} |(m,n)\rangle$ with $|(m,n)\rangle \in \mathfrak{H}_{ext}$. By this procedure we obtain a map $\mathbf{k} \to \hat{H}(\mathbf{k}) = \langle\mathbf{k}| \hat{H} |\mathbf{k}\rangle$ from the momentum space into the parameter space $\mathcal{M}_H$ of the Hamiltonian. In the single–particle picture, the parameter space $\mathcal{M}_H$ is determined by the behaviour of the system under time–reversal (TR), particle–

hole (PH) and sublattice (SL) symmetry. All possibilities for $\mathcal{M}_H$ have been classified by Altland and Zirnbauer, as in table C.1. Moreover, periodicity implies the existence of a 2D reciprocal lattice Λ^* on the (quasi–)momentum space such that invariance under mappings $\mathbf{k} \to \mathbf{k}+\mathbf{Q}$ with $\mathbf{Q} \in \Lambda^*$ is guaranteed; $\hat{H}(\mathbf{k}+\mathbf{Q}) = \hat{H}(\mathbf{k})$. We identify a fundamental region of the momentum space, called the Brillouin zone ($\mathcal{BZ}$), from which the whole plane can be reconstructed by action of the lattice Λ^*. On a formal level one defines the action $\Lambda^* \times \mathbb{R}^2 \to \mathbb{R}^2$, $(\mathbf{Q}, \mathbf{k}) \mapsto \mathbf{k}+\mathbf{Q}$, where Λ^* operates as the finitely generated abelian group $\mathbb{Z}^2$ on the momentum space. One can demonstrate that physically relevant topology is encoded in the maps we have just generically described, i.e.

$$\mathcal{BZ} \to \mathcal{M}_H, \quad \mathbf{k} \mapsto \hat{H}(\mathbf{k}), \tag{1.26}$$

where $\mathcal{M}_H$ is one of the coset spaces in C.1.

The Lieb, Kagome and Ruby Lattice. We point out the most remarkable features of the 2-D lattices in Figure 1.3 with respect to itinerant electrons. Considering a tight–binding model of the lattices, which is basically a Hamiltonian (1.1) including only (nn)–terms, we get the following pictures: 1) The electronic Lieb lattice resembles a band structure with 2 conic bands touching the third flat band situated in the middle of the spectrum [57]. 2) The picture of the electronic Kagome lattice bands is similar to Figure 3.4 b), however with striking differences to a polaritonic system [19]. 3) The ruby lattice shows a more complex picture of 6 bands in total [24], where various hopping parameter implementations have been studied. All three examples share a common property of the gap opening mechanism: Introducing spin-orbit (SO) induced (nnn)–coupling of the form $it\sum_{\langle\langle i,j\rangle\rangle\alpha\beta}(\mathbf{e}^1_{ij} \times \mathbf{e}^2_{ij})\hat{a}^\dagger_{i\alpha}\sigma_{\alpha\beta}\hat{a}_{j\beta}$ allows for a gap opening in the spectrum and drives the system into an insulating phase. Since these spin–orbit couplings preserve time–reversal symmetry $\hat{\mathcal{T}}$, we must have $\hat{\mathcal{T}}^2 = -\mathbb{1}$ for fermions. This limits available options for coset spaces of the Hamiltonians according to the Altland–Zirnbauer table. Hence, one expects to find $\mathbb{Z}_2$–valued insulating phases in $D = 2$,

as has been indeed confirmed in the above cases. In contrast, specific arrangements of polaritonic systems provide a platform for breaking time reversal symmetry (TRS) in two dimensions, and thereby engineering Chern insulators.

Topological Analysis

Brillouin zone $\mathcal{BZ}$. The action $\Lambda^* \times \mathbb{R}^2 \to \mathbb{R}^2$ on the momentum space yields $\mathcal{BZ} = \mathbb{R}^2/\Lambda^* \cong \mathbb{T}^2$ for the Brillouin zone via identification. All 2D periodic (translational invariant) lattices Λ yield the same result and, $\mathcal{BZ}$ will have torus topology, Figure 1.5 b). The maps of investigation are therefore $f\colon \mathbb{T}^2 \to \mathcal{M}$. The induced maps on the level of homology and cohomology are given by

$$f_*\colon H_k(\mathbb{T}^2;\mathbb{R}) \to H_k(\mathcal{M};\mathbb{R}), \tag{1.27}$$

$$f^*\colon H^k(\mathcal{M};\mathbb{R}) \to H^k(\mathbb{T}^2;\mathbb{R}). \tag{1.28}$$

H_k, H^k denote the homology and cohomology groups of the spaces, respectively. f_*, f^* are the corresponding (dual) homomorphisms between the groups. f^* is of the pullback map type. The isomorphism $H^k(\mathcal{M};\mathbb{R}) \cong H_k(\mathcal{M};\mathbb{R})$ is guaranteed if the coset space $\mathcal{M}$ is compact. Computation of homology groups is facilitated provided that the space admits a cell decomposition (CW–complex). In particular, we calculate first over $\mathbb{Z}$: $H_2(\mathbb{T}^2;\mathbb{Z}) = \mathbb{Z}$, $H_1(\mathbb{T}^2;\mathbb{Z}) = \mathbb{Z} \oplus \mathbb{Z}$. One can then just replace $\mathbb{Z}$ by $\mathbb{R}$.

Implications. The map $\mathbf{k} \to \hat{H}(\mathbf{k})$ implies another relevant point: if the space $\mathcal{M}$ has a fibre bundle, then one can construct a fibre bundle over $\mathbb{T}^2$ with the same fibres; this is known as a *Bloch bundle*. This follows from a general result: Let $f\colon \mathcal{N} \to \mathcal{M}$ be a map between manifolds and assume $\mathcal{M}$ admits a fibre bundle structure $(E, \pi, \mathcal{M}, F)$, $\pi\colon E \to \mathcal{M}$, then there exists a pull back bundle $f^\bullet E$ over $\mathcal{N}$, which has the same fibre F (Steenrod [51, 25]).

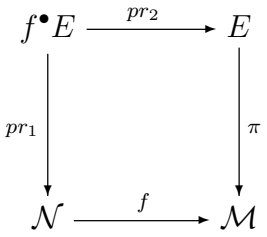

Figure 1.4: Induction of a pullback bundle $f^\bullet E$ over $\mathcal{N}$ from $f\colon \mathcal{N} \to \mathcal{M}$. The diagram is commutative, $\pi \circ pr_2 = f \circ pr_1$.

If we have two homotopic maps $f \sim g\colon \mathcal{N} \to \mathcal{M}$, then the induced bundles $f^\bullet E$ and $g^\bullet E$ will be equivalent [51]. We can combine this statement with a result about cell complexes [59]: If $\mathcal{M}, \mathcal{N}$ are manifolds which admit a cell decomposition and $f\colon \mathcal{M} \to \mathcal{N}$ is a map, then there exists a homotopic cellular map g such that

$$f \sim g\colon \mathcal{M} \to \mathcal{N}, \quad g(X^n) \subseteq Y^n, \tag{1.29}$$

where X^n, Y^n are n-skeletons - these are unions of cells[3] up to dimension n, e.g.

$$X^n = \bigcup_{\{e|\,\dim e \leq n\}} e. \tag{1.30}$$

Note that $X^0 \subset X^1 \subset X^2 \subset \cdots \subset X^n$. This facilitates the understanding of Bloch bundles to some extent since f needs to be described up to homotopy. An illustration is given by the following

Example 6 *($\mathbb{T}^2 \to \mathbb{S}^2 = \mathbb{C}P^1$) The torus $\mathbb{T}^2 = \mathbb{S}^1 \times \mathbb{S}^1$ has the cell decomposition: one 0-cell e^0, two 1-cells $\{e_1^1 = e^0 \times e^1, e_2^1 = e^1 \times e^0\}$ and one 2-cell $e^2 = e^1 \times e^1$. $\mathbb{S}^2$ has an even simpler decomposition: one 0-cell c^0 and one 2-cell c^2. By the previous discussion $f\colon \mathbb{T}^2 \to \mathbb{S}^2$ is homotopic to a cellular map, and we must have*

$$f(e^0) = c^0, \quad f(e_1^1) = f(e_2^1) = c^0.$$

[3] A cell e^n is homeomorphic to $\mathbb{R}^n$ and to an open n–ball; $e^n \approx \mathbb{R}^n \approx \mathbb{D}^{\circ n}$.

The decision whether f is topologically trivial or not depends on $f(e^2)$. If $f(e^2) = c^0$, then it is definitely a trivial map. However, non–trivial mappings arise if not all points of the 2-cell of the torus are mapped onto the 0-cell of the sphere.

Assume we have an (abelian) Berry curvature $\mathcal{F} \in \mathfrak{u}(1) \otimes \Omega^2(\mathcal{M})$ assigned to some eigenstate over $\mathcal{M}$ and derived from a (synthetic) gauge field $\mathcal{A}$ (see Chapter 2 and appendix B for details). The equation of motion for the gauge field $\mathcal{A}$ is $d\mathcal{F} = 0$, since $\mathcal{F} = d\mathcal{A}$ (locally) and then $d\mathcal{F} = d^2\mathcal{A} \equiv 0$ follows. So, $\mathcal{F}$ is a closed 2-form, i.e. $[F] \in H^2(\mathcal{M})$. Note that $\mathcal{F} = d\mathcal{A}$ has to be read as a local equation and does not generally apply as a global condition on $\mathcal{M}$. Thus, the cohomology class $[\mathcal{F}]$ is non–zero and this has various topologically non–trivial effects, such as non–vanishing Chern numbers which are strong indicators of topological phases of light–matter. The pullback map in (1.28) gives a Berry curvature $f^*\mathcal{F}$ which is associated with the Bloch bundle over $\mathbb{T}^2$ (Brillouin zone), and $f^*[\mathcal{F}] \in H^2(\mathbb{T}^2)$. Since $H^2(\mathbb{T}^2; \mathbb{R}) = \mathbb{R}$ this curvature is generally non–trivial, but can turn out to be trivial, if f is null–homotopic.

Other topologies. Can a 2D Brillouin zone have another topology than $\mathbb{T}^2$? First of all, one should refer to such topologies as *non–standard* or *atypical*. Recall that $\mathbb{T}^2$ has been obtained by a map $\mathbb{R}^2 \to \mathbb{R}^2/\Lambda^* \cong \mathbb{T}^2$, where Λ^* is a discrete (translational) subgroup of the full euclidean group $E(2)$, $\Lambda^* < E(2)$. The extension of the idea is to take other non–trivial discrete subgroups G of $E(2)$ which provide us with an action $G \times \mathbb{R}^2 \to \mathbb{R}^2$. This construction yields a specific tessellation of the plane. The search condition for G is that the orbit space $\mathbb{R}^2/G$ should be compact, and G is called a *plane–crystallographic group* [14]. Hence, together with the projection $\pi \colon \mathbb{R}^2 \to \mathbb{R}^2/G$, the space $\mathbb{R}^2/G$ becomes a compact, connected 2D–manifold.

Now, combinatorial topology provides the following classification: A compact, connected and closed 2–dimensional manifold $\mathcal{S}$ with genus $g \geq 1$ is the connected

sum of either tori $\mathbb{T}^2$ or projective planes $\mathbb{P}^2$ (see [38] for a proof),

$$\mathcal{S} \cong \begin{cases} \mathbb{T}^2 \# \cdots \# \mathbb{T}^2 & \text{if orientable,} \\ \mathbb{P}^2 \# \cdots \# \mathbb{P}^2 & \text{if non–orientable.} \end{cases} \tag{1.31}$$

(a) $\mathbb{T}^2 \# \mathbb{T}^2$ (b) $\mathbb{T}^2$

Figure 1.5: Two examples of oriented, compact, connected 2-manifolds. The Brillouin zone $\mathcal{BZ}$ of a translational invariant two–dimensional crystal lattice is $\mathbb{T}^2$ in Fig. (b). Fig. a) shows an oriented genus 2 surface.

Gedankenexperiment: Let Hamiltonian $\hat{H}$ be invariant under a plane crystallographic group G such that $\mathbb{R}^2/G$ is non–orientable, for instance a projective plane $\mathbb{P}^2$ or Klein bottle $\mathbb{P}^2 \# \mathbb{P}^2$. The underlying lattice can be thought to be generated by glide reflections, or similar group elements which are not discrete translations. Consider the abelian Berry curvature $[\mathcal{F}] \in H^2(\mathcal{M})$, where $\mathcal{M}$ describes a coset space of the Hamiltonian, as in C.1. Due to G–symmetry the Hamiltonian must be already uniquely determined on the fundamental region $\mathbb{R}^2/G$ (atypical $\mathcal{BZ}$). As an example assume $\mathbb{R}^2/G \cong \mathbb{P}^2$. Then, the corresponding map $f\colon \mathbb{P}^2 \to \mathcal{M}$, $f\colon \mathbf{k} \mapsto \hat{H}(\mathbf{k})$ provides on the cohomological part $f^*\colon H^2(\mathcal{M}) \to H^2(\mathbb{P}^2)$. Here, we note that $H^2(\mathbb{P}^2; \mathbb{R}) = 0$, as a consequence of being a non–orientable surface. Hence, $f^*\mathcal{F}$ must be globally trivial, i.e. $f^*\mathcal{F} = d\mathcal{A}$ on all $\mathbb{P}^2$, and consequently all (first) Chern numbers $\mathcal{C}$ vanish: $\mathcal{C} = \frac{1}{2\pi} \int_{\mathbb{P}^2} f^*\mathcal{F} = \frac{1}{2\pi} \int_{\mathbb{P}^2} d\mathcal{A} = 0$. The topology of the band structure appears to be trivial, since a global potential exists. This extends to all non–orientable surfaces, in particular to the Klein bottle $\mathbb{P}^2 \# \mathbb{P}^2$.

Chapter 2

Berry Structures

For the analysis of topological effects we shall encounter, it is crucial to understand concepts like *Berry phases*, *connections* and *curvatures*.

2.1 Numerical Approach

First of all, we take a numerical approach for the derivation as it will make it feasible to apply the methods in more complex contexts and implement them as codes, if necessary. For complex systems, it is almost inevitable to have a corresponding approximation on a grid.

2.1.1 Abelian Berry Phase

The discovery of the Berry phase [6, 7] showed that the standard, i.e. initially formulated, adiabatic theorem of quantum theory was incomplete in a sense: During an adiabatic cyclic evolution a quantum state can acquire a geometrical phase, along with its usual dynamical phase factor. It turns out that this geometrical phase, today known as *Berry phase*, is non–integrable and depends on the path traced out in the parameter space.

Let $|\Psi_1\rangle$, $|\Psi_2\rangle$ be some non–orthogonal states, then

$$\langle\Psi_1|\Psi_2\rangle = |\langle\Psi_1|\Psi_2\rangle|e^{-i\gamma_{12}} \tag{2.1}$$

where $\gamma_{12} = -\arg\langle\Psi_1|\Psi_2\rangle$ is the relative phase of the states. A gauge transformation

$$|\Psi_k\rangle \longrightarrow e^{i\alpha_k}|\Psi_k\rangle \tag{2.2}$$

yields a shift of the relative phase

$$-\gamma_{12} \longrightarrow -\gamma_{12} + \alpha_2 - \alpha_1. \tag{2.3}$$

Therefore, the relative phase of two states is not a potential candidate for an observable - simply because it is not a gauge invariant. Consider now N states $|\Psi_i\rangle \in \mathfrak{H}_i$ ($\dim \mathfrak{H}_i = 1 \forall i$) arranged on a grid configuration and take a loop $\mathcal{C}$ which connects them. This is possible whenever we can assign copies of the same Hilbert space to each node of the lattice.

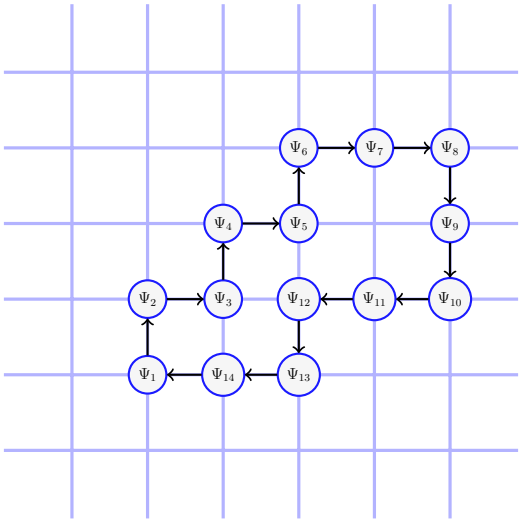

Figure 2.1: Construction of a Berry phase. A sample loop $\mathcal{C}$ which connects states on a grid configuration.

Definition 7 *The discrete version of a Berry phase corresponding to the loop $\mathcal{C}$ may be given by*

$$\gamma_{\mathcal{C}} = -\arg\left(\langle\Psi_1|\Psi_2\rangle\langle\Psi_2|\Psi_3\rangle\cdots\langle\Psi_N|\Psi_1\rangle\right), \quad N \geq 3. \tag{2.4}$$

This can be also written as $\gamma_{\mathcal{C}} = \gamma_{12} + \gamma_{23} + \cdots + \gamma_{N1} \mod 2\pi$ (see Figure 2.1).

Proposition 8 *$\gamma_{\mathcal{C}}$ is gauge invariant and hence an observable. An equivalent representation is*

$$\gamma_{\mathcal{C}} = -\arg \mathrm{Tr} \left(\prod_{i=1}^{N} (|\Psi_i\rangle \langle \Psi_i| \right). \tag{2.5}$$

Proof. Consider $\mathfrak{H}$ as a separable Hilbert space with an orthonormal basis $\{|m\rangle\}$. Define the operator $\hat{\mathcal{O}} = \prod_{i=1}^{N} (|\Psi_i\rangle \langle \Psi_i|)$ with corresponding states $|\Psi_i\rangle$ over the grid, then

$$\begin{aligned} \mathrm{Tr}(\hat{\mathcal{O}}) = \sum_m \langle m| \hat{\mathcal{O}} |m\rangle &= \sum_m \langle m|\Psi_1\rangle \langle \Psi_1|\Psi_2\rangle \cdots \langle \Psi_N|m\rangle \\ &= \langle \Psi_1|\Psi_2\rangle \langle \Psi_2|\Psi_3\rangle \cdots \langle \Psi_N|\Psi_1\rangle \\ &= |A| \exp\left(-i \sum_{k=1} \gamma_{k,k+1} \right), \end{aligned}$$

where $\sum_m |m\rangle \langle m| = \hat{\mathbb{1}}$ has been used, and $|A|$ is the product modulus. This entity is represented as the trace of an operator, hence it must be gauge invariant. ■

Note that we have assigned one–dimensional projectors $\hat{P}_i = |\Psi_i\rangle \langle \Psi_i|$ to each lattice site i, making use of an eigenstate of the Hamiltonian. We will see that in this case we are led to an *abelian Berry phase*. However, these ideas can be developed further, yielding the construction of a non–abelian Berry connection and related concepts.

This enables us to introduce plaquettes which form a grid over some orientable surface $\mathcal{S}$. Since each plaquette can be thought as a sufficiently small rectangle with coordinates (n, m), $(n+1, m)$, $(n+1, m+1)$, $(n, m+1)$, we can define a phase sum around the boundary of each plaquette by

$$\Gamma_{nm} := \gamma_{(n,m),(n+1,m)} + \gamma_{(n+1,m),(n+1,m+1)} + \gamma_{(n+1,m+1),(n,m+1)} + \gamma_{(n,m+1),(n,m)}, \tag{2.6}$$

where γ_{ij} represent the usual relative phases. From this, we may compute the previously defined Berry phase or, equivalently, the *flux* through the rectangle, denoted by Ω_{nm}, by observing that

$$\Omega_{nm} = -\arg\left(e^{-i\Gamma_{nm}} \right) \tag{2.7}$$

holds. Let us now take the product over pairs (n, m) of grid point coordinates:

$$\prod_{n,m} e^{-i\Omega_{nm}} = e^{-i\sum_{n,m}\Omega_{nm}} = e^{i\sum_{n,m}\arg\left(e^{-i\Gamma_{nm}}\right)} \tag{2.8}$$

$$= e^{i\sum_{n,m}(-\Gamma_{nm})}. \tag{2.9}$$

With the relation $\gamma_{\partial\mathcal{S}} = \sum_{n,m}\Gamma_{nm}$ we obtain

$$e^{-i\sum_n\sum_m\Omega_{nm}} = e^{-i\gamma_{\partial\mathcal{S}}}. \tag{2.10}$$

Here, $\gamma_{\partial\mathcal{S}}$ is the phase acquired by moving around the boundary $\partial\mathcal{S}$ of the surface $\mathcal{S}$. The reason for that is of topological origin: Phase contributions γ_{ij} from interior edges of neighbouring rectangles cancel each other due to opposite orientations. Thus, only the boundary contribution remains. This proves

Corollary 9

$$\left(\sum_n\sum_m\Omega_{nm} - \gamma_{\partial\mathcal{S}}\right) \in 2\pi\mathbb{Z}. \tag{2.11}$$

The (first) Chern number

It is possible to define the Chern number by a formal introduction of characteristic forms and classes from differential topology [37]. Although this program might be beneficial from the point of view of mathematical elegance, we take here an alternative numerical approach. Assume we have a closed surface $\mathcal{S}$, in particular $\partial S = \emptyset$. Then $\gamma_{\partial\mathcal{S}} = 0$ and the previous corollary yields $\sum_{n,m}\Omega_{nm} \in 2\pi\mathbb{Z}$. This allows us to define a topological number

Definition 10 *(Chern number) The Chern number is given by*

$$\mathcal{C} := \frac{1}{2\pi}\sum_{n,m}\Omega_{nm}, \tag{2.12}$$

where the flux Ω_{nm} is defined via Eq. (2.7) and the sum runs over the whole grid covering the closed surface.

Crucial properties, which immediately follow from the definition, are:

- $\mathcal{C}$ is gauge–invariant (observable).
- $\mathcal{C}$ is a topological invariant (insensitive to homeomorphisms and even homotopic deformations).
- $\mathcal{C} \in \mathbb{Z}$.

The theoretical description leads to an efficient algorithm for the computation of the Chern number.

Algorithm 11 *(CHN-AL)*

1. *Define a grid* (i, j) *on the surface* $\mathcal{S}$*;* $i, j = 1, \cdots, N$.
2. *For each node, solve the eigenvalue equation* $\hat{H}(i,j)\,|\Psi_n(i,j)\rangle = E_n(i,j)\,|\Psi_n(i,j)\rangle$ *with non–degenerate* $E_n(i,j)$*, and store eigenstates* $|\Psi_n(i,j)\rangle$ *in an array.*
3. *For each square extract the 4 phases between the nearest neighbour eigenstates, e.g.* $\gamma_{(i,j),(i+1,j)} = -\arg(\langle\Psi_n(i,j)|\Psi_n(i+1,j)\rangle)$*. Subsequently, build the sum* Γ_{ij} *as in* (2.6) *and compute* $\Omega_{ij}^{(n)} = -\arg(\exp(-i\Gamma_{ij}))$.
4. *Sum all fluxes* $\Omega_{ij}^{(n)}$ *through the* $(N-1)^2$ *squares to obtain the Chern number* $\mathcal{C}^{(n)} = \frac{1}{2\pi}\sum_{ij}\Omega_{ij}^{(n)}$ *which corresponds to the nth level.*

This can be efficiently coded in Python with its numerical library for operating with high–dimensional arrays[1]. The results of Fukui et al. confirm the fast convergence of this method, even for a coarse discretization of the underlying space [18].

2.1.2 Berry connection and curvature

Analysis of Berry's connection

Assume the underlying parameter space, e.g. through generation of synthetic dimensions, is a manifold $\mathcal{M}$ of dimension n. The parametrization on $\mathcal{M}$ shall be given by $\mathbf{R} = (R_1, \ldots, R_n) \in \mathbb{R}^n$, and Hilbert states are denoted by $\Psi(\mathbf{R})$. In a more

[1] Codes have been written by the author.

rigorous fashion the parametrization is constructed through an atlas $\{(U_i, \varphi_i)\}$ of the differentiable manifold[2] [33]; then $U \ni p \mapsto \varphi(p) \in \mathbb{R}^n$. A deviation by $\Delta\mathbf{R} \in \varphi(U)$ leads to a phase change given by the relation

$$e^{-i\Delta\gamma} = \frac{\langle\Psi(\mathbf{R})|\Psi(\mathbf{R}+\Delta\mathbf{R})\rangle}{|\langle\Psi(\mathbf{R})|\Psi(\mathbf{R}+\Delta\mathbf{R})\rangle|}. \tag{2.13}$$

We expand the above expression in terms of Taylor's formula and compute up to second order

$$-i\Delta\gamma = \langle\Psi(\mathbf{R})|\nabla_{\mathbf{R}}\Psi(\mathbf{R})\rangle|_{\mathbf{R}+\varsigma\Delta\mathbf{R}}\Delta\mathbf{R} + \mathcal{O}((\Delta\mathbf{R})^2). \tag{2.14}$$

Under the assumption of non–degeneracy of the states we define an entity in the limit $\Delta\mathbf{R} \to 0$ which precisely describes the phase change acquired (Berry connection).

Definition 12 *(Gauge field/Berry connection) The so called gauge or Berry connection is given by*

$$\mathcal{A}(\boldsymbol{R}) = i\langle\Psi(\boldsymbol{R})|\nabla_{\boldsymbol{R}}\Psi(\boldsymbol{R})\rangle. \tag{2.15}$$

We test the results by probing them with (local) $U(1)$ gauge transformations

$$|\Psi(\mathbf{R})\rangle \longrightarrow e^{i\alpha(\mathbf{R})}|\Psi(\mathbf{R})\rangle =: |\Psi'(\mathbf{R})\rangle \tag{2.16}$$

$$\nabla_{\mathbf{R}}|\Psi(\mathbf{R})\rangle \longrightarrow \nabla_{\mathbf{R}}\left(e^{i\alpha(\mathbf{R})}|\Psi(\mathbf{R})\rangle\right) = ie^{i\alpha(\mathbf{R})}(\nabla_{\mathbf{R}}\alpha(\mathbf{R}))|\Psi(\mathbf{R})\rangle + e^{i\alpha(\mathbf{R})}\nabla_{\mathbf{R}}|\Psi(\mathbf{R})\rangle \tag{2.17}$$

Hence, for the gauge transformed connection we compute

$$\mathcal{A}'(\mathbf{R}) = i\langle\Psi'(\mathbf{R})|\nabla_{\mathbf{R}}\Psi'(\mathbf{R})\rangle \tag{2.18}$$

$$= i\left(i\nabla_{\mathbf{R}}\alpha(\mathbf{R})\langle\Psi(\mathbf{R})|\Psi(\mathbf{R})\rangle + \langle\Psi(\mathbf{R})|\nabla_{\mathbf{R}}\Psi(\mathbf{R})\rangle\right) \tag{2.19}$$

$$= -\nabla_{\mathbf{R}}\alpha(\mathbf{R}) + \mathcal{A}(\mathbf{R}) \tag{2.20}$$

[2]Most of the physical examples carry a differentiable structure and can be considered as differentiable manifolds. The atlas consists of charts U_i covering $\mathcal{M}$ and homeomorphisms $\varphi_i : U_i \to \mathbb{R}^n$. For overlapping charts $U_i \cap U_j \neq \emptyset$ the diffeomorphic maps $\varphi_j \circ \varphi_i^{-1} : \varphi_i(U_i \cap U_j) \to \varphi_j(U_i \cap U_j)$ belong to the C^∞–class. However, for some cases a C^m–class would be sufficient [33].

Altogether, we get formulas similar to transformations in quantum electrodynamics (QED), which is known to be a $U(1)$–gauge theory:

$$|\Psi(\mathbf{R})\rangle \longrightarrow e^{i\alpha(\mathbf{R})}\,|\Psi(\mathbf{R})\rangle \tag{2.21}$$

$$\mathcal{A}(\mathbf{R}) \longrightarrow \mathcal{A}(\mathbf{R}) - \nabla_{\mathbf{R}}\alpha(\mathbf{R}) \tag{2.22}$$

Proceeding with the construction and by parametrization of a smooth loop $\mathcal{C}$ in the manifold, we can write for the Berry phase according to our previous results

$$\gamma_{\mathcal{C}} = -\arg\left(e^{-i\sum_{k=1}^{N}\gamma_{k,k+1}}\right) + \mathcal{R}, \tag{2.23}$$

where the first sum on the RHS represents a term corresponding to a polygonal approximation of the curve $\mathcal{C}$, the second term $\mathcal{R}$ is the truncation or approximation error. By considering finer subdivisions and taking the limit $N \to \infty$ at the end of the calculation, we observe that $\mathcal{R} \to 0$ and

$$\gamma_{\mathcal{C}} = -\arg\left(e^{-i\oint_{\mathcal{C}}\mathcal{A}(\mathbf{R})\,d\mathbf{R}}\right). \tag{2.24}$$

The gauge invariance is obviously preserved in this limit.

Remark 13 *There exist specific cases where the Berry phase vanishes identically; i.e. for dimension one or zero. In any case, we will be considering systems with $n \geq 2$. So, the Berry phases will have a potential effect as we shall see in due course.*

Berry curvature as a two-form

We can regard $\mathcal{A}(\mathbf{R})d\mathbf{R}$ as an one–form $\mathcal{A} = \mathcal{A}_\mu(\mathbf{R})dR^\mu$.[3] The generalized *theorem of Stokes* implies for a 2–chain σ

$$\int_{\partial\sigma}\mathcal{A} = \int_{\sigma} d\mathcal{A}, \tag{2.25}$$

where $d\mathcal{A}$ denotes the exterior differential of $\mathcal{A}$.

$$d\mathcal{A} = \partial_\nu\mathcal{A}_\mu(\mathbf{R})dR^\nu \wedge dR^\mu = \frac{1}{2}(\partial_\nu\mathcal{A}_\mu(\mathbf{R})dR^\nu \wedge dR^\mu + \partial_\mu\mathcal{A}_\nu(\mathbf{R})dR^\mu \wedge dR^\nu) \tag{2.26}$$

[3] This is the Einstein summation convention.

Taking advantage of the antisymmetry $dR^\mu \wedge dR^\nu = -dR^\nu \wedge dR^\mu$ of the wedge algebra we obtain

$$d\mathcal{A} = \frac{1}{2} \underbrace{\left(\partial_\nu \mathcal{A}_\mu(\mathbf{R}) - \partial_\mu \mathcal{A}_\nu(\mathbf{R})\right)}_{\mathcal{F}_{\nu\mu}} dR^\nu \wedge dR^\mu = \mathcal{F}. \tag{2.27}$$

$d\mathcal{A}$ is interpreted as the (Berry) *curvature* 2–form $\mathcal{F}$ with components $\mathcal{F}_{\nu\mu}$. In analogy to the numerical treatment of the preceding section we are in the position to transfer the ideas on Chern numbers: Consider a two–dimensional submanifold $\mathcal{S}$ (closed surface) of $\mathcal{M}$, then we have

$$\mathcal{C} = \frac{1}{2\pi} \int_{\mathcal{S}} \mathcal{F} \in \mathbb{Z}. \tag{2.28}$$

By varying the parameters accordingly in the parameter space, we trace out a cycle, which is the boundary $\partial\sigma$ of a 2–chain σ (surface). Then, the accumulated Berry phase is predicted to be

$$\gamma_{\partial\sigma} = \oint_{\partial\sigma} \mathcal{A}(\mathbf{R})\, d\mathbf{R} = i \oint_{\partial\sigma} \langle \Psi(\mathbf{R}) | \nabla_{\mathbf{R}} \Psi(\mathbf{R}) \rangle \; d\mathbf{R} = \int_\sigma \mathcal{F}. \tag{2.29}$$

The Chern number can be regarded as a measure for the global obstruction of a fibres bundle from a trivial one.

Time Evolution of states

Eigenstates are computed from $\hat{H}(\mathbf{R}(t)) \, |n;\mathbf{R}(t)\rangle = E_n(\mathbf{R}(t)) \, |n;\mathbf{R}(t)\rangle$, where we have $|n;\mathbf{R}(t)\rangle \in \mathfrak{H}_{E_n}$ (adiabatic condition) and eigenvalues are non–degenerate. The solution of the time–dependent Schrödinger equation $i\frac{\partial}{\partial t} \, |\Psi(t)\rangle = \hat{H}(\mathbf{R}(t)) \, |\Psi(t)\rangle$ can be formally written as

$$|\Psi(t)\rangle = e^{-i\int_0^t E_n(\mathbf{R}(s))\, ds} e^{i\gamma_n(t)} \, |n;\mathbf{R}(t)\rangle \, . \tag{2.30}$$

The initial condition is $|\Psi(0)\rangle = |n;\mathbf{R}(0)\rangle$. A path $\Gamma\colon [0,t] \to \mathcal{M}$ from $\mathbf{R}(0)$ to $\mathbf{R}(t)$ implies the evolution $|n;\mathbf{R}(0)\rangle \to |n;\mathbf{R}(t)\rangle$, but the state now acquires next to the usual dynamical phase (first factor on the RHS (2.30)) also a geometrical phase (2$^{\text{nd}}$ factor on the RHS). A self–consistent solution requires $\gamma_n(t) = i\int_0^t \langle n;\mathbf{R}(s)| \, \frac{\partial}{\partial s} \, |n;\mathbf{R}(s)\rangle \; ds$ (Berry phase). Non–adiabatic evolutions lead to the generalized Aharonov–Anandan phase [1].

2.1.3 Non–abelian Berry phase and U(n)–fibres

Wilczek and Zee were the first to notice the appearance of gauge structures in simple (quantum) dynamical systems [60]. We focus on adiabatic evolutions, as in Figure 2.1, however, now for a degenerate spectrum of the Hamiltonian. This will explain the emergence of non–abelian, e.g. $U(n)$–fibres, and provide the backbone for engineering and simulating non–trivial bundles in cold atomic and condensed matter systems.

Spectral decomposition and action of $U(n)$

Let $\hat{H}(\mathbf{R})$ be a finite–dimensional Hamiltonian, $\{E(\mathbf{R})\}$ the set of its eigenvalues and $\mathfrak{H}_E$ the corresponding eigen–spaces, such that the full Hilbert space can be written as

$$\mathfrak{H} = \bigoplus_E \mathfrak{H}_E \cong \mathfrak{H}_{E_1} \oplus \cdots \oplus \mathfrak{H}_{E_s}, \tag{2.31}$$

according to the spectral decomposition of the Hamiltonian.

For the following analysis, we focus on one of the subspaces with some energy E and assume that $\dim \mathfrak{H}_E = n$, which, in other words, is an n-fold degeneracy (n finite and $n > 1$). Then, we prepare the system in a state belonging to $\mathfrak{H}_E$. During an adiabatic evolution on the manifold the dimension of this subspace remains constant, i.e. $\dim \mathfrak{H}_E(\mathbf{R}_i) = \dim \mathfrak{H}_E(\mathbf{R}_j)$ for any two connected points $\mathbf{R}_i, \mathbf{R}_j$. A convenient basis $\mathcal{B}_{\mathfrak{H}_E}$ is given by the eigenvectors $|\Psi_a(i)\rangle, a = 1, \ldots, n$, where i refers to the lattice site or, equivalently, $\mathbf{R}_i$. However, we notice immediately that there exists some arbitrariness in this selection, since any unitary rotated basis will do the same job. These local gauge transformations are given by

$$|\Psi_a(i)\rangle \longrightarrow |\Psi'_a(i)\rangle := \mathcal{U}(i)\,|\Psi_a(i)\rangle = \sum_{b=1}^{n} \mathcal{U}_{ba}(i)\,|\Psi_b(i)\rangle\,, \tag{2.32}$$

the $n \times n$–matrix $\mathcal{U}(i) := (\mathcal{U}_{ab}(i))$ describes a local $U(n)$–transformation.

In this way, we see how the action of the Lie Group $U(n)$ comes into play, giving rise to $U(n)$–fibres of the bundle. The crucial point is how the total space P

of the bundle can be reconstructed from this information. The base space B can be seen as a connected component $\mathcal{M}$ of the full parameter space of the Hamiltonian and the fibres are given by $U(n)$ at each of the points of the manifold $\mathcal{M}$. One possibility for P would be the trivial bundle $\mathcal{M} \times U(n)$ with data structure $(\mathcal{M} \times U(n), pr_1, \mathcal{M}, U(n))$, $pr_1 \colon \mathcal{M} \times U(n) \to \mathcal{M}$. But, in principle there might exist non–trivial fibre bundles $(P, \pi, \mathcal{M}, U(n))$, $\pi \colon P \to \mathcal{M}$, with the same base space $\mathcal{M}$ and fibre $U(n)$, but inequivalent total space, i.e. $P \neq \mathcal{M} \times U(n)$. To some extent this information is encoded in the Chern number. More generally, it can be demonstrated that so called characteristic classes can distinguish between the different twisting of the bundles. Famous candidates are given by the Chern classes; see [37, 39] for details.

Wilson line, Wilson loop and gauge connection

We develop a construction of Wilson structures for tunable Hamilton operators with a degenerate spectrum. The projector onto the eigenspace $\mathfrak{H}_{E_n}$ and the site i is constructed via

$$\hat{\mathbb{P}}_i = \sum_{a=1}^{n} |\Psi_a(i)\rangle \langle \Psi_a(i)| , \tag{2.33}$$

and the gauge transformation of the projector is written as

$$\hat{\mathbb{P}}'_i = \mathcal{U}(i) \hat{\mathbb{P}}_i \mathcal{U}(i)^\dagger, \quad \mathcal{U}(i) \in U(n). \tag{2.34}$$

Useful properties are $\hat{\mathbb{P}}_i^\dagger \hat{\mathbb{P}}_i = \hat{\mathbb{P}}_i \hat{\mathbb{P}}_i^\dagger = \hat{\mathbb{P}}_i$ and $\hat{\mathbb{P}}_i^\dagger = \hat{\mathbb{P}}_i$. Now, consider some path Γ in $\mathcal{M}$ which connects the points $i = 1, \ldots, M$ of the lattice 2.1 in the corresponding order under the adiabatic condition, and define the concatenated operator

$$\begin{aligned} \hat{\mathbb{P}}(\Gamma) &:= \hat{\mathbb{P}}_M \circ \hat{\mathbb{P}}_{M-1} \circ \cdots \circ \hat{\mathbb{P}}_2 \circ \hat{\mathbb{P}}_1 = \hat{\mathbb{P}}_M \hat{\mathbb{P}}_{M-1} \cdots \hat{\mathbb{P}}_2 \hat{\mathbb{P}}_1 \\ &= \sum_{a_M=1}^{n} \sum_{a_{M-1}=1}^{n} \cdots \sum_{a_1=1}^{n} \langle \Psi_{a_M}(M) | \Psi_{a_{M-1}}(M-1) \rangle \cdots \langle \Psi_{a_2}(2) | \Psi_{a_1}(1) \rangle \\ &\quad \times |\Psi_{a_M}(M)\rangle \langle \Psi_{a_1}(1)| . \end{aligned} \tag{2.35}$$

This operator does not share properties of the projectors (2.33), and, it is not unitary. The derived discrete version of a gauge transformation rule for $\hat{\mathbb{P}}(\Gamma)$ is

$$\begin{aligned}\hat{\mathbb{P}}(\Gamma) \longrightarrow \hat{\mathbb{P}}(\Gamma)' = (\mathcal{U}(M)\hat{\mathbb{P}}_M\mathcal{U}(M)^\dagger)(\mathcal{U}(M-1)\hat{\mathbb{P}}_{M-1}\mathcal{U}(M-1)^\dagger)\cdots \\ \times (\mathcal{U}(2)\hat{\mathbb{P}}_2\mathcal{U}(2)^\dagger)(\mathcal{U}(1)\hat{\mathbb{P}}_1\mathcal{U}(1)^\dagger).\end{aligned} \tag{2.36}$$

Definition 14 *Let $\hat{\mathcal{W}}(\Gamma)$ be the $n \times n$-matrix with entries given by*

$$\mathcal{W}_{ab}(\Gamma) := \langle \Psi_a(M)| \hat{\mathbb{P}}(\Gamma) |\Psi_b(1)\rangle , \tag{2.37}$$

Γ describes the path connecting the sites $1, \ldots, M$ in the assigned order.

The overlaps $\langle \Psi_{a_k}(k)|\Psi_{a_l}(l)\rangle$ of states between neighbouring lattice sites k and l, as in (2.35), give rise to a gauge connection. From now on, we will focus on manifolds rather than discrete lattices (lattice sites constructed so far shall be regarded as auxiliary constructions on the grid). Re-writing the expression for a differentiable manifold, the overlaps are computed with Taylor's formula

$$\langle \Psi_a(\mathbf{R}+\Delta\mathbf{R})|\Psi_b(\mathbf{R})\rangle = \delta_{ab} + \langle \nabla_{\mathbf{R}}\Psi_a(\mathbf{R})|\Psi_b(\mathbf{R})\rangle\,|_{\mathbf{R}+\varsigma\Delta\mathbf{R}}\Delta\mathbf{R} + \mathcal{O}((\Delta\mathbf{R})^2). \tag{2.38}$$

Definition 15 *(Non–abelian gauge field) The vector–valued matrix $\mathcal{A} = (\mathcal{A}^{(n)}_{ab})$ with matrix elements*

$$\mathcal{A}^{(n)}_{ab}(\boldsymbol{R}) = i\,\langle \Psi_a(\boldsymbol{R})|\nabla_{\boldsymbol{R}}\Psi_b(\boldsymbol{R})\rangle \tag{2.39}$$

is called non–abelian gauge field. The index n is assigned to the energy level E_n.

As can be seen, the gauge field (2.39) has a similar form as the previously defined abelian field. In fact, we can show that $\left(i\mathcal{A}^{(n)}_{ab}\right) \in \mathfrak{u}(n)$: Relation $\langle \Psi_a(\mathbf{R})|\Psi_b(\mathbf{R})\rangle = \delta_{ab}$ implies $\langle \Psi_a(\mathbf{R})|\nabla_{\mathbf{R}}\Psi_b(\mathbf{R})\rangle = -\langle \Psi_b(\mathbf{R})|\nabla_{\mathbf{R}}\Psi_a(\mathbf{R})\rangle^*$, hence, $\mathcal{A}_{ab} = \mathcal{A}^*_{ba}$, which describes a hermitian matrix. Then, the exponential map yields $\exp(i(\mathcal{A}_{ab})) \in U(n)$, which confirms the statement. The gauge transformation rule for $\mathcal{A}$ is

$$\mathcal{A}'_\mu = \mathcal{U}\mathcal{A}_\mu\mathcal{U}^{-1} + \mathcal{U}\partial_\mu\mathcal{U}^{-1}, \tag{2.40}$$

utilizing the mathematical convention (B.13). We are now prepared to show that $\Gamma \mapsto \hat{\mathcal{W}}(\Gamma)$ provides an assignment rule for a connection on the bundle which is determined by the gauge field. For convenience, we may omit index n of the energy level E_n.

Lemma 16 *The map* $\Gamma \mapsto \hat{\mathcal{W}}(\Gamma)$ *has the following properties*

$$\hat{\mathcal{W}}(\Gamma' \circ \Gamma) = \hat{\mathcal{W}}(\Gamma')\hat{\mathcal{W}}(\Gamma) \tag{2.41}$$

$$\hat{\mathcal{W}}(\Gamma : \boldsymbol{R} \to \boldsymbol{R} + \Delta\boldsymbol{R}) = \hat{\mathbb{1}} + \mathcal{A}\Delta\boldsymbol{R} + \mathcal{O}((\Delta\boldsymbol{R})^2) \tag{2.42}$$

Proof. For the first part of the statement, we have

$$\begin{aligned}
\mathcal{W}_{ab}(\Gamma' \circ \Gamma) &= \langle \Psi_a(M')| \hat{\mathbb{P}}_{M'} \circ \hat{\mathbb{P}}_{M'-1} \circ \cdots \circ \hat{\mathbb{P}}_{N+1} \circ \hat{\mathbb{P}}_N \circ \hat{\mathbb{P}}_{N-1} \circ \cdots \circ \hat{\mathbb{P}}_1 |\Psi_b(1)\rangle \\
&= \langle \Psi_a(M')| \underbrace{\hat{\mathbb{P}}_{M'} \circ \cdots \circ \hat{\mathbb{P}}_N}_{\hat{\mathcal{P}}(\Gamma')} \circ \underbrace{\hat{\mathbb{P}}_N}_{\sum_m |\Psi_m(N)\rangle\langle\Psi_m(N)|} \circ \underbrace{\hat{\mathbb{P}}_N \circ \cdots \circ \hat{\mathbb{P}}_1}_{\hat{\mathcal{P}}(\Gamma)} |\Psi_b(1)\rangle \\
&= \sum_{m=1}^{n} \mathcal{W}_{am}(\Gamma')\mathcal{W}_{mb}(\Gamma),
\end{aligned}$$

where we have used $\hat{\mathbb{P}}_N^3 = \hat{\mathbb{P}}_N$ to decompose the above operator product in three parts. With regards to the second part of the statement,

$$\begin{aligned}
\mathcal{W}_{ab}(\Gamma : \mathbf{R} \to \mathbf{R} + \Delta\mathbf{R}) &= \langle \Psi_a(\mathbf{R} + \Delta\mathbf{R})| \hat{\mathbb{P}}_{\mathbf{R}+\Delta\mathbf{R}} \hat{\mathbb{P}}_{\mathbf{R}} |\Psi_b(\mathbf{R})\rangle = \langle \Psi_a(\mathbf{R} + \Delta\mathbf{R})|\Psi_b(\mathbf{R})\rangle \\
&= \delta_{ab} + i\mathcal{A}_{ab}\Delta\mathbf{R} + \mathcal{O}((\Delta\mathbf{R})^2),
\end{aligned}$$

where use has been made of definition (2.39) and equation (2.38). ■

We parametrize the path $\Gamma\colon [0,t] \to \mathcal{M}$ by $s \mapsto \mathbf{R}(s)$ and observe that following expression must hold according to the previous lemma

$$\hat{\mathcal{W}}(\mathbf{R}(s + \Delta s)) = \hat{\mathcal{W}}(\mathbf{R}(s) \to \mathbf{R}(s) + \Delta\mathbf{R}(s))\hat{\mathcal{W}}(\mathbf{R}(s)) \tag{2.43}$$

$$= (\hat{\mathbb{1}} + i\mathcal{A}\Delta\mathbf{R})\hat{\mathcal{W}}(\mathbf{R}(s)). \tag{2.44}$$

Then, taking the limit we compute

$$\lim_{\Delta s \to 0} \frac{1}{\Delta s}[\hat{\mathcal{W}}(\mathbf{R}(s + \Delta s)) - \hat{\mathcal{W}}(\mathbf{R}(s))] = \lim_{\Delta s \to 0} i\mathcal{A}\frac{\Delta\mathbf{R}}{\Delta s}\hat{\mathcal{W}}(\mathbf{R}(s)) \tag{2.45}$$

$$= i\mathcal{A}_\mu(\mathbf{R}(s))\dot{\mathbf{R}}^\mu(s)\hat{\mathcal{W}}(\mathbf{R}(s)). \tag{2.46}$$

Since the LHS of the above equation is simply a derivative with respect to s, we arrive at the fundamental differential equation for the Wilson line of a smooth path

$$\frac{d}{ds}\hat{\mathcal{W}}(\mathbf{R}(s)) = i\mathcal{A}_\mu(\mathbf{R}(s))\dot{\mathbf{R}}^\mu(s)\hat{\mathcal{W}}(\mathbf{R}(s)). \tag{2.47}$$

An obvious approach for obtaining a solution can be provided if we state it as an integral equation - this means

$$\hat{\mathcal{W}}(\mathbf{R}(t)) = \hat{\mathcal{W}}(\mathbf{R}(0)) + i\int_0^t \mathcal{A}_\mu(\mathbf{R}(s))\dot{\mathbf{R}}^\mu(s)\hat{\mathcal{W}}(\mathbf{R}(s))\,ds. \tag{2.48}$$

Theorem 17 *A solution of the integral equation* (2.48) *is given by*

$$\hat{\mathcal{W}}(\boldsymbol{R}(t)) = \mathcal{T}\exp\left(i\int_0^t \mathcal{A}_\mu \dot{\boldsymbol{R}}^\mu\,ds\right)\hat{\mathcal{W}}(\boldsymbol{R}(0)) \tag{2.49}$$

where the initial value condition is $\hat{\mathcal{W}}(\boldsymbol{R}(0)) = \hat{\mathbb{1}}$ *and* $\mathcal{T}$ *is the time–ordering operator*[4].

Proof. Equation (2.48) provides us with the possibility of solving (2.47) by the well known Picard-Lindelöf iteration for differential equations. The iteration sequence $(\hat{\mathcal{W}}_n)_{n\in\mathbb{N}}$ starts with $\hat{\mathcal{W}}_0 = \hat{\mathcal{W}}(\mathbf{R}(0))$ and the elements of the sequence are defined as

$$\hat{\mathcal{W}}_n(\mathbf{R}(t)) = \hat{\mathcal{W}}(\mathbf{R}(0)) + i\int_0^t \mathcal{A}_\mu(\mathbf{R}(s))\dot{\mathbf{R}}^\mu(s)\hat{\mathcal{W}}_{n-1}(\mathbf{R}(s))\,ds. \tag{2.50}$$

The first few terms are

$$\begin{aligned}
\hat{\mathcal{W}}_1(\mathbf{R}(t)) &= \hat{\mathcal{W}}(\mathbf{R}(0)) + i\int_0^t \mathcal{A}_\mu(\mathbf{R}(s_1))\dot{\mathbf{R}}^\mu(s_1)\hat{\mathcal{W}}(\mathbf{R}(0))\,ds_1,\\
\hat{\mathcal{W}}_2(\mathbf{R}(t)) &= \hat{\mathcal{W}}(\mathbf{R}(0)) + i\int_0^t ds_1\mathcal{A}_\mu(\mathbf{R}(s_1))\dot{\mathbf{R}}^\mu(s_1)\hat{\mathcal{W}}(\mathbf{R}(0)) +\\
& i^2\int_0^t ds_1\mathcal{A}_\mu(\mathbf{R}(s_1))\dot{\mathbf{R}}^\mu(s_1)\int_0^{s_1} ds_2\mathcal{A}_\nu(\mathbf{R}(s_2))\dot{\mathbf{R}}^\nu(s_2)\hat{\mathcal{W}}(\mathbf{R}(0)).
\end{aligned}$$

By using the abbreviation $\mathcal{A}_\mu(\mathbf{R}(s_i))\dot{\mathbf{R}}^\mu(s_i) = \hat{\Xi}(s_i)$ and the time ordering $0 \le s_n \le s_{n-1}\cdots \le s_1 \le t$ we can assign to the n-th term

$$\begin{aligned}
& i^n\int_0^t ds_1\int_0^{s_1} ds_2\cdots\int_0^{s_{n-1}} ds_n\hat{\Xi}(s_1)\hat{\Xi}(s_2)\cdots\hat{\Xi}(s_n)\hat{\mathcal{W}}(\mathbf{R}(0))\\
&= \frac{i^n}{n!}\int_0^t ds_1\int_0^t ds_2\cdots\int_0^t ds_n\mathcal{T}(\hat{\Xi}(s_1)\hat{\Xi}(s_2)\cdots\hat{\Xi}(s_n))\hat{\mathcal{W}}(\mathbf{R}(0))
\end{aligned}$$

[4]More details on time–ordered products can be found in [58].

So,

$$\hat{\mathcal{W}}_n(\mathbf{R}(t)) = \sum_{k=0}^{n} \frac{i^k}{k!} \int_0^t ds_1 \int_0^t ds_2 \cdots \int_0^t ds_k \mathcal{T}(\hat{\Xi}(s_1)\hat{\Xi}(s_2)\cdots\hat{\Xi}(s_k))\hat{\mathcal{W}}(\mathbf{R}(0)) \tag{2.51}$$

With an appropriate operator norm $\|\cdot\|$, we see that the RHS of (2.47) has the global Lipschitz-condition

$$\left\|\Xi(s)\hat{\mathcal{W}}(\mathbf{R}(s)) - \Xi(s)\hat{\mathcal{X}}(\mathbf{R}(s))\right\| \leq \max\left\|\Xi(s)\right\|_{s\in[0,t]} \left\|\hat{\mathcal{W}}(\mathbf{R}(s)) - \hat{\mathcal{X}}(\mathbf{R}(s))\right\|.$$

According to Picard-Lindelöf, $\hat{\mathcal{W}} := \lim_{n\to\infty} \hat{\mathcal{W}}_n$ exists and is unique over the whole time interval. Taking the limit $n \to \infty$ on both sides of (2.51) yields

$$\begin{aligned}\hat{\mathcal{W}}(\mathbf{R}(t)) &= \sum_{k=0}^{\infty} \frac{i^k}{k!} \int_0^t ds_1 \int_0^t ds_2 \cdots \int_0^t ds_k \mathcal{T}(\hat{\Xi}(s_1)\hat{\Xi}(s_2)\cdots\hat{\Xi}(s_k))\hat{\mathcal{W}}(\mathbf{R}(0)) \\ &= \mathcal{T}\exp\left(i\int_0^t \hat{\Xi}(s)\,ds\right)\hat{\mathcal{W}}(\mathbf{R}(0)),\end{aligned}$$

and $\hat{\mathcal{W}}(\mathbf{R}(0)) = \hat{\mathbb{1}}$, since it is the Wilson line to a constant path. ■

The path ordering method of operators can be considered as a consequence of the time–ordering process [58], as is suggested by the above proof. Notice that $\mathcal{A}_\mu \dot{\mathbf{R}}^\mu\, ds$ represents a $\mathfrak{u}(n)$–valued one–form $\mathcal{A} = \mathcal{A}_\mu d\mathbf{R}^\mu$. Thus, the theorem above leads to

Corollary 18 *The Wilson line (operator) corresponding to a path Γ connecting two points in $\mathcal{M}$ can be formally written as*

$$\hat{\mathcal{W}}(\Gamma) = \mathcal{P}\exp\left(i\int_\Gamma \mathcal{A}_\mu d\boldsymbol{R}^\mu\right), \tag{2.52}$$

with $\mathcal{A}_\mu d\boldsymbol{R}^\mu \in \mathfrak{u}(n)\otimes\Omega^1(\mathcal{M})$ and $\mathcal{P}$ as the path–ordering operator.

The *Wilson loop operator* $\hat{\mathcal{W}}(\mathcal{C})$ is obtained from (2.52) by setting $\Gamma = \mathcal{C}$ for a loop. The behaviour of the Wilson operators under gauge transformations is relevant for the computation of observables. For this goal, one can consider $\hat{\mathcal{W}}(\Delta\Gamma)$ for sufficiently small paths $\Delta\Gamma$, as all Wilson lines can be built by such pieces according to (2.41) and (2.42).

Proposition 19 *Let $\hat{\mathcal{W}}(\Gamma)$ be the Wilson line (operator) for a path Γ which connects the start point $\boldsymbol{R}_1$ and end point $\boldsymbol{R}_2$. Then the gauge transformed Wilson line is*

$$\hat{\mathcal{W}}(\Gamma)' = \mathcal{U}(\boldsymbol{R}_2)\hat{\mathcal{W}}(\Gamma)\mathcal{U}(\boldsymbol{R}_1)^{-1}, \quad \mathcal{U}^{-1} = \mathcal{U}^{\dagger}. \tag{2.53}$$

Unlike the abelian Berry phase $\exp(i\gamma_{\mathcal{C}})$, the Wilson loop operator is not gauge–invariant and therefore, it is not directly observable. However, gauge invariant observables can be derived from the Wilson loop operator.

Time Evolution

We focus on cyclic adiabatic evolutions: Let $|\Psi(0)\rangle = |\Psi_a\rangle \in \mathfrak{H}_{E_n(\mathbf{R}(0))}$ be the initial condition and consider the evolution of the state along a loop $\mathcal{C}$ in the manifold, such that $\mathbf{R}(0) = \mathbf{R}(T)$ holds for the period T of the cycle; $\hat{H}(\mathbf{R}(t))\,|\Psi_a(t)\rangle = E_n(\mathbf{R}(t))\,|\Psi_a(t)\rangle$. The formal solution to $i\frac{\partial}{\partial t}\,|\Psi(t)\rangle = \hat{H}(\mathbf{R}(t))\,|\Psi(t)\rangle$ is

$$|\Psi(T)\rangle = e^{-i\int_0^T E_n(\mathbf{R}(s))\,ds}\hat{\mathcal{W}}(\mathcal{C})\,|\Psi_a\rangle\,. \tag{2.54}$$

Again, a dynamic and geometric factor occur for the evolved state. The geometric factor is the Wilson loop operator.

Wilson loop and non–abelian Berry Curvature

We derive now a significant relation between the Wilson loop operator $\hat{\mathcal{W}}(\mathcal{C})$ and the curvature of the fibre bundle. Let $\mathcal{C}_{\square}$ be a small square on the manifold whose edges are aligned with the ν, μ–coordinates. One can compose the Wilson loop of four Wilson lines according to our lemma, each corresponding to an edge

$$\hat{\mathcal{W}}(\mathcal{C}_{\square}) = \hat{\mathcal{W}}(\Gamma_4)\hat{\mathcal{W}}(\Gamma_3)\hat{\mathcal{W}}(\Gamma_2)\hat{\mathcal{W}}(\Gamma_1) = \exp(W^{\dagger})\exp(Z^{\dagger})\exp(Y)\exp(X), \tag{2.55}$$

with operators defined by gauge fields along the rectangle

$$X = ia\mathcal{A}_{\mu}(x + \varsigma\hat{\mu}) \tag{2.56}$$

$$Y = ia\mathcal{A}_{\nu}(x + \hat{\mu} + \varsigma\hat{\nu}) \tag{2.57}$$

$$Z = ia\mathcal{A}_{\mu}(x + \hat{\nu} + \varsigma\hat{\mu}) \tag{2.58}$$

$$W = ia\mathcal{A}_{\nu}(x + \varsigma\hat{\nu}) \tag{2.59}$$

Proposition 20 *Up to leading order $\mathcal{O}(a^3)$ (a side length of the square) the Wilson loop operator for $\mathcal{C}_\square$ is*

$$\hat{\mathcal{W}}(\mathcal{C}_\square) = \exp(ia^2\mathcal{F}_{\mu\nu} + \mathcal{O}(a^3)), \tag{2.60}$$

$$\mathcal{F}_{\mu\nu} = \partial_\mu \mathcal{A}_\nu - \partial_\nu \mathcal{A}_\mu - i[\mathcal{A}_\mu, \mathcal{A}_\nu], \tag{2.61}$$

where $\mathcal{F}_{\mu\nu}$ is known to be the local form of the curvature.

The complete computation is carried out in subsection B.1.1. We recognize $\mathcal{F}_{\mu\nu}$ as the field strength components of a non–abelian Yang–Mills field. The Yang–Mills field strength is known from high energy physics, quantum chromodynamics (QCD) etc.

Wilson action. From the above discussion it is actually straightforward to construct a gauge invariant action, by taking sums over traces of the Wilson operators. The Wilson action for a $SU(n)$ gauge theory on a lattice can be defined via, see e.g. [61, 11],

$$S_W(U) = \frac{1}{2g^2} \sum_\square \Re \operatorname{Tr} \hat{\mathcal{W}}(\mathcal{C}_\square), \tag{2.62}$$

which with the help of (2.60) can be written as

$$S_W(U) = \frac{1}{2g^2} \sum_\square \Re \operatorname{Tr} \left(\mathbb{1} + ia^2\mathcal{F}_{\mu\nu} - \frac{1}{2}a^4 \mathcal{F}_{\mu\nu}\mathcal{F}_{\mu\nu} + \mathcal{O}(a^5) \right) \tag{2.63}$$

$$= \frac{1}{2g^2} \sum_\square (n - \frac{1}{2}a^4 \operatorname{Tr}\left(\mathcal{F}_{\mu\nu}\mathcal{F}_{\mu\nu}\right) + \mathcal{O}(a^5)), \tag{2.64}$$

where g is a coupling constant and the sum runs over all plaquettes in the manifold. The first term is an irrelevant constant when considering the path integral

$$Z = \int \mathcal{D}U e^{S_W(U)}, \tag{2.65}$$

and main contributions come from $\operatorname{Tr}(\mathcal{F}_{\mu\nu}\mathcal{F}_{\mu\nu})$.

Although Wilson introduced his action in seminal papers in the context of QCD [61], one can argue that it must also play a crucial role in condensed matter systems. One of the promising platforms on which this can be achieved are highly

tunable ultracold atom systems where internal atomic levels are coupled to light (e.g. Chap. 4 section 2). The original idea was based on a formulation of the QCD action on a discrete space-time lattice using path integrals. From that point it is a short path to the interpretation and evaluation of observables in terms of stochastic tools, Monte-Carlo or microcanonical ensembles [11, 12]. It is worth to make a remark about a crucial topological point - since the Minkowski space-time is contractible, the resulting fibre bundle of the system will be trivial [51, 59]. This is the case for all gauge theories defined over Minkowski space-time. Also, one cannot control the space-time variables itself in this context. However, in tunable condensed matter platforms, such as cold atom systems, one can utilize the parameter space as the base space manifold of a fibre bundle. It turns out that these parameter spaces are topologically non-trivial, e.g. spherical, and can therefore naturally host monopole-like structures. The principle of unprecedented control of the coupled laser fields to atomic states allows to navigate through the parameter space and measure, for instance, $\langle \hat{\mathcal{W}}(\mathcal{C}) \rangle$ etc.

Generating synthetic non–abelian gauge fields. As discussed, we have shown that a necessary condition for simulating non–abelian gauge fields is to create a tunable, degenerate subspace of states. One general set up scheme consists of resonant coupling of N ground states $\{|i\rangle_g \, | i = 1, \cdots, N\}$ to an excited state $|\Psi\rangle_e$ via laser fields (see [47] for more details).

2.2 Advanced Methods and Tools

In this section we investigate mathematical tools which shall prove to be essential for the understanding of topological phases of matter.

2.2.1 Topological Quantities I

Take a closed $\mathbb{R}$–valued differential 1–form ω living on a (connected and compact) finite–dimensional manifold $\mathcal{M}$. Denote by $\pi_1(\mathcal{M})$ the first homotopy group of

the manifold. Then regard the following map $\gamma \mapsto \int_\gamma \omega$, where $\gamma\colon [0,1] \to \mathcal{M}$ is a closed path, i.e. $\gamma(0) = \gamma(1)$. Consider another loop β starting at the same base point and which is homotopic to γ (short: $\gamma \sim \beta$), then we have the following invariance by the *monodromy lemma* $\int_\gamma \omega = \int_\beta \omega$. This gives us the possibility to induce a map which assigns to every homotopy class $[\gamma] \in \pi_1(\mathcal{M})$ a unique real number

$$[\gamma] \mapsto h_\omega([\gamma]) := \int_\gamma \omega. \tag{2.66}$$

Thus, we have constructed a well-defined map $h_\omega\colon \pi_1(\mathcal{M}) \to \mathbb{R}$ which is also a group homomorphism $h_\omega([\alpha \cdot \beta]) = h_\omega([\alpha]) + h_\omega([\beta])$. As can be seen, the value of the integral depends solely on the 1-form ω and the loop homotopy class $[\gamma]$. Moreover, every loop can be seen as one–cycle in the homology class which provides us with a map $\pi_1(\mathcal{M}) \to H_1(\mathcal{M}, \mathbb{R})$ (homomorphism), as a special case of *Hurewicz's theorem*. De Rham's theorem asserts a non–degenerate and bilinear pairing $(\cdot,\cdot)\colon H^k(\mathcal{M}) \times H_k(\mathcal{M}) \to \mathbb{R}$ which reduces to

$$\int_\gamma \omega = ([\omega], [\gamma]), \quad [\omega] \in H^1(\mathcal{M}), [\gamma] \in H_1(\mathcal{M}). \tag{2.67}$$

The value of the integral depends only on the classes: If one replaces ω by $\omega + df$ or γ by $\gamma + \partial c$, where df is the derivative of some function and ∂c is the boundary of some 2-cycle, then the result turns out to be invariant due to Stokes theorem. In particular, the winding number can be constructed as a one–form:

Condition 21 *(winding form ω_W) Referring to $\mathbb{R}^2 - \{0\}$ (one can also take $\mathbb{R}^2$ minus any other point and modify the formulas):*

- $\omega_W = f_1 dx_1 + f_2 dx_2$ *(local coordinate representation)*
- $\partial_2 f_1 = \partial_1 f_2$*;* $\partial_i := \frac{\partial}{\partial x_i}$ *(integrability condition & local exactness)*
- $\int_{\partial D(0;R)} \omega_W = 2\pi n$*,* $n \in \mathbb{Z}$*, where $D(0;R)$ is a disk with radius R and centre 0 and ∂D is its boundary (circle).*

One can show that these conditions are necessary and sufficient for a winding form.

Proposition 22 *A suitable winding 1-form in* $\mathbb{R}^2 - \{0\}$ *can be given by*

$$\omega_W = \frac{1}{r^2}(-ydx + xdy), \quad r = \sqrt{x^2 + y^2}. \tag{2.68}$$

It is easy to check that it is closed, $d\omega_W = 0$. The manifold $\mathbb{R}^2 - \{0\}$ is homotopic to $\mathbb{S}^1$, hence the first homology group is $H_1(\mathbb{S}^1; \mathbb{R}) = \mathbb{R}$. De Rham's theorem implies for the cohomology group $H^1(\mathbb{S}^1; \mathbb{R}) = \mathbb{R}$ due to the general duality isomorphism $H_k(\mathcal{M}) \cong H^k(\mathcal{M})$ for compact manifolds $\mathcal{M}$. So, $H^1(\mathbb{S}^1)$ is generated by the cohomology class $[\omega_W]$. This means that any other closed 1–form ω must be given by $\omega = a\omega_W + df$ with $a \in \mathbb{R}$. Since df is the derivative of some function, it will have no effect when we integrate over some cycle.

Application to SSH model. Calculating the winding numbers for the SSH phases using $\mathbf{d}(k)$ we get

$$\frac{1}{2\pi} \int_{\partial D(v;w)} \omega_W = 1, \quad w > v \tag{2.69}$$

$$\frac{1}{2\pi} \int_{\partial D(v;w)} \omega_W = 0, \quad w < v \tag{2.70}$$

This demonstrates the existence of precisely two phases of the system. The chiral symmetry of the SSH model implies a vanishing z–component[5] in the Hamiltonian which leads in fact to a reduction of the parameter space, i.e. $\mathbb{R}^3 - \{0\} \to \mathbb{R}^2 - \{0\}$ or $\mathbb{S}^2 \to \mathbb{S}^1$. Hence, by virtue of homology–cohomology duality of $\mathbb{S}^1$ there is only one non–trivial closed 1-form (unique up to cohomology).

2.2.2 Topological Quantities II

In order to extend the theory to non–abelian gauge fields and describe higher Chern numbers one needs to deal with covariant differential calculus. Two main points for the motivation are:

- For non–abelian gauge fields $\mathcal{A}$ the curvature $\mathcal{F}$ cannot be simply written as $d\mathcal{A}$ (not even locally). Instead, it is $\mathcal{F}_{\mu\nu} = \partial_\mu \mathcal{A}_\nu - \partial_\nu \mathcal{A}_\mu + [\mathcal{A}_\mu, \mathcal{A}_\nu]$, as has been shown in (B.13) and stated in (2.61).

[5] Diagonal entries in $\hat{H}(k)$ vanish.

- Manifolds with $H^2(\mathcal{M}) = 0$ have vanishing first Chern numbers. Thus, we need to define a generalized tensor–wedge operation $\hat{\otimes}$ for the construction of higher degree forms consisting of non–abelian curvature $\mathcal{F}$.

Definition 23 *(Covariant differential $d_{\mathcal{A}}$ of forms) Let ω be a vector-valued r–form, i.e. $\omega \in V \otimes \Omega^r(\mathcal{M})$, and let $\mathcal{A}$ be a gauge field on the manifold $\mathcal{M}$, which acts on vector space V via a representation $R\colon \mathfrak{g} \to End(V)$. One defines*

$$d_{\mathcal{A}}\omega := d\omega + \mathcal{A} \wedge \omega \tag{2.71}$$

as the exterior covariant differential of ω with respect to gauge field $\mathcal{A}$. d is the standard exterior derivative and $\wedge$ denotes the wedge product for forms.

Applying this definition to $\mathcal{A}$ we obtain the correct formula for the curvature,

$$d_{\mathcal{A}}\mathcal{A} = d\mathcal{A} + \mathcal{A} \wedge \mathcal{A} = \frac{1}{2}(\partial_\mu \mathcal{A}_\nu - \partial_\nu \mathcal{A}_\mu) dx^\mu \wedge dx^\nu + \mathcal{A}_\mu \cdot \mathcal{A}_\nu dx^\mu \wedge dx^\nu \tag{2.72}$$

$$= \frac{1}{2}(\partial_\mu \mathcal{A}_\nu - \partial_\nu \mathcal{A}_\mu + [\mathcal{A}_\mu, \mathcal{A}_\nu]) dx^\mu \wedge dx^\nu = \mathcal{F}. \tag{2.73}$$

In this formalism the Bianchi identity is written as $d_{\mathcal{A}}\mathcal{F} = d^2_{\mathcal{A}}\mathcal{A} = 0$ (equation of motion for gauge field $\mathcal{A}$).

Definition 24 *(Exterior tensor–wedge product $\hat{\otimes}$) Let η be a V–valued r-form and ω a W–valued s-form. The resulting $(V \otimes W)$–valued (r+s)-form $\eta\hat{\otimes}\omega$ is written as*

$$\eta\hat{\otimes}\omega = (\eta^a \wedge \omega^b) v_a \otimes w_b, \tag{2.74}$$

where v_a and w_b are the basis elements of vector spaces V and W, respectively. For the components we have

$$\eta^a = \frac{1}{r!}\eta^a_{\mu_1 \cdots \mu_r} dx^{\mu_1} \wedge \cdots \wedge dx^{\mu_r}, \tag{2.75}$$

$$\omega^b = \frac{1}{s!}\omega^b_{\nu_1 \cdots \nu_s} dx^{\nu_1} \wedge \cdots \wedge dx^{\nu_s}. \tag{2.76}$$

Using the component representation we may write in total

$$\eta\hat{\otimes}\omega = \frac{1}{r!s!}\eta^a_{\mu_1 \cdots \mu_r}\omega^b_{\nu_1 \cdots \nu_s}(v_a \otimes w_b) dx^{\mu_1} \wedge \cdots \wedge dx^{\mu_r} \wedge dx^{\nu_1} \wedge \cdots \wedge dx^{\nu_s}. \tag{2.77}$$

The action of the operator $d_{\mathcal{A}}$ on $\eta\hat{\otimes}\omega$ yields the useful formula

$$d_{\mathcal{A}}(\eta\hat{\otimes}\omega) = (d_{\mathcal{A}}\eta)\hat{\otimes}\omega + (-1)^r\eta\hat{\otimes}(d_{\mathcal{A}}\omega). \tag{2.78}$$

We take the nth tensor-wedge product of the non–abelian Berry curvature $\mathcal{F}$ to obtain the $\mathfrak{g}^{\otimes n}$–valued (2n)–form

$$\underbrace{\mathcal{F}\hat{\otimes}\mathcal{F}\hat{\otimes}\cdots\hat{\otimes}\mathcal{F}}_{n} \in \mathfrak{g}^{\otimes n}\otimes\Omega^{2n}(\mathcal{M}). \tag{2.79}$$

This entity is the key for the construction of characteristic forms and and corresponding classes (Hirzebruch, Milnor [21, 39]). However, it is necessary to extract a gauge–invariant real–valued differential form out of (2.79). I shall briefly describe this mathematical procedure.

Characteristic cohomological form. Let $P\colon \mathfrak{g}\times\cdots\times\mathfrak{g}\to\mathbb{R}$ be a G–invariant symmetric polynomial P of degree n (linear in each argument). Then consider $P\to R_P$ such that $\mathcal{F}\hat{\otimes}\mathcal{F}\hat{\otimes}\cdots\hat{\otimes}\mathcal{F}\to R_P(\mathcal{F}\hat{\otimes}\mathcal{F}\hat{\otimes}\cdots\hat{\otimes}\mathcal{F})\in\mathbb{R}\otimes\Omega^{2n}(\mathcal{M})$, which is a mapping

$$R_P\colon \mathfrak{g}^{\otimes n}\otimes\Omega^{2n}(\mathcal{M})\to\mathbb{R}\otimes\Omega^{2n}(\mathcal{M}), \tag{2.80}$$

with the full structure

$$R_P(\mathcal{F}\hat{\otimes}\mathcal{F}\hat{\otimes}\cdots\hat{\otimes}\mathcal{F}) = \frac{1}{2^n}\mathcal{F}^{a_1}_{\mu_1\nu_1}\cdots\mathcal{F}^{a_n}_{\mu_n\nu_n}P(T_{a_1},\ldots,T_{a_n})dx^{\mu_1}\wedge dx^{\nu_1}\wedge\cdots\wedge dx^{\mu_n}\wedge dx^{\nu_n}, \tag{2.81}$$

where $\{T_a\}$ constitutes a basis of the Lie algebra $\mathfrak{g}$ of the group. It is straightforward to show that form (2.81) is gauge–invariant and closed (characteristic): 1) Local gauge transformation $\mathcal{F}(x)\to\mathcal{F}^g(x)=g(x)\mathcal{F}(x)g^{-1}(x)$ yields

$$R_P(\mathcal{F}^g\hat{\otimes}\cdots\hat{\otimes}\mathcal{F}^g) = R_P(\mathcal{F}\hat{\otimes}\cdots\hat{\otimes}\mathcal{F}) \tag{2.82}$$

since the polynomial part is G–invariant $P(T^g_{a_1},\ldots,T^g_{a_n})=P(T_{a_1},\ldots,T_{a_n})$ by construction (invariant under the adjoint transformation). 2) To show that (2.81) is closed we observe the commuting relation $d\circ R_P = R_P\circ d_{\mathcal{A}}$ and apply the Bianchi identity $d_{\mathcal{A}}\mathcal{F}=0$ to each of the factors in $\mathcal{F}\hat{\otimes}\cdots\hat{\otimes}\mathcal{F}$ via rule (2.78) on the RHS.

For a closed manifold with $\dim \mathcal{M} = 2n$, we may define a topological number $N(\mathcal{A})$ for gauge field $\mathcal{A}$

$$N(\mathcal{A}) = \int_{\mathcal{M}} R_P(\mathcal{F}\hat{\otimes}\mathcal{F}\hat{\otimes}\cdots\hat{\otimes}\mathcal{F}) = \left([R_P(\mathcal{F}^{\hat{\otimes}n})], [\mathcal{M}]\right). \tag{2.83}$$

Since $N(\mathcal{A})$ remains constant for variations $\mathcal{A} \to \mathcal{A} + \delta\mathcal{A}$, it is a homotopy invariant for gauge–field configurations. In equation (2.83) we have included the expression in terms of the pairing $H^{2n}(\mathcal{M}) \times H_{2n}(\mathcal{M}) \to \mathbb{R}$. A powerful and detailed demonstration of these methods is given in Chap. 4 sec. 2, where a synthetic high–dimensional space is generated via hyperfine level coupling in cold Rubidium atoms.

2.3 Two–Level System: Monopole and 'hidden' structures

In order to understand the emergence of non–trivial fibre bundles and monopoles in synthetic dimensions, we begin our study with a generic two–level system which supports a topologically stable monopole configuration. It can be considered as a basic unit for engineering topologically stable defects.

2.3.1 Hamiltonian

Consider the generic Hamiltonian[6] for spin–1/2 fermions

$$\hat{H}(\mathbf{R}) = \mathbf{R}\cdot\vec{\sigma} = \begin{pmatrix} R_z & R_x - iR_y \\ R_x + iR_y & -R_z \end{pmatrix}, \tag{2.84}$$

where $\mathbf{R} = R(\sin\theta\cos\varphi, \sin\theta\sin\varphi, \cos\theta)$, $R := ||\mathbf{R}||$. To have a particular system in mind, we can think of spin–1/2 particles coupled to a rotating magnetic field. It also turns out that various models, such as the Haldane model, are described by the same type of Hamiltonian $\hat{H}(\mathbf{k})$ on the momentum–space level.

[6] In general, one can set $\hat{H}(\mathbf{R}) = \epsilon\hat{\mathbb{1}} + \mathbf{R}\cdot\vec{\sigma}$. This additional term only causes an energy shift of the gap. So, we can neglect the ϵ term in the following discussion.

Berry connection, curvature, Chern numbers

Since $\hat{H}^2 = R^2\hat{1}$ the energy eigenvalues are given by $E = \pm R$. We compute the eigenstates by rewriting $(\hat{H} - E)\psi = 0$ as

$$\begin{pmatrix} \cos\theta \pm 1 & \sin\theta e^{-i\varphi} \\ \sin\theta e^{i\varphi} & -\cos\theta \pm 1 \end{pmatrix} \begin{pmatrix} \psi_1 \\ \psi_2 \end{pmatrix} = \begin{pmatrix} 0 \\ 0 \end{pmatrix}. \tag{2.85}$$

A standard computation leads to

$$|+, \mathbf{R}\rangle = \begin{pmatrix} \cos\frac{\theta}{2} \\ \sin\frac{\theta}{2}e^{i\varphi} \end{pmatrix}, \quad |-, \mathbf{R}\rangle = \begin{pmatrix} \sin\frac{\theta}{2}e^{-i\varphi} \\ -\cos\frac{\theta}{2} \end{pmatrix}. \tag{2.86}$$

The ground state corresponding to $E = -R$ is denoted by $|-, \mathbf{R}\rangle$ and the excited states is $|+, \mathbf{R}\rangle$. The system is obviously *gapped* and no degeneracies occur for $\mathbf{R} \neq 0$. This signals a potential *topological singularity* in the origin $\mathbf{R} = 0$. For convenience, we calculate the ground state gauge connection in the chosen coordinate system

$$\mathcal{A}_R^{(-)} = i \langle -, \mathbf{R}| \partial_R |-, \mathbf{R}\rangle = 0, \tag{2.87}$$

$$\mathcal{A}_\theta^{(-)} = i \langle -, \mathbf{R}| \partial_\theta |-, \mathbf{R}\rangle = i \begin{pmatrix} \sin\frac{\theta}{2}e^{-i\varphi} \\ -\cos\frac{\theta}{2} \end{pmatrix}^\dagger \frac{1}{2} \begin{pmatrix} \cos\frac{\theta}{2}e^{-i\varphi} \\ \sin\frac{\theta}{2} \end{pmatrix} = 0, \tag{2.88}$$

$$\mathcal{A}_\varphi^{(-)} = i \langle -, \mathbf{R}| \partial_\varphi |-, \mathbf{R}\rangle = i \begin{pmatrix} \sin\frac{\theta}{2}e^{-i\varphi} \\ -\cos\frac{\theta}{2} \end{pmatrix}^\dagger \begin{pmatrix} -i\sin\frac{\theta}{2}e^{-i\varphi} \\ 0 \end{pmatrix} = \sin^2\left(\frac{\theta}{2}\right). \tag{2.89}$$

The curvature components are $\mathcal{F}_{\theta\varphi}^{(-)} = \partial_\theta \mathcal{A}_\varphi^{(-)} - \partial_\varphi \mathcal{A}_\theta^{(-)} = \frac{1}{2}\sin\theta$, and the curvature two-form is $\mathcal{F} = \mathcal{F}_{\theta\varphi}^{(-)} d\theta \wedge d\varphi$. Thus, it is straightforward to see that the Chern number is given by

$$\mathcal{C}^{(-)} = \frac{1}{2\pi}\int_{\mathbb{S}^2} \mathcal{F} = 1. \tag{2.90}$$

This indicates a topologically non–trivial fibre bundle structure corresponding to the ground level of the system. Moreover, the Chern number of the excited state is $\mathcal{C}^{(+)} = -1$.

2.3.2 A topological model and fibre bundle structure

The natural emergence of a gauge field and curvature, as described in the previous section, requires us to propose a model for the fibre bundle structure. A suitable mathematical strategy which can be modified to other situations is the following: Consider the space

$$\mathcal{X}_H := \left\{ \hat{H} = \sum_{i=1}^{3} R_i \hat{\sigma}_i | \quad ||\mathbf{R}|| \neq 0 \right\}. \tag{2.91}$$

This space is $\mathbb{R}^3 - \{0\}$ which has a deformation retract onto $\mathbb{S}^2$, i.e. we have a homotopy $\mathbb{R}^3 - \{0\} \sim \mathbb{S}^2$. A coset/homogeneous space representation is given by $SO(3)/SO(2) = \mathbb{S}^2$. We introduce a group action on the above space

$$SU(2) \times \mathcal{X}_H \to \mathcal{X}_H, \quad (\mathcal{U}, \hat{H}) \mapsto \mathcal{U}\hat{H}\mathcal{U}^\dagger, \tag{2.92}$$

$$\sum_{i=1}^{3} R_i \mathcal{U}\sigma_i\mathcal{U}^\dagger = \sum_{i=1}^{3} R_i \phi(\mathcal{U})^k{}_i \sigma_k. \tag{2.93}$$

The mapping $\mathcal{U} \mapsto \phi(\mathcal{U})$ is obviously a surjective homomorphism $\phi\colon SU(2) \to SO(3)$. This can be seen by introducing the bilinear form $\mathrm{Tr}(\hat{H}(\mathbf{R}_1)\hat{H}(\mathbf{R}_2))$, and observing that $\mathrm{Tr}(\hat{H}(\mathbf{R}_1)\hat{H}(\mathbf{R}_2)) = \langle \mathbf{R}_1 | \mathbf{R}_2 \rangle$ holds, where $\langle .|. \rangle$ denotes the standard scalar product in euclidean $\mathbb{R}^3$. Combining the map ϕ with the canonical projection $\pi\colon SO(3) \to SO(3)/SO(2)$ onto the coset space gives

$$\mathbb{S}^3 \xrightarrow{\approx} SU(2) \xrightarrow{\phi} SO(3) \xrightarrow{\pi} SO(3)/SO(2) \xrightarrow{\approx} \mathbb{S}^2. \tag{2.94}$$

The geometrical construction and the Chern number $\mathcal{C} = 1$ suggest that projection $\tilde{\pi} := \pi \circ \phi\colon \mathbb{S}^3 \to \mathbb{S}^2$ is non–trivial and equivalent to a Hopf map. The diffeomorphisms are indicated by $\approx$ in the above diagram. This corresponds to a principal bundle $(\mathbb{S}^3, \pi, \mathbb{S}^2, U(1))$. The fibre $U(1)$ of the bundle is inherited from $SO(2)$ via isomorphism $U(1) \cong SO(2)$.

Proposition 25 *Let $X \subset \mathbb{R}^n$ be compact and convex and let $X^\circ \neq \emptyset$ be its (non–empty) interior. Then, there exists a homeomorphism $X \approx \mathbb{D}^n$.*

Based on this proposition we derive $\mathbb{D}^n \times \mathbb{D}^m \approx \mathbb{D}^{n+m}$ for arbitrary balls $\mathbb{D}^n$, $\mathbb{D}^m$. Applying this result to $\mathbb{D}^4$, we compute $\mathbb{D}^4 = \mathbb{D}^2 \times \mathbb{D}^2$ and

$$\mathbb{S}^3 = \partial\mathbb{D}^4 = (\partial\mathbb{D}^2 \times \mathbb{D}^2) \cup (\mathbb{D}^2 \times \partial\mathbb{D}^2) = \mathbb{S}^1 \times \mathbb{D}^2 \cup \mathbb{D}^2 \times \mathbb{S}^1, \tag{2.95}$$

which provides the topological information that $\mathbb{S}^3$ is the union of two solid tori $(\mathbb{D}^2 \times \mathbb{S}^1)$ intersecting each other along their common boundary – i.e. the two–dimensional torus $\mathbb{T}^2 = \mathbb{S}^1 \times \mathbb{S}^1$. As can be seen, we have derived this without referring to any particular parametrization of $\mathbb{S}^3$. Due to the fibre bundle structure we have another interesting feature - using $\mathbb{S}^1$–fibres we can cover and partition $\mathbb{S}^3$ by copies of non-intersecting circles

$$\mathbb{S}^3 = \bigcup_{p\in\mathbb{S}^2} \pi^{-1}(p) = \bigcup_{p} \mathbb{S}^1_p, \quad \pi\colon \mathbb{S}^3 \to \mathbb{S}^2. \tag{2.96}$$

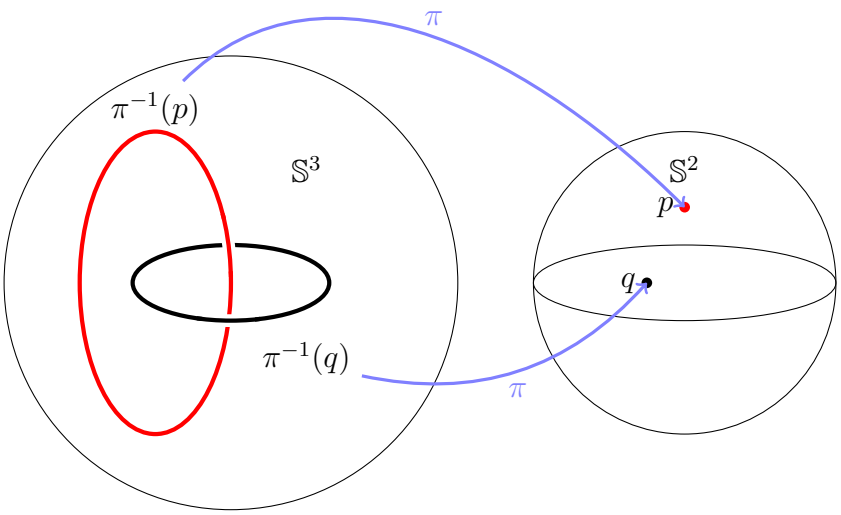

Figure 2.2: 'Visualization' of the Hopf map $\pi\colon \mathbb{S}^3 \to \mathbb{S}^2$. The linked red and black circles correspond to the fibres $\pi^{-1}(p)$ and $\pi^{-1}(q)$, respectively. They are mapped onto p and q in $\mathbb{S}^2$. Note that not all loops are linked in this non-trivial way.

To sum up, we have a obtained a Hopf fibration $(\mathbb{S}^3, \pi, \mathbb{S}^2, \mathbb{S}^1)$ exploiting the ground level configuration of the system (2.84). The non–trivial topology is confirmed by the Chern number $\mathcal{C} = 1$. It is remarkable to notice that a known

two–level quantum system admits a non–trivial fibre bundle structure of the Hopf type. These topologically intricate relations go beyond the level of computing eigenvalues and eigenstates of the system.

2.3.3 Constructions: Linking and Hopf invariant

The fibre bundle structure in the two–level system is related to a map $f: \mathbb{S}^3 \to \mathbb{S}^2$. We give a construction in terms of a rational function.

Example 26 *A Hopf map can be represented as a rational function in complex variables* (z_1, z_2)

$$\pi: \mathbb{S}^3 \to \mathbb{C}^*, \quad \pi(z_1, z_2) := \frac{z_1}{z_2}, \tag{2.97}$$

where $\mathbb{S}^3 = \{(z_1, z_2) \in \mathbb{C}^2 | |z_1|^2 + |z_2|^2 = 1\}$ *and we allow* z_2 *to be zero with the restriction made by the compactification process of the plane, i.e.* $\mathbb{C}^* := \mathbb{C} \cup \{\infty\} \cong \mathbb{S}^2$.

In other words, $\pi(z_1, z_2) := \frac{z_1}{z_2}$ provides a mapping from $\mathbb{S}^3$ to $\mathbb{C}^* = \mathbb{C} \cup \{\infty\}$ which is homeomorphic to $\mathbb{S}^2$, in symbols $\mathbb{C}^* \cong \mathbb{S}^2$. The mapping $\pi: \mathbb{S}^3 \to \mathbb{S}^2$ has precisely the features of a principal $U(1)$–bundle $(\mathbb{S}^3, \pi, \mathbb{S}^2, U(1))$, and it was first considered by H. Hopf [22] in pure topology.

Remarks on Linking

Equation (2.96) and Figure 2.2 suggest that one can define a linking number between two loops: Take $a, b \in \mathbb{S}^2$ $(a \neq b)$, then $\pi^{-1}(a)$ and $\pi^{-1}(b)$ describe two non–intersecting circles which may be linked in a particular way in the space $\mathbb{S}^3$ or, equivalently in $\mathbb{R}^3 \cup \{\infty\}$. The algebraic number of intersections of one circle with the surface bounded by the other circle may be regarded as a linking number $l(\pi^{-1}(a), \pi^{-1}(b))$. However, this number can be studied through a more general topological approach. There exist also topologically non–trivial solutions of the free Maxwell equations that resemble linking and knot structures [26, 44].

Hopf invariant

Let $f\colon \mathbb{S}^3 \to \mathbb{S}^2$ be a differentiable map. The construction is based on the homology–cohomology duality of compact manifolds. For that, let ω be a normalized volume form on $\mathbb{S}^2$, i.e. $\omega \in \Omega^2(\mathbb{S}^2)$ and

$$\int_{\mathbb{S}^2} \omega = 1. \tag{2.98}$$

The map f naturally induces homomorphisms of homology and cohomology groups, respectively

$$f_*\colon H_k(\mathbb{S}^3) \to H_k(\mathbb{S}^2), \tag{2.99}$$

$$f^*\colon H^k(\mathbb{S}^2) \to H^k(\mathbb{S}^3), \tag{2.100}$$

where f^* denotes the dual (adjoint) map to f_*. The pullback mapping $f^*\omega \in \Omega^2(\mathbb{S}^3)$ produces a closed two-form on the sphere $\mathbb{S}^3$, $f^*[\omega] \in H^2(\mathbb{S}^3)$. De Rham's theorem yields the isomorphism $H^2(\mathbb{S}^3) \cong H_2(\mathbb{S}^3) = 0$, which implies that any closed two-form on $\mathbb{S}^3$ must be exact. In particular,

$$f^*\omega = d\sigma_f \tag{2.101}$$

where σ_f is a one-form on $\mathbb{S}^3$ which can be calculated by solving the set of differential equations given by (2.101). Now, using the wedge product $\wedge$, we construct the 3-form

$$f^*\omega \wedge \sigma_f. \tag{2.102}$$

This form on $\mathbb{S}^3$ must be proportional to the volume form on the three–sphere.

Definition 27 *The Hopf invariant of a differentiable map $f\colon \mathbb{S}^3 \to \mathbb{S}^2$ is given by*

$$H(f) := \int_{\mathbb{S}^3} f^*\omega \wedge \sigma_f. \tag{2.103}$$

$H(f)$ is indeed an invariant since homotopic maps $f \sim g\colon \mathcal{M} \to \mathcal{N}$ of manifolds $\mathcal{M}, \mathcal{N}$ give rise to identical homomorphisms $f_* = g_*\colon H_k(\mathcal{M}) \to H_k(\mathcal{N})$ [38]. Thus $f^* = g^*\colon H^k(\mathcal{M}) \to H^k(\mathcal{N})$, from which we see that $H(f) = H(g)$ for $f \sim g$.

2.3.4 Qubit state geometry and Qubit maps

Until now, we have been dealing with the Hopf map of the two–level quantum system in a somewhat abstract sense. In fact, we have constructed the fibre bundle from the base space (bottom–up approach). A reverse approach can be given for the $\mathbb{S}^3$ Hopf fibration, if we make use of basic results from quantum optics and quantum information theory. This will shed light on the relevant physics part. We recall what a single qubit state is: The term qubit was first introduced in the remarkable work of B. Schumacher [50] stating its importance as a basic storage unit for quantum information and computation.

Definition 28 *(Single qubit state) Let $\mathfrak{H}_2$ be the Hilbert space of a two–level quantum system with a basis $\{|0\rangle, |1\rangle\}$. A (single) qubit state $|\Psi\rangle \in \mathfrak{H}_2$ is given by*

$$|\Psi\rangle = z_1 |0\rangle + z_2 |1\rangle, \quad z_1, z_2 \in \mathbb{C}, \quad |z_1|^2 + |z_2|^2 = 1. \tag{2.104}$$

We denote the set of all such qubit states by $\mathfrak{Q}(\mathfrak{H}_2)$.

$\mathfrak{Q}(\mathfrak{H}_2)$ inherits its topology from $\mathfrak{H}_2$. It is then straightforward to observe the one-to-one correspondence between a point $(z_1, z_2) \in \mathbb{S}^3$ and a qubit state $|\Psi\rangle$ as in (2.104). In fact, we have more, i.e. a diffeomorphism $\mathfrak{Q}(\mathfrak{H}_2) \approx \mathbb{S}^3$:

$$\mathfrak{Q}(\mathfrak{H}_2) \overset{\phi}{\longleftrightarrow} \mathbb{S}^3 \tag{2.105}$$

This *qubit geometry* allows for a *qubit (state) map*

$$\mathcal{Q}\colon \mathfrak{Q}(\mathfrak{H}_2) \to \mathcal{X}, \tag{2.106}$$

$$|\Psi\rangle \longrightarrow \hat{\rho}_\Psi = |\Psi\rangle \langle\Psi|, \tag{2.107}$$

which is a mapping onto the set $\mathcal{X}$ of pure state 2×2–density matrices.

Proposition 29 *The fibres of the map are $\mathcal{Q}^{-1}(|\Psi\rangle \langle\Psi|) = \{e^{i\alpha} |\Psi\rangle \,|\, \alpha \in \mathbb{R}\} \approx \mathbb{S}^1$.*

Thus, the fibre is simply the phase degree of freedom of a state. Since $|\Psi\rangle$ is non–vanishing, the mapping yields the desired Hopf map by observing that (2.107) is

$$\mathbb{S}^3 \approx \mathfrak{Q}(\mathfrak{H}_2) \longrightarrow \mathcal{X} \sim \mathbb{S}^2, \tag{2.108}$$

or, equivalently, in a rigorous description

$$\mathbb{S}^3 \xrightarrow{\phi} \mathfrak{Q}(\mathfrak{H}_2) \xrightarrow{\mathcal{Q}} \mathcal{X} \xrightarrow{r} \mathbb{S}^2, \tag{2.109}$$

where ϕ denotes a diffeomorphism, $\mathcal{Q}$ is the qubit map and r is a deformation retract onto the Bloch sphere $\mathbb{S}^2$. From the parametrization we represent the density matrix as

$$\hat{\rho}_\Psi = |z_1|^2 \, |0\rangle \langle 0| + z_1 z_2^* \, |0\rangle \langle 1| + z_1^* z_2 \, |1\rangle \langle 0| + |z_2|^2 \, |1\rangle \langle 1| = \sum_{i=1}^{3} R_i \hat{\sigma}_i + \frac{1}{2}\hat{\mathbb{1}}, \tag{2.110}$$

such that

$$R_1 = \Re(z_1 z_2^*), \tag{2.111}$$

$$R_2 = \Im(z_1 z_2^*), \tag{2.112}$$

$$R_3 = |z_1|^2 - \frac{1}{2}. \tag{2.113}$$

The equations (2.110)-(2.113) imply that the spectrum $\mathrm{Spec}(\hat{\rho}_\Psi)$ is equivalent to that of matrices in $\mathcal{X}_H$, defined in (2.91), up to some constant shift. Indeed, the composition $r \circ \mathcal{Q} \circ \phi$ yields the map $\pi \colon \mathbb{S}^3 \to \mathbb{S}^2$ of the $\mathbb{S}^3$–Hopf fibration, with the correct fibre $\mathbb{S}^1$, as indicated in proposition (29). An alternative method to reproduce the simple rational representation of the Hopf map is provided by using the density matrix $\hat{\rho}_\Psi$ and make a projection:

$$z_1 \, |0\rangle + z_2 \, |1\rangle = |\Psi\rangle \longrightarrow \frac{\langle 0| \, \hat{\rho}_\Psi \, |\Psi\rangle}{\langle 1| \, \hat{\rho}_\Psi \, |\Psi\rangle} = \frac{\langle 0|\Psi\rangle}{\langle 1|\Psi\rangle} = \frac{z_1}{z_2}. \tag{2.114}$$

Chapter 3

Polariton Graphs, Topological Insulators, Fibrations

3.1 Technical Achievements and Prerequisites

The hybrid light-matter structure of (exciton)–polaritons enables us to design and engineer synthetic Chern insulators. Two remarkable properties are: (1) The possibility of having a Zeeman splitting by the application of external magnetic fields [31], (2) a spin–orbit type of coupling (SOC) due to TE–TM (transverse electric, transverse magnetic) splitting [42, 48]. A quite recent design of a polaritonic honeycomb lattice, related to Haldane's model, has been achieved in the work of Klembt [31]. Such a realization of Chern numbers $\mathcal{C} = \pm 2$ has been predicted in the context of polaritonic topological insulators, utilizing graphene or honeycomb–like geometries [41]. By the bulk–boundary principle the non–trivial bulk topology corresponds to topologically protected edge states. A similar goal has been reached in the ultracold atom field: by loading atoms in an optical lattice of the honeycomb form, consisting of two triangular sub-lattices A/B with (nnn)-couplings, and then inducing laser-assisted (nn)–tunnelling between the sub-lattices A and B [29].

Note on Symmetry Classes

The three classes of time–reversal (TR), particle–hole (PH) and chiral/sublattice (SL) symmetry have been used to classify the coset spaces of single particle Hamiltonians [2] (table C.1). The topological structure of the coset space determines the existence of topological phases in a particular real dimension D via the homotopy group π_D. One can show by direct comparison of π_D of all coset spaces for $D = 2$ that symmetry class A Hamiltonians are of potential interest for engineering two–dimensional Chern insulators (characterized by a $\mathbb{Z}$–invariant). In these systems all three symmetries are absent. The existence of single positive flat bands with no negative counterparts in the band spectrum is a perfect indicator for PHS and SLS breaking. This follows directly from the discussion in appendix C. Although this is a strong condition, it is not the only possibility to determine absence of these symmetries within the band structure. The Kagome lattice with only nn–terms has such a flat band (see Figure 3.4 b) and thus, is a suitable candidate. It remains to break TRS in this specific lattice.

3.1.1 Derivation - The polaritonic lattice Hamiltonian

We arrange polariton microcavity pillars in a lattice configuration which allows for a hopping between nearest neighbour sites via junctions (for technical details see [31, 41]). The polaritons can have internal longitudinal (L) or transverse (T) polarization modes. Moreover, we may apply an external magnetic field $\mathcal{B}$ to the system. Hence, we conclude that the tight–binding polaritonic Hamiltonian is

$$\hat{H} = \sum_{i,p} U_p \hat{a}^\dagger_{p,i} \hat{a}_{p,i} + \sum_{\langle ij\rangle,p,p'} \langle p,i|\, \mathcal{J}\, |p',j\rangle\, \hat{a}^\dagger_{p,i} \hat{a}_{p',j} + h.c., \tag{3.1}$$

subscripts i, j run over lattice sites and $p \in \{L, T\}$ denotes the linear polarization mode of micro-cavity polaritons. The on–site potentials can be written as $U_p = \mathcal{B}\sigma\delta_{\sigma\sigma'}$, with $\sigma = \pm$ describing circular polarization. The longitudinal–transverse basis can be transformed into the circular basis via $\frac{1}{\sqrt{2}}(|L\rangle \pm i\,|T\rangle) = |\pm\rangle$, as inferred

from QED practice:

$$\hat{a}_{L,j} = \frac{1}{\sqrt{2}}(\hat{a}_{+,j} + \hat{a}_{-,j}) \tag{3.2}$$

$$\hat{a}_{T,j} = \frac{i}{\sqrt{2}}(\hat{a}_{+,j} - \hat{a}_{-,j}) \tag{3.3}$$

For (nn)–sites $\langle ij \rangle$ we find only diagonal terms in the $\{L, T\}$–basis, i.e. $\langle L, i| \mathcal{J} |L, j\rangle = -t - \delta t$ and $\langle T, i| \mathcal{J} |T, j\rangle = -t + \delta t$ ($t, \delta t > 0$). These results are strongly supported by a careful numerical analysis of the spinor component polariton wavefunction (methods [41]). The parameter δt is due to the presence of TE–TM splitting in a junction connecting two sites. From this observation and (3.2), (3.3), we only need the following expressions

$$\hat{a}^\dagger_{L,i}\hat{a}_{L,j} = \frac{1}{2}(\hat{a}^\dagger_{+,i}\hat{a}_{+,j} + \hat{a}^\dagger_{-,i}\hat{a}_{-,j} + \hat{a}^\dagger_{-,i}\hat{a}_{+,j} + \hat{a}^\dagger_{+,i}\hat{a}_{-,j}), \tag{3.4}$$

$$\hat{a}^\dagger_{T,i}\hat{a}_{T,j} = \frac{1}{2}(\hat{a}^\dagger_{+,i}\hat{a}_{+,j} + \hat{a}^\dagger_{-,i}\hat{a}_{-,j} - \hat{a}^\dagger_{-,i}\hat{a}_{+,j} - \hat{a}^\dagger_{+,i}\hat{a}_{-,j}). \tag{3.5}$$

Peierls–phase free Hamiltonian. We insert the above equations into Eq. (3.1)

$$\begin{aligned}\hat{H} &= \mathcal{B}\sum_{i,\sigma}\sigma\hat{a}^\dagger_{\sigma,i}\hat{a}_{\sigma,i} - t\sum_{\langle ij\rangle}(\hat{a}^\dagger_{L,i}\hat{a}_{L,j} + \hat{a}^\dagger_{T,i}\hat{a}_{T,j} + h.c.) - \delta t\sum_{\langle ij\rangle}(\hat{a}^\dagger_{L,i}\hat{a}_{L,j} - \hat{a}^\dagger_{T,i}\hat{a}_{T,j} + h.c.) \\ &= \mathcal{B}\sum_{i,\sigma}\sigma\hat{a}^\dagger_{\sigma,i}\hat{a}_{\sigma,i} - t\sum_{\langle ij\rangle,\sigma}(\hat{a}^\dagger_{\sigma,i}\hat{a}_{\sigma,j} + h.c.) - \delta t\sum_{\langle ij\rangle}(\hat{a}^\dagger_{+,i}\hat{a}_{-,j} + \hat{a}^\dagger_{-,i}\hat{a}_{+,j} + h.c.).\end{aligned} \tag{3.6}$$

The first part results from Zeeman–splitting, the second term comes from (nn)–hopping and the last sum consists of cross–polarized terms from TE-TM splitting.

Geometrical origin of Peierls type phases and full Hamiltonian. So far, we have neglected Peierls–type phases $\exp(i\theta_{ij})$. We now show that these type of phases exist in principle between cross–polarized polaritons of neighbouring sites.

Let $\hat{\mathcal{U}}(\theta) = \exp(-i\theta\hat{\sigma}_y)$ be the rotation operator acting on circular polarization states $|\sigma\rangle$, $\sigma = \pm$. Then,

$$\hat{\sigma}_y |\sigma\rangle = \sigma |\sigma\rangle , \tag{3.7}$$

$$\hat{\mathcal{U}}(\theta) |\sigma\rangle = e^{-i\theta\sigma} |\sigma\rangle . \tag{3.8}$$

Let $\theta_{ij} \equiv \theta$ be the angle specifying the direction of the vector which connects the sites i, j along the junction. Consider the adjoint operation of the operator $\hat{\mathcal{U}}$ on elements forming $\hat{H} \in End(\mathfrak{H})$, i.e. on the space $End(\mathfrak{H}) \cong \mathfrak{H} \otimes \mathfrak{H}^*$:

$$|\sigma, i\rangle \langle \sigma', j| \longrightarrow \hat{\mathcal{U}}(\theta) |\sigma, i\rangle \langle \sigma', j| \hat{\mathcal{U}}^\dagger(\theta) = e^{-i\theta\sigma} e^{i\theta\sigma'} |\sigma, i\rangle \langle \sigma', j| \tag{3.9}$$

$$= \begin{cases} |\sigma, i\rangle \langle \sigma, j| & \text{if } \sigma = \sigma', \\ e^{\pm 2i\theta} |\sigma, i\rangle \langle \sigma', j| & \text{if } \sigma \neq \sigma'. \end{cases} \tag{3.10}$$

We see that non–trivial phases arise between cross–polarized polaritons in a 2D lattice configuration, i.e. we have transformations

$$\hat{a}^\dagger_{\sigma,i} \hat{a}_{\sigma',j} \longrightarrow e^{-i\theta(\sigma-\sigma')} \hat{a}^\dagger_{\sigma,i} \hat{a}_{\sigma',j}. \tag{3.11}$$

To account for this, we derive for the *full Hamiltonian*

$$\hat{H} = \mathcal{B} \sum_{i,\sigma} \sigma \hat{a}^\dagger_{\sigma,i} \hat{a}_{\sigma,i} - t \sum_{\langle ij \rangle, \sigma} (\hat{a}^\dagger_{\sigma,i} \hat{a}_{\sigma,j} + h.c.) - \delta t \sum_{\langle ij \rangle} (e^{2i\theta_{ij}} \hat{a}^\dagger_{+,i} \hat{a}_{-,j} + e^{-2i\theta_{ij}} \hat{a}^\dagger_{-,i} \hat{a}_{+,j} + h.c.). \tag{3.12}$$

Within our scheme, non–trivial phases can only occur in at least dimension $D = 2$. In strictly one–dimensional systems the Hamiltonian will have the reduced form 3.6. In other words, the phases are determined by the geometry of the 2-dimensional polaritonic lattice. The analysis reveals a purely geometrical origin of the phases, with a distinct reason than in systems considered by Peierls in his seminal work [43]. Recent advances even suggest the realization of Peierls-type phases (substitutions) in one–dimensional lattices of ultracold neutral atoms [28].

3.2 Polaritonic Lattices and Topological Band Structures

Our next step consists of proposing lattice structures which are subject to Hamiltonian (3.12). The resulting excition–polariton insulators are examined by a thorough analysis of the bulk topology.

3.2.1 Square Lattice Crystal

$\mathbf{R}(m,n) = a(m\mathbf{e}_x + n\mathbf{e}_y)$, $m,n \in \mathbb{Z}$ describes the Bravais lattice vectors Figure 3.1, a is the characteristic lattice spacing. First, we perform a Fourier transformation

$$|\mathbf{k}\rangle = \frac{1}{\sqrt{N}} \sum_{(m,n)\in\mathbb{Z}^2} e^{i\mathbf{k}\cdot\mathbf{R}(m,n)} \,|(m,n)\rangle\,, \tag{3.13}$$

and matrix computation

$$\langle\mathbf{k}|\,\hat{a}^\dagger_{\sigma,i}\hat{a}_{\sigma',j}\,|\mathbf{k}\rangle = \langle\mathbf{k}|(m,n)\rangle\,\langle(m',n')|\mathbf{k}\rangle\,|\sigma\rangle\,\langle\sigma'| = \frac{1}{N}e^{-i\mathbf{k}\cdot\mathbf{R}(m-m',n-n')}\,|\sigma\rangle\,\langle\sigma'|\,. \tag{3.14}$$

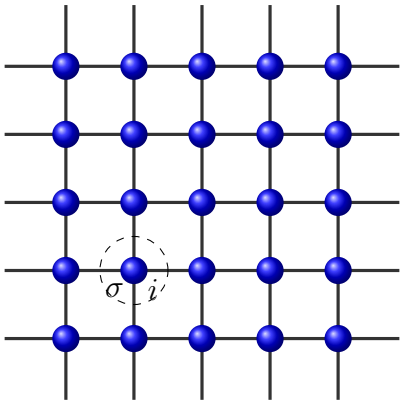

Figure 3.1: 2D polaritonic square lattice structure (connected microcavity pillars). $\sigma = \pm$ refers to the circular polarization of a polariton at site $i = (m,n)$ (unit cell).

In detail, the calculation yields with respect to joint pairs (m,n) and $(m',n') \in \{(m+1,n);(m,n+1)\}$

$$\mathcal{B}\sum_{i,\sigma}\sigma\hat{a}^\dagger_{\sigma,i}\hat{a}_{\sigma,i} \longrightarrow \mathcal{B}\sum_{i,\sigma}\sigma\frac{1}{N}\,|\sigma\rangle\,\langle\sigma| = \mathcal{B}\hat{\sigma}_z, \tag{3.15}$$

$$\begin{aligned} t\sum_{\langle ij\rangle,\sigma}(\hat{a}^\dagger_{\sigma,i}\hat{a}_{\sigma,j} + h.c.) \longrightarrow & t\frac{1}{N}\sum_i (e^{iak_x} + e^{-iak_x} + e^{iak_y} + e^{-iak_y}) \otimes \hat{\mathbb{1}}_2 \\ & = 2t(\cos(ak_x) + \cos(ak_y)) \otimes \hat{\mathbb{1}}_2 \end{aligned} \tag{3.16}$$

$$\begin{aligned}
&\delta t \sum_{\langle ij \rangle} (e^{i2\theta_{ij}} \hat{a}^\dagger_{+,i} \hat{a}_{-,j} + e^{-i2\theta_{ij}} \hat{a}^\dagger_{-,i} \hat{a}_{+,j} + h.c.) \\
&\qquad \longrightarrow \delta t \frac{1}{N} \sum_i \sum_{m \in \{x,y\}} \left(e^{iak_m} e^{i2\theta_m} |+\rangle \langle -| + e^{iak_m} e^{-i2\theta_m} |-\rangle \langle +| + h.c. \right) \\
&\qquad = 2\delta t \begin{pmatrix} 0 & \cos(ak_x) e^{i2\theta_x} + \cos(ak_y) e^{i2\theta_y} \\ \cos(ak_x) e^{-i2\theta_x} + \cos(ak_y) e^{-i2\theta_y} & 0 \end{pmatrix}
\end{aligned} \tag{3.17}$$

We have used $\sum_i = N$ for the summation over the unit cells. Thus, with $\theta_x = 0$ and $\theta_y = \frac{\pi}{2}$:

$$\begin{aligned}
\hat{H}(\mathbf{k}) =& \mathcal{B}\hat{\sigma}_z - 2t(\cos(ak_x) + \cos(ak_y))\hat{\mathbb{1}}_2 \\
&- 2\delta t \begin{pmatrix} 0 & \cos(ak_x) - \cos(ak_y) \\ \cos(ak_x) - \cos(ak_y) & 0 \end{pmatrix}
\end{aligned} \tag{3.18}$$

The Chern number of the lowest band can be calculated by

$$\mathcal{C} = \frac{1}{4\pi} \int_{\mathbb{T}^2} n(\mathbf{k}) \cdot (\partial_{k_x} n(\mathbf{k}) \times \partial_{k_y} n(\mathbf{k})) d^2k. \tag{3.19}$$

Since $n(\mathbf{k}) = (n_x(\mathbf{k}), 0, n_z(\mathbf{k}))$, we obtain the trivial result $\mathcal{C} = 0$. This is discussed in the next section from a slightly different point of view.

Homological - Cohomological View

We consider the effect on the first Chern number $\mathcal{C}$ by a map $h\colon \mathbb{T}^2 \to \mathbb{S}^2$. First note that we can write

$$\mathcal{C} = \frac{1}{2\pi} \int_{\mathbb{S}^2} \mathcal{F} = \frac{1}{2\pi} \left([\mathcal{F}], [\mathbb{S}^2] \right), \tag{3.20}$$

where $(,)$ describes the pairing between cohomology–homology classes. The induced dual homomorphisms on the level of homology and cohomology are (again)

$$h_*\colon H_k(\mathbb{T}^2; \mathbb{R}) \to H_k(\mathbb{S}^2; \mathbb{R}) \tag{3.21}$$

$$h^*\colon H^k(\mathbb{S}^2; \mathbb{R}) \to H^k(\mathbb{T}^2; \mathbb{R}) \tag{3.22}$$

For $k = 2$ we know that $H_2(\mathbb{S}^2;\mathbb{Z}) = H_2(\mathbb{T}^2;\mathbb{Z}) = \mathbb{Z}$, so $h_*|_{\mathbb{Z}} \colon \mathbb{Z} \to \mathbb{Z}$. The generators of the homology groups are given by the classes $[\mathbb{T}^2]$, $[\mathbb{S}^2]$ of the corresponding two–cycles (surfaces). Therefore,

$$h_*([\mathbb{T}^2]) = q \cdot [\mathbb{S}^2], \quad q \in \mathbb{Z}. \tag{3.23}$$

The integer q is called *degree* of the map h, $q = \deg h$. It is a homotopy invariant since homotopic maps between topological spaces induce identical homomorphisms between the homology groups. Multiplying the degree with the original Chern number yields

$$q \cdot \mathcal{C} = \frac{1}{2\pi}\left([\mathcal{F}], h_*[\mathbb{T}^2]\right) = \frac{1}{2\pi}\left(h^*[\mathcal{F}], [\mathbb{T}^2]\right) = \frac{1}{2\pi}\int_{\mathbb{T}^2} h^*\mathcal{F}. \tag{3.24}$$

The new Chern number obtained over the Brillouin zone is now $q \cdot \mathcal{C}$ (multiplied with the degree of h). Map h turns out to be topologically trivial for the polariton square lattice, i.e. $\deg h = 0$ and thus, the (lowest) band has zero Chern number.

3.2.2 Kagome Lattice – Fresh Perspectives of the bulk

The standard form of a Kagome lattice is given by (nn)–hopping processes and the unit cell consists of three sites or levels denoted by A, B, C (Figure 3.2). We conclude from the periodic arrangement of this unit cell forming the lattice that the Fourier transformed Hamiltonian describes 3 bands over $\mathcal{BZ}$. However, one can advance this idea since each site of a polaritonic lattice must have two polarization modes ($\sigma = \pm$) assigned to it. This would generally double the number of bands and we get a total number of 6 bands which makes the system relevant for topological material study, e.g. topological insulators.

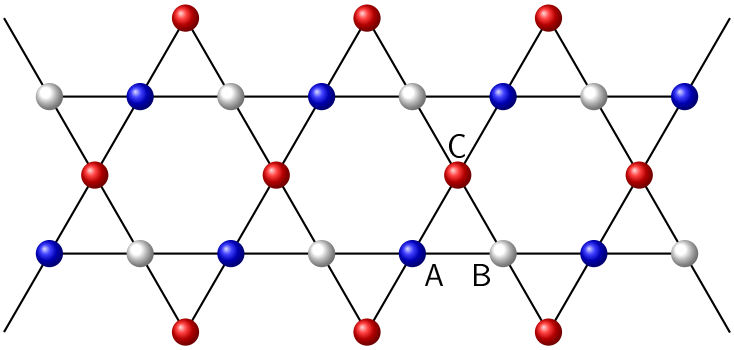

Figure 3.2: 2D polaritonic Kagome lattice structure (snapshot). Primitive unit cell vectors are $\mathbf{d}_1 = a(1,0)$ (A-B), $\mathbf{d}_2 = a(1/2, \sqrt{3}/2)$ (A-C). A unit cell is represented by the triangle $\triangle$ABC.

The translation vectors for shifting of unit cells are: $\mathbf{a}_i = 2\mathbf{d}_i$ (see fig. 3.2). Therefore, Kagome Bravais lattice unit cells are found at points $\mathbf{R}(m,n) = m\mathbf{a}_1 + n\mathbf{a}_2, m, n \in \mathbb{Z}$, with vectors $\mathbf{a}_1, \mathbf{a}_2$ being the generators of the lattice.

Polariton Kagome Hamiltonian and its Fourier transform

We now analyse and reduce the three terms of Eq. (3.12) with respect to the Kagome geometry. The Hamiltonian acts on the $6N$-dim. Hilbert space $\mathfrak{H}_N \otimes \mathfrak{H}_3 \otimes \mathfrak{H}_2$: The Zeeman–energy term is simply $\hat{H}_{\text{kagome, (Zeem.)}} = \hat{\mathbb{1}}_N \otimes \hat{\mathbb{1}}_3 \otimes \mathcal{B}\hat{\sigma}_z$. Hence, applying a magnetic field allows to break TRS.

Nomenclature	Meaning
(m,n)	unit cell in the Kagome lattice
$\sigma = \pm$	polarization mode
$\hat{A}/\hat{A}^\dagger, \hat{B}/\hat{B}^\dagger, \hat{C}/\hat{C}^\dagger$	annihilation/creation operators for the levels in a unit cell

Table 3.1: Labels for operators in the Kagome lattice Hamiltonian.

nn–sum $\hat{H}_{\text{kagome},(nn)}$ of the Hamiltonian. The nn–hopping term of the Hamiltonian is ($\mathcal{B}=0$, $\delta t=0$)

$$\begin{aligned}
\hat{H}_{\text{kagome, (nn)}} &= \sum_{(m,n),\sigma} \hat{A}^{\dagger}_{\sigma,(m,n)}\hat{B}_{\sigma,(m,n)} + \hat{A}^{\dagger}_{\sigma,(m,n)}\hat{C}_{\sigma,(m,n)} + h.c. \\
&+ \sum_{(m,n),\sigma} \hat{B}^{\dagger}_{\sigma,(m,n)}\hat{C}_{\sigma,(m,n)} + \hat{B}^{\dagger}_{\sigma,(m,n)}\hat{A}_{\sigma,(m+1,n)} + h.c. \\
&+ \sum_{(m,n),\sigma} \hat{C}^{\dagger}_{\sigma,(m,n)}\hat{B}_{\sigma,(m-1,n+1)} + \hat{C}^{\dagger}_{\sigma,(m,n)}\hat{A}_{\sigma,(m,n+1)} + h.c. \\
&= \mathbb{1}_N \otimes \begin{pmatrix} 0 & 1 & 1 \\ 1 & 0 & 1 \\ 1 & 1 & 0 \end{pmatrix} \otimes \mathbb{1}_2 + \sum_{m,n} |m,n\rangle \langle m+1,n| \otimes |B\rangle \langle A| \otimes \mathbb{1}_2 + h.c. \\
&+ \sum_{m,n} |m,n\rangle \langle m-1,n+1| \otimes |C\rangle \langle B| \otimes \mathbb{1}_2 + h.c. \\
&+ \sum_{m,n} |m,n\rangle \langle m,n+1| \otimes |C\rangle \langle A| \otimes \mathbb{1}_2 + h.c.
\end{aligned} \tag{3.25}$$

The Fourier transformed Hamiltonian is obtained from $\hat{H}(\mathbf{k})_{\text{kagome, (nn)}} = \langle \mathbf{k}| \hat{H}_{\text{kagome, (nn)}} |\mathbf{k}\rangle$ by inserting (3.13), in this case using Kagome lattice vectors $\mathbf{R}(m,n)$.

$$\hat{H}(\mathbf{k})_{\text{kagome, (nn)}} = -t \begin{pmatrix} 0 & 1+e^{-i\mathbf{k}\cdot\mathbf{R}(1,0)} & 1+e^{-i\mathbf{k}\cdot\mathbf{R}(0,1)} \\ 1+e^{i\mathbf{k}\cdot\mathbf{R}(1,0)} & 0 & 1+e^{-i\mathbf{k}\cdot\mathbf{R}(-1,1)} \\ 1+e^{i\mathbf{k}\cdot\mathbf{R}(0,1)} & 1+e^{i\mathbf{k}\cdot\mathbf{R}(-1,1)} & 0 \end{pmatrix} \otimes \mathbb{1}_2 \tag{3.26}$$

Cross–polarized part $\hat{H}_{\text{kagome, (cp)}}$ of the Hamiltonian. We proceed with the cross–polarized terms on the Kagome lattice. For this purpose, we calculate e.g.

$$\begin{aligned}
&\sum_{m,n} \hat{A}^{\dagger}_{+,(m,n)}\hat{B}_{-,(m,n)}e^{i2\theta_{AB}} + \hat{A}^{\dagger}_{-,(m,n)}\hat{B}_{+,(m,n)}e^{-i2\theta_{AB}} + h.c. \\
&= \mathbb{1}_N \otimes |A\rangle \langle B| \otimes |+\rangle \langle -|\, e^{i2\theta_{AB}} + \mathbb{1}_N \otimes |A\rangle \langle B| \otimes |-\rangle \langle +|\, e^{-i2\theta_{AB}} + h.c. \\
&= \mathbb{1}_N \otimes (|A\rangle \langle B| + |B\rangle \langle A|) \otimes \underbrace{\begin{pmatrix} 0 & e^{i2\theta_{AB}} \\ e^{-i2\theta_{AB}} & 0 \end{pmatrix}}_{X_{AB}=X^{\dagger}_{AB}}
\end{aligned} \tag{3.27}$$

With respect to the pairs (A, C) and (B, C), the computation yields similar results. The sum of these terms is

$$\mathbb{1}_N \otimes \begin{pmatrix} 0_2 & X_{AB} & X_{AC} \\ X_{AB} & 0_2 & X_{BC} \\ X_{AC} & X_{BC} & 0_2 \end{pmatrix}. \tag{3.28}$$

We also need to evaluate the following sums

$$\sum_{m,n} |m,n\rangle \langle m+1,n| \otimes \left(|B\rangle \langle A| \otimes |+\rangle \langle -| \, e^{2i\theta_{AB}} + |B\rangle \langle A| \otimes |-\rangle \langle +| \, e^{-2i\theta_{AB}} \right) + h.c. \tag{3.29}$$

$$\sum_{m,n} |m,n\rangle \langle m-1,n+1| \otimes \left(|C\rangle \langle B| \otimes |+\rangle \langle -| \, e^{2i\theta_{BC}} + |C\rangle \langle B| \otimes |-\rangle \langle +| \, e^{-2i\theta_{BC}} \right) + h.c. \tag{3.30}$$

$$\sum_{m,n} |m,n\rangle \langle m,n+1| \otimes \left(|C\rangle \langle A| \otimes |+\rangle \langle -| \, e^{2i\theta_{AC}} + |C\rangle \langle A| \otimes |-\rangle \langle +| \, e^{-2i\theta_{BC}} \right) + h.c. \tag{3.31}$$

The above expressions are now evaluated by squeezing them between Bloch states $|\mathbf{k}\rangle$:

$$\left\{ |B\rangle \langle A| \, e^{i\mathbf{k}\cdot\mathbf{R}(1,0)} + e^{-i\mathbf{k}\cdot\mathbf{R}(1,0)} \, |A\rangle \langle B| \right\} \otimes X_{AB} \tag{3.32}$$

$$\left\{ |C\rangle \langle B| \, e^{i\mathbf{k}\cdot\mathbf{R}(-1,1)} + e^{-i\mathbf{k}\cdot\mathbf{R}(-1,1)} \, |B\rangle \langle C| \right\} \otimes X_{BC} \tag{3.33}$$

$$\left\{ |C\rangle \langle A| \, e^{i\mathbf{k}\cdot\mathbf{R}(0,1)} + e^{-i\mathbf{k}\cdot\mathbf{R}(0,1)} \, |A\rangle \langle C| \right\} \otimes X_{AC} \tag{3.34}$$

In total, performing the appropriate Fourier transformation on eq. (3.28), and adding the above cross–polarized terms yields a 6×6–matrix

$$\hat{H}(\mathbf{k})_{\text{kagome, (cp)}} = -\delta t \begin{pmatrix} 0_2 & (1 + e^{-i\mathbf{k}\cdot\mathbf{R}(1,0)})X_{AB} & (1 + e^{-i\mathbf{k}\cdot\mathbf{R}(0,1)})X_{AC} \\ (1 + e^{i\mathbf{k}\cdot\mathbf{R}(1,0)})X_{AB} & 0_2 & (1 + e^{-i\mathbf{k}\cdot\mathbf{R}(-1,1)})X_{BC} \\ (1 + e^{i\mathbf{k}\cdot\mathbf{R}(0,1)})X_{AC} & (1 + e^{i\mathbf{k}\cdot\mathbf{R}(-1,1)})X_{BC} & 0_2 \end{pmatrix} \tag{3.35}$$

Complete Bloch Hamiltonian. The Bloch Hamiltonian is the sum of the computed operators, $\hat{H}(\mathbf{k})_{\text{kagome,(Zeem.)}} + \hat{H}(\mathbf{k})_{\text{kagome, (nn)}} + \hat{H}(\mathbf{k})_{\text{kagome, (cp)}}$, i.e.

$$\hat{H}(\mathbf{k}) = \begin{pmatrix} \mathcal{B}\hat{\sigma}_z & \mathcal{M}_{AB}(\mathbf{k}) & \mathcal{M}_{AC}(\mathbf{k}) \\ \mathcal{M}^{\dagger}_{AB}(\mathbf{k}) & \mathcal{B}\hat{\sigma}_z & \mathcal{M}_{BC}(\mathbf{k}) \\ \mathcal{M}^{\dagger}_{AC}(\mathbf{k}) & \mathcal{M}^{\dagger}_{BC}(\mathbf{k}) & \mathcal{B}\hat{\sigma}_z \end{pmatrix}, \tag{3.36}$$

with 2×2–matrices defined by

$$\mathcal{M}_{\mathbf{d}}(\mathbf{k}) = -2e^{-i\mathbf{k}\cdot\mathbf{d}} \cos(\mathbf{k}\cdot\mathbf{d}) \begin{pmatrix} t & \delta t e^{2i\theta_{\mathbf{d}}} \\ \delta t e^{-2i\theta_{\mathbf{d}}} & t \end{pmatrix}. \tag{3.37}$$

Numerical Analysis

For the numerical computation of the energy bands resulting from the Bloch Hamiltonian (3.36), we set $a = 1$ for the lattice geometry. Furthermore, by scaling with respect to nearest-neighbour hopping amplitude $t = 1$ we numerically solve the eigenvalue problem $\hat{H}(\mathbf{k})\,|u_m(\mathbf{k})\rangle = E_m(\mathbf{k})\,|u_m(\mathbf{k})\rangle$. The band structure is computed for different values of the magnetic field $\mathcal{B}$ and TE-TM splitting parameter δt.

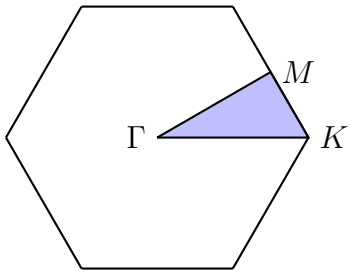

Figure 3.3: Schematic of the hexagonal $\mathcal{BZ}$ for the Kagome lattice. In accordance with the hexagonal shape, the computation of the energy bands can be performed along the closed path $\Gamma - K - M - \Gamma$ of high symmetry points.

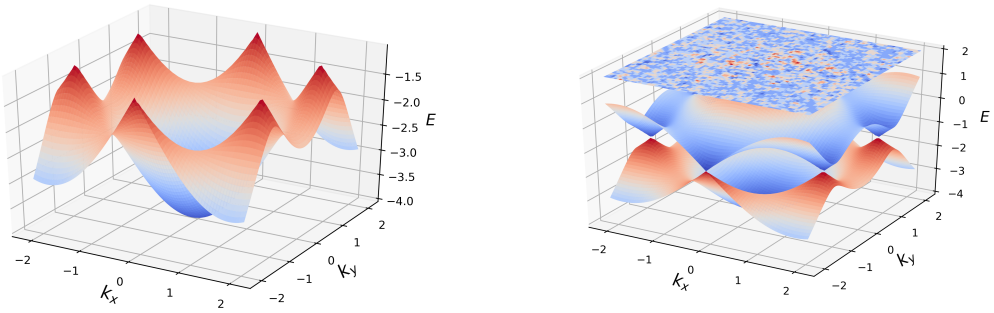

(a) Kagome ground state level for $\mathcal{B} = 0$, $\delta t = 0$. (b) Kagome band structure for $\mathcal{B} = 0$, $\delta t = 0$.

Figure 3.4: 3D representation of the polaritonic Kagome band structure. Figure a) shows the lowest band and the symmetric arrangement of cones (K) in hexagonal form. In b) we see all three bands - the two lowest bands touch at appropriate Dirac points, while the highest band is completely flat.

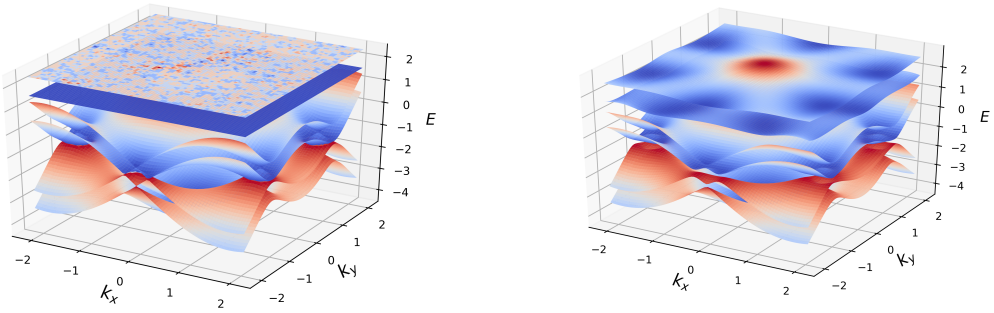

(a) Kagome band structure $\mathcal{B} = 0.4$, $\delta t = 0$. (b) Kagome band structure for $\mathcal{B} = 0.4$, $\delta t = 0.2$.

Figure 3.5: 3D representation of the polaritonic Kagome band structure by including non–zero values for the magnetic field and the TE-TM splitting parameter. All 6 bands are displayed.

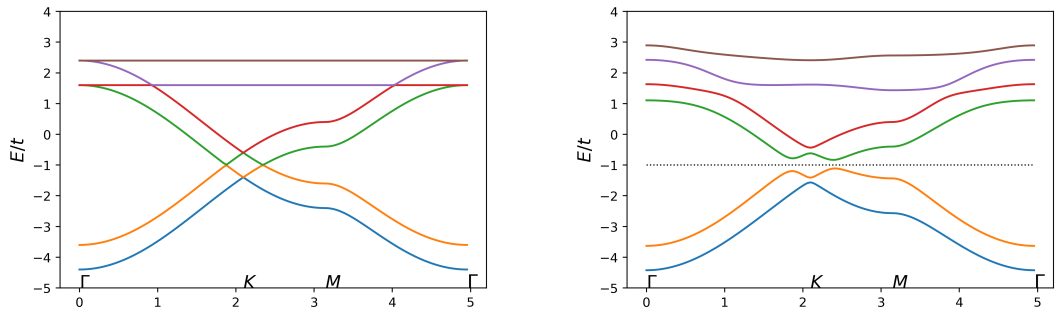

(a) Kagome lattice bands for $\mathcal{B} = 0.4$, $\delta t = 0$. (b) Kagome lattice bands for $\mathcal{B} = 0.4$, $\delta t = 0.2$

Figure 3.6: Gap opening mechanism in the polaritonic Kagome lattice by the interplay between the magnetic field $\mathcal{B}$ and the TE-TM splitting parameter δt. Crystallographic coordinates are used in $\mathcal{BZ}$ (Figure 3.3), marking the points Γ (centre of the hexagon), K (Dirac cone), M. Computation reveals a gap opening around $E_g = -1$ (see b), distinguishing between upper/lower bands.

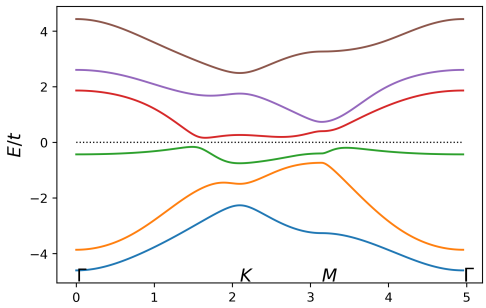

(a) Kagome lattice bands for $\mathcal{B} = 0.4$, $\delta t = 0.6$

Figure 3.7: Polaritonic Kagome lattice band structure for adjusting of the parameters to $\mathcal{B} = 0.4$, $\delta t = 0.6$. The diagram shows now a potential gap around $E_g = 0$.

Topological Polariton Insulator

The band structure of Figure 3.6 b) suggests that there are $U(1)$–bundles over $\mathcal{BZ}$ for all the bands, since no band touching points exist. The band gap allows to calculate the Chern numbers for the two lowest bands below $E_g = -1$

$$\mathcal{C} = \sum_{\{i:E_i<-1\}} \mathcal{C}^{(i)} = \frac{1}{2\pi} \sum_{\{i:E_i<-1\}} \int_{\mathcal{BZ}} \mathcal{F}^{(i)} = \frac{1}{2\pi} \sum_{\{i:E_i<-1\}} \int_{\mathbb{T}^2} \mathcal{F}^{(i)}(\mathbf{k}), \tag{3.38}$$

where $\mathcal{C}^{(i)}$ denotes the first Chern number of the i-th band, $\mathcal{BZ} = \mathbb{T}^2$. It is the non–zero sum of Chern numbers of the populated bands below the gap which supports the topological insulating phase of the exciton–polariton crystal.

PARAMETERS	BAND :	E_1	E_2	E_3	E_4	E_5	E_6
$\mathcal{B} = 0.4$, $\delta t = 0.2$	$\mathcal{C}^{(i)}$ num.:	$-1.0(0)$	$3.0(0)$	$-2.0(0)$	$-1.9(9)$	$2.9(9)$	$-0.9(9)$
$\mathcal{B} = 0.4$, $\delta t = 0.6$	$\mathcal{C}^{(i)}$ num.:	$-1.0(0)$	$3.0(0)$	$-2.0(0)$	$-2.0(0)$	$3.0(0)$	$-0.9(9)$
	$\mathcal{C}^{(i)}$ theor.:	-1	3	-2	-2	3	-1

Table 3.2: Numerically extracted Chern numbers $\mathcal{C}^{(i)}$ for all six bands, for the cases in Figure 3.6 b) and Figure 3.7. According to the algorithm, the computation has been performed using a discretization on a grid of 50×50 sites over the Brillouin zone $[0, \pi] \times [-\frac{\pi}{\sqrt{3}}, \frac{\pi}{\sqrt{3}}]$, where fluxes Ω_{nm} through each plaquette were obtained. The net flux gives the Chern number $\mathcal{C}^{(i)} = \frac{1}{2\pi} \sum_{n,m} \Omega^{(i)}_{nm}$ of the i-th band. The numerical errors are indicated within the brackets. Note that $\sum \mathcal{C}^{(i)} = 0$, which is expected since the Berry curvatures of all bands sum up to zero (see appendix B.3).

From table 3.2 and Figure 3.6 b) we see that for $\mathcal{B} = 0.4$, $\delta t = 0.2$

$$\mathcal{C} = \sum_{\{i:E_i<-1\}} \mathcal{C}^{(i)} = 2, \tag{3.39}$$

and this represents a $\mathcal{C} = 2$–Chern insulator. On the other hand, we get a trivial Chern insulator ($\mathcal{C} = \sum_{\{i:E_i<0\}} \mathcal{C}^{(i)} = 0$) for parameter values $\mathcal{B} = 0.4$ and $\delta t = 0.6$ (Figure 3.7).

Mapping Structure $\mathbf{k} \longrightarrow \hat{H}(\mathbf{k}) \longrightarrow \hat{\mathbb{P}}(\mathbf{k}) \sim \hat{\mathbb{O}}(\mathbf{k})$. Consider the band structures in Figure 3.6 b) and Figure 3.7, where we have different numbers of valence bands below the gap. With the help of the Altland–Zirnbauer symmetry classification C.1 we notice that $\hat{H}(\mathbf{k})$ must represent a point in a Grassmannian, since its symmetry class is A. A topological insulator is determined by its valence Bloch bundle, or in other words, by the valence bands below the energy gap. For that we need a projector $\hat{\mathbb{P}}(\mathbf{k}) = \sum_a |u_a(\mathbf{k})\rangle \langle u_a(\mathbf{k})|$ onto the subspace of eigenstates $|u_a(\mathbf{k})\rangle$ corresponding to the valence bands, or the equivalent spectral–flattened operator $\hat{\mathbb{O}}(\mathbf{k}) = \hat{\mathbb{1}} - 2\hat{\mathbb{P}}(\mathbf{k})$ (3.45). The figures of the numerical results imply the following scenarios[1]:

- $\delta t = 0.2$, $\mathcal{B} = 0.4$: $\hat{\mathbb{O}}(\mathbf{k}) \in \mathbb{G}_{2,6}(\mathbb{C})$ (16-dimensional Grassmannian).
- $\delta t = 0.6$, $\mathcal{B} = 0.4$: $\hat{\mathbb{O}}(\mathbf{k}) \in \mathbb{G}_{3,6}(\mathbb{C})$ (18-dimensional Grassmannian).

This means we have in fact a map

$$f_{\delta t,\mathcal{B}} \colon \mathbb{T}^2 \to \mathbb{G}_{m,6}(\mathbb{C}), \tag{3.40}$$

depending on the experimental parameters δt, $\mathcal{B}$, and m being the valence band number. Then, one may apply the results of Milnor, Stasheff [39], which suggest a construction method of cell decompositions for Grassmann manifolds. This gives us the right to construct a cellular map $g_{\delta t,\mathcal{B}}$ which is homotopic to $f_{\delta t,\mathcal{B}}$, as indicated in eq. (1.29), Chap. 1,

$$f_{\delta t,\mathcal{B}} \sim g_{\delta t,\mathcal{B}} \colon \mathbb{T}^2 \to X^2 \hookrightarrow \mathbb{G}_{m,6}(\mathbb{C}), \tag{3.41}$$

X^2 is the 2–skeleton of $\mathbb{G}_{m,6}$. This sets a restriction to the image of the torus $\mathbb{T}^2$: $g_{\delta t,\mathcal{B}}(\mathbb{T}^2) \subseteq X^2$. In addition, the existence of a potential monopole in a Grassmannian yields the following interpretation (see Figure 3.3): The two-dimensional Brillouin zone is mapped into the 2-skeleton of the Grassmann manifold, and possibly encloses the monopole in a non–trivial way. The observed non-zero Chern

[1] See next section for details of the complete derivation.

numbers $\mathcal{C}^{(i)}$ measure the net flux of the monopole field (expressed as Berry curvature $\mathcal{F}^{(i)}$ of a band), which then penetrates through the surface. This is expressed by the formula $\mathcal{C}^{(i)} = \frac{1}{2\pi}\int_{\mathbb{T}^2}\mathcal{F}^{(i)}(\mathbf{k})$.

Discussion. The gap opening mechanism has been verified for parameter values $\delta t = 0.2$, $B \in [0.3, 0.5]$ by a numerical simulation. There is also a gap for adjusting the magnetic field to $\mathcal{B} = 0.4$ and taking values $\delta t \in [0.2, 0.45]$ - also, we note that no band degeneracies occur for these values which clearly supports the construction of $U(1)$–bundles assigned to each band. From the numerical simulation we learn that the gap opening mechanism strongly depends on the interplay between the magnetic field and TE-TM splitting parameter. This parameter plays here an analogous role as the spin–orbit coupling (SOC) in electronic systems. Realistic parameter values (in units) are $\delta t = 50 - 200\mu eV$, $\mathcal{B} = 100 - 200\mu eV$ [41]. As a comparison, the gap size in polaritonic systems ($100 \sim 150\mu eV$) exceeds the spin-orbit gap in graphene [62] by a factor of at least 10^2. Driving the system into the $\mathcal{C} = 0$–phase requires larger values for δt - this is within reach as new results on cavity structures suggest [16]. Bulk–boundary correspondence predicts the existence of edge mode states at the interface of areas of differing Chern numbers. Propagation of these states is insensitive to perturbations and defects due to their topological origin. For the Kagome lattice, edge mode state analysis can be carried out by (non–resonant) excitation of polariton condensation into energy states in the band gap. The experimental realization should be analogous to Ref. [31], but the theoretical study of the mode dynamics will be done elsewhere.

3.2.3 General Methods for Topological Bands

We consider a Bloch Hamiltonian $\hat{H}(\mathbf{k})$ based on the assumption of translation invariance of the system in D dimensions and take $|u_a(\mathbf{k})\rangle$ as corresponding Bloch states. For the following discussion no further symmetry conditions are imposed.

$$\hat{H}(\mathbf{k})\,|u_a(\mathbf{k})\rangle = E_a(\mathbf{k})\,|u_a(\mathbf{k})\rangle\,, \quad \mathbf{k} \in \mathcal{BZ}, \tag{3.42}$$

where a refers to the band number, $a \in \{1, \ldots, n+m\}$. The ground state of a topological insulator is determined by the occupied bands below some gap.

Definition 30 *(Projection operator $\hat{\mathbb{P}}(\boldsymbol{k})$)*

$$\hat{\mathbb{P}}(\boldsymbol{k}) := \sum_{a=1}^{m} |u_a(\boldsymbol{k})\rangle \langle u_a(\boldsymbol{k})| , \tag{3.43}$$

m is the number of occupied (valence) bands.

One checks immediately the usual properties of a projector:

- $\hat{\mathbb{P}}^{\dagger}(\mathbf{k}) = \hat{\mathbb{P}}(\mathbf{k})$
- $\hat{\mathbb{P}}^{2}(\mathbf{k}) = \hat{\mathbb{P}}(\mathbf{k})$

Definition 31 *(Analytical index) The analytical index of the projector $\hat{\mathbb{P}}(\boldsymbol{k})$ is*

$$\mathrm{ind}(\hat{\mathbb{P}}) := \dim \ker(\hat{\mathbb{P}}) - \dim \ker(\hat{\mathbb{P}}^{\perp}), \tag{3.44}$$

where $\hat{\mathbb{P}}^{\perp}$ is the orthogonal complement to $\hat{\mathbb{P}}$, i.e. $\hat{\mathbb{P}}^{\perp} = \hat{\mathbb{1}} - \hat{\mathbb{P}}$.

The projector gives zero eigenvalues when being applied to unoccupied band states. These states are the zero modes of $\hat{\mathbb{P}}$ and span the kernel $\ker(\hat{\mathbb{P}})$. In the same way, occupied band states are the zero modes of $\hat{\mathbb{P}}^{\perp}$ and they span the kernel $\ker(\hat{\mathbb{P}}^{\perp})$. For convenience we can re-define the operator:

Definition 32 *(involution operator $\hat{\mathbb{O}}(\boldsymbol{k})$)*

$$\hat{\mathbb{O}}(\boldsymbol{k}) = \hat{\mathbb{1}} - 2\hat{\mathbb{P}}(\boldsymbol{k}). \tag{3.45}$$

This new operator can be regarded as a *spectral–flattened Hamiltonian*. $\hat{\mathbb{O}}(\mathbf{k})$ has the properties:

1. $\hat{\mathbb{O}}^{\dagger}(\mathbf{k}) = \hat{\mathbb{O}}(\mathbf{k})$ (hermitian)
2. $\hat{\mathbb{O}}(\mathbf{k})\hat{\mathbb{O}}^{\dagger}(\mathbf{k}) = \hat{\mathbb{O}}^{2}(\mathbf{k}) = \hat{\mathbb{1}}$ (unitary)
3. $\mathrm{Tr}\left(\hat{\mathbb{O}}(\mathbf{k})\right) = n - m$

Note that $\dim\ker(\hat{\mathbb{P}}(\mathbf{k})) = n$ and $\dim\ker(\hat{\mathbb{P}}^{\perp}(\mathbf{k})) = m$. Hence, the index can be written as

$$\mathrm{Tr}\left(\hat{\mathbb{O}}(\mathbf{k})\right) = n - m = \mathrm{ind}(\hat{\mathbb{P}}(\mathbf{k})). \tag{3.46}$$

The class of all involution operators with the three given properties shall be denoted as $IU_{n,m}$. The operator $\hat{\mathbb{O}}$ is a unitary $(n+m)$-matrix with m eigenvalues $\lambda = -1$ and n eigenvalues $\lambda = 1$, corresponding to filled and empty bands, respectively. Let $\hat{\mathbb{O}} \in IU_{n,m}$, $\mathcal{U} \in U(n+m)$ and regard the action

$$U(n+m) \times IU_{n,m} \to IU_{n,m}, \tag{3.47}$$

$$(\mathcal{U}, \hat{\mathbb{O}}) \mapsto \mathcal{U}\hat{\mathbb{O}}\mathcal{U}^{\dagger}. \tag{3.48}$$

One sees immediately that all 3 properties remain invariant under this transformation (conjugation operation). In particular, this is true for the analytical index ind (3.46) under the conjugation operation (3.48). From a geometrical point of view we have generated an *orbit* within $IU_{n,m}$. We show that this single orbit actually covers all $IU_{n,m}$.

Lemma 33 *$U(n+m)$ acts transitively on $IU_{n,m}$ by conjugation operation in equation (3.48). In other words $IU_{n,m}$ is a homogeneous $U(n+m)$-space.*

Proof. Let $\mathbb{V} \in IU_{n,m}$ be some involution operator. Then $\exists \mathcal{W} \in \mathbb{U}(n+m)$:

$$\mathcal{W}\mathbb{V}\mathcal{W}^{\dagger} = \mathrm{Diag}(\lambda_1, \ldots, \lambda_{n+m}), \quad \lambda_i = \pm 1.$$

Since $\mathrm{Tr}\,(\mathbb{V}) = n - m$ we can re-arrange the eigenvalues to get

$$\mathbb{D} := \mathrm{Diag}(\underbrace{+1 \ldots, +1}_{n}, \underbrace{-1, \ldots, -1}_{m})$$

This is achieved by using permutation matrices $\mathcal{P}_{\pi}$ ($\pi \in S_{n+m}$) which are orthogonal (hence unitary). Combining all that together, we have $\mathbb{V} = \mathcal{U}\mathbb{D}\mathcal{U}^{\dagger}$ with the unitary operator $\mathcal{U} := (\mathcal{P}_{\pi}\mathcal{W})^{\dagger}$. ∎

From a group theoretical perspective it follows that there exists a bijection

$$IU_{n,m} \leftrightarrow U(n+m)/I_{\mathbb{D}}, \tag{3.49}$$

where $I_{\mathbb{D}}$ is the isotropy group of $\mathbb{D}$ - this is defined by

$$I_{\mathbb{D}} = \{\mathcal{U} \in U(n+m) | \mathcal{U}\mathbb{D} = \mathbb{D}\mathcal{U}\}. \tag{3.50}$$

It is straightforward to calculate this isotropy group

$$I_{\mathbb{D}} = U(n) \times U(m) \tag{3.51}$$

$$IU_{n,m} \approx U(n+m)/\left(U(n) \times U(m)\right) \tag{3.52}$$

Result (3.52) is more than just a bijection. The space $IU_{n,m}$ can be assigned a subspace topology, in particular Hausdorff space topology. Moreover, the action of $U(n+m)$ on $IU_{n,m}$ is continuous - this is true for the induced map and for the inverse map since $U(n+m)$ is compact and $IU_{n,m}$ Hausdorff. For that reason (3.52) is a homeomorphism between topological spaces. This topological space is actually known as Grassmann manifold or *Grassmannian* $\mathbb{G}_{m,n+m}(\mathbb{C})$ [2]

Notation 34 $\mathbb{G}_{m,n+m}(\mathbb{C}) := U(n+m)/\left(U(n) \times U(m)\right)$

The dimension of the Grassmann manifold $\mathbb{G}_{m,n+m}(\mathbb{C})$ is

$$\dim[U(n+m)/(U(n) \times U(m))] = (n+m)^2 - (n^2+m^2) = 2nm. \tag{3.53}$$

The major statement we will show in subsequent sections is:

Claim 35 *The band numbers m (valence bands) and n (empty bands) determine the Bloch bundle structure of a Chern insulator in symmetry class A*[3].

For the rest of the discussion, we focus on symmetry class A Hamiltonians in real dimension D. The momentum space Hamiltonian has been transformed stepwise

$$\hat{H}(\mathbf{k}) \longrightarrow \hat{\mathbb{P}}(\mathbf{k}) \longrightarrow \hat{\mathbb{O}}(\mathbf{k}). \tag{3.54}$$

[2]Since it is compact it can be embedded into $\mathbb{R}^N$ for sufficiently large N due to Whitney's theorem. Grassmannians are fundamental objects in pure geometry, and they have recently started to appear in the context of topological phases in condensed matter [2, 30]. Remarkably, they also seem to play a central role for scattering amplitudes in particle physics.

[3]As deduced from the Altland–Zirnbauer table in Figure C.1.

Operator $\hat{\mathbb{O}}$ is an equivalent replacement of the original Hamiltonian up to homotopy. The outlined construction provides a map f

$$f\colon \mathbb{T}^D \to U(n+m)/\left(U(n)\times U(m)\right), \quad f\colon \mathbf{k}\mapsto \hat{\mathbb{O}}(\mathbf{k}), \tag{3.55}$$

where the Brillouin zone $\mathcal{BZ}$ has been identified with the D–dimensional torus $\mathbb{T}^D$. An *adiabatic deformation* of the Hamiltonian $\hat{H}(\mathbf{k})$ implies a continuous change of the parameters upon which the Hamiltonian depends, and we are naturally led to the homotopy class $[f]$ of (3.55) - i.e. $[f]\in\{\mathbb{T}^D,\mathbb{G}_{m,n+m}(\mathbb{C})\}$. However, it seems sufficient to understand homotopy classes $\{\mathbb{S}^D,\mathbb{G}_{m,n+m}(\mathbb{C})\}\cong\pi_D(\mathbb{G}_{m,n+m}(\mathbb{C}))$.

Corollary 36 *The gapped topological phases in dimension D are characterized by homotopy group $\pi_D(\mathbb{G}_{m,n+m}(\mathbb{C}))$.*

This corollary is an immediate consequence following from the classification of symmetry–protected gapped Hamiltonians by Altland and Zirnbauer. Topological phase transitions are associated with topology changes and can occur under certain parameter variations (see Chap. 4 sec. 1). It is important to understand how symmetry protection in terms of TRS, PHS and SLS alters the target space of the Hamiltonian. For that purpose, let us consider

Example 37 *(SLS protected Hamiltonian) Let $\hat{H}$ be only invariant under sublattice symmetry (SLS) $\hat{\mathcal{S}}$, $\hat{\mathcal{S}}\hat{H}\hat{\mathcal{S}}^\dagger=-\hat{H}$ (C.10). As in the case of the SSH model, we may perform an equivalence transformation on $\hat{H}$ which yields an off–diagonal block matrix form*

$$\hat{H}(\boldsymbol{k})\sim\begin{pmatrix} 0_n & \mathcal{M}(\boldsymbol{k})\\ \mathcal{M}^\dagger(\boldsymbol{k}) & 0_n\end{pmatrix},$$

$\mathcal{M}(\boldsymbol{k})\in U(n)$. Since $\pi_2(U(n))=0$, it is impossible to find topological insulators in dimension $D=2$ for such SLS protected Hamiltonians. However, in real dimension $D=3$ we may find $\mathbb{Z}$–valued topological phases due to $\pi_3(U(n))=\pi_3(SU(2))=\mathbb{Z}$, $n\geq 2$.

3.2.4 Exploiting Fibrations and Homotopy Sequences

Firstly, I demonstrate the existence of a synthetic monopole in the coset space of symmetry class A Hamiltonians by the application of exact sequences of homotopy groups for fibre bundles or Serre fibrations. This perspective allows to supplement our findings made in the numerical analysis of the Kagome lattice: The Berry curvature is generated by a monopole in the parameter space of the Hamiltonian. Secondly, I provide a characterization of the valence Bloch bundles associated with the Chern insulators on the Kagome lattice.

Definition 38 *(Stiefel manifold $\mathbb{V}_{k,n}(\mathbb{C})$) The Stiefel manifold is defined as the set of ordered orthonormal k-frames in $\mathbb{C}^n$:*

$$\mathbb{V}_{k,n}(\mathbb{C}) := \left\{(e_1,\ldots,e_k) \in \mathbb{C}^{n\times k} |\, \langle e_i|e_j\rangle = \delta_{ij}\right\} \tag{3.56}$$

First action on $\mathbb{V}_{k,n}$. The action on the Stiefel manifold is $U(n)\times\mathbb{V}_{k,n}(\mathbb{C})\to\mathbb{V}_{k,n}(\mathbb{C})$, $(\mathcal{U},(e_1,\ldots,e_k))\mapsto(\mathcal{U}e_1,\mathcal{U}e_2,\ldots,\mathcal{U}e_k)$, and it is transitive, which also applies to $SU(n)$. The isotropy group of the ordered tuple $(e_1,\ldots,e_k)$ is $U(n-k)$ (or $SU(n-k)$). Therefore, by the same token as given in the preceding paragraph, the manifold can be described as a homogeneous space

$$\mathbb{V}_{k,n}(\mathbb{C}) \cong U(n)/U(n-k) \cong SU(n)/SU(n-k). \tag{3.57}$$

Remark 39 *Let G be a Lie group and $H < G$ a closed subgroup, then G/H will be the base manifold of a fibre bundle $(G,\pi,G/H,H)$ with the canonical projection $\pi\colon G\to G/H$ and fibre H. So, $H\xrightarrow{i}G\xrightarrow{\pi}G/H$. This well known fact can be exploited for the computation of exact homotopy sequences.*

The corresponding long exact homotopy sequence for $\mathbb{V}_{k,n}$ is

$$\cdots\xrightarrow{\partial_*}\pi_m(SU(n-k))\xrightarrow{i_*}\pi_m(SU(n))\xrightarrow{\pi_*}\pi_m(\mathbb{V}_{k,n}(\mathbb{C}))\xrightarrow{\partial_*}\pi_{m-1}(SU(n-k))\xrightarrow{i_*}\cdots \tag{3.58}$$

We also need to compute some groups $\pi_m(U(n))$. First, it is known that spheres $\mathbb{S}^{2n-1}$ can be written as $\mathbb{S}^{2n-1} = U(n)/U(n-1) = SU(n)/SU(n-1)$ which constitutes a principal fibration with the exact sequences:

$$\cdots \xrightarrow{\partial_*} \pi_m(U(n-1)) \xrightarrow{i_*} \pi_m(U(n)) \xrightarrow{\pi_*} \pi_m(\mathbb{S}^{2n-1}) \xrightarrow{\partial_*} \pi_{m-1}(U(n-1)) \xrightarrow{i_*} \cdots \tag{3.59}$$

$$\cdots \xrightarrow{\partial_*} \pi_m(SU(n-1)) \xrightarrow{i_*} \pi_m(SU(n)) \xrightarrow{\pi_*} \pi_m(\mathbb{S}^{2n-1}) \xrightarrow{\partial_*} \pi_{m-1}(SU(n-1)) \xrightarrow{i_*} \cdots \tag{3.60}$$

From the last two sequences we derive: $\pi_m(U(n)) = \pi_m(U(n-1))$ and $\pi_m(SU(n)) = \pi_m(SU(n-1))$ for $m < 2n-2$, since in this case $\pi_{m+1}(\mathbb{S}^{2n-1}) = \pi_m(\mathbb{S}^{2n-1}) = 0$. By induction we obtain some useful results: $\pi_0(U(n)) = \pi_0(U(1)) = 0$ (connected Lie groups). $\pi_1(U(n)) = \pi_1(U(2)) = \pi_1(SU(2) \times U(1)) = \pi_1(\mathbb{S}^3 \times \mathbb{S}^1) = \pi_1(\mathbb{S}^1) = \mathbb{Z} \quad (n \geq 2)$. Also, $\pi_1(SU(n)) = \pi_1(SU(2)) = 0$ and $\pi_2(SU(n)) = \pi_2(SU(2)) = \pi_2(\mathbb{S}^3) = 0$. As a consequence from this and (3.58), we obtain for the lowest dimensional homotopy groups of the Stiefel manifold $\pi_0(\mathbb{V}_{k,n}) = \pi_1(\mathbb{V}_{k,n}) = \pi_2(\mathbb{V}_{k,n}) = 0, (n-k \geq 2)$.

Second action on $\mathbb{V}_{k,n}$. We also have an action $U(k) \times \mathbb{V}_{k,n}(\mathbb{C}) \to \mathbb{V}_{k,n}(\mathbb{C})$, $(\mathcal{U}, (e_1, \ldots, e_k)) \mapsto (\mathcal{U}e_1, \mathcal{U}e_2, \ldots, \mathcal{U}e_k)$ where $\mathcal{U}$ is now a unitary $k \times k$–matrix. As before, the action is transitive, but the stabilizer is trivial, i.e. $\mathbb{1}_k$. Employing (3.57) the resulting space is

$$\mathbb{V}_{k,n}/U(k) \cong U(n)/(U(n-k) \times U(k)) = \mathbb{G}_{k,n}(\mathbb{C}), \tag{3.61}$$

which is a Grassmannian. We obtain the principal fibration $(\mathbb{V}_{k,n}(\mathbb{C}), \mathbb{G}_{k,n}(\mathbb{C}), U(k))$ for the Grassmann manifold with the projection $\pi\colon \mathbb{V}_{k,n}(\mathbb{C}) \to \mathbb{G}_{k,n}(\mathbb{C})$. Correspondingly, the exact homotopy sequence is

$$\cdots \xrightarrow{\partial_*} \pi_m(U(k)) \xrightarrow{i_*} \pi_m(\mathbb{V}_{k,n}(\mathbb{C})) \xrightarrow{\pi_*} \pi_m(\mathbb{G}_{k,n}(\mathbb{C})) \xrightarrow{\partial_*} \pi_{m-1}(U(k)) \xrightarrow{i_*} \cdots \tag{3.62}$$

From all that we compute: $\pi_0(\mathbb{G}_{k,n}(\mathbb{C})) = \pi_1(\mathbb{G}_{k,n}(\mathbb{C})) = 0$. Moreover, because of the vanishing homotopy groups of $\mathbb{V}_{k,n}$ for $d = 1, 2$, sequence (3.62) yields the

$\pi_0(\mathbb{G}_{k,n}(\mathbb{C}))$	$\pi_1(\mathbb{G}_{k,n}(\mathbb{C}))$	$\pi_2(\mathbb{G}_{k,n}(\mathbb{C}))$
0	0	$\mathbb{Z}$

Table 3.3: Summary of low–dimensional homotopy groups for the Grassmann manifold $\mathbb{G}_{k,n}(\mathbb{C})$ (coset space of symmetry class A).

isomorphism $\pi_2(\mathbb{G}_{k,n}(\mathbb{C})) = \pi_1(U(k)) = \mathbb{Z}$. This proves the existence of monopoles in the coset space of symmetry class A Hamiltonians. At the same time, we obtain a characterization of gapped phases of topological insulators for dimension $D = 2$. In summary we have shown

Lemma 40 *$\mathbb{G}_{k,n}(\mathbb{C})$ contains a monopole, and it admits a principal bundle of the type $(\mathbb{V}_{k,n}(\mathbb{C}), \mathbb{G}_{k,n}(\mathbb{C}), U(k))$ with respect to the band structure, in which case k is the number of valence bands and n is the total band number.* □

Monopole, Hurewicz's relation and non–trivial Berry curvature. There exists a remarkable relation between the artificial monopole configuration in the coset space, the aspherical property of $\mathbb{G}_{k,n}(\mathbb{C})$ in dimensions $D < 2$, and the resulting non–trivial curvature $\mathcal{F}$ assigned to the bands over the Brillouin zone $\mathbb{T}^2$. The link for this line of thought is:

Remark 41 *(Hurewicz Theorem) A topological space X admits a homomorphism $\pi_k(X) \to H_k(X, \mathbb{Z})$. If the space X is aspherical for dimensions $i < k$, i.e. $\pi_i(X) = 0$, then $\pi_k(X) \xrightarrow{\sim} H_k(X, \mathbb{Z})$ is an isomorphism for $k \geq 2$.*

Putting together Hurewicz's theorem with the results of table 3.3 we conclude that $H_2(\mathbb{G}_{k,n}(\mathbb{C})) = \mathbb{Z}$ holds. One also infers $H^2(\mathbb{G}_{k,n}(\mathbb{C}); \mathbb{R}) \cong \mathbb{R}$ on the cohomological level. Since this is a one–generator group, all closed 2-forms, e.g. abelian Berry curvatures over the manifold, are effectively constructed from the single generator, denoted by $[\mathcal{F}]$. The map $f_{\delta t, \mathcal{B}} \colon \mathbb{T}^2 \to \mathbb{G}_{m,m+n}(\mathbb{C})$ gives rise to Berry curvatures for the various Bloch bands by the pull-back operation

$$f^*_{\delta t, \mathcal{B}} \mathcal{F}^{(i)} = \frac{1}{2} \mathcal{F}^{(i)}_{\mu\nu} \frac{\partial y^\mu}{\partial k^\alpha} \frac{\partial y^\nu}{\partial k^\beta} dk^\alpha \wedge dk^\beta, \tag{3.63}$$

where a local parametrization $y = y(\mathbf{k})$ of $f_{\delta t,\mathcal{B}}$ has been chosen on the torus manifold . The abelian curvature components $\mathcal{F}^{(i)}_{\mu\nu}$ are given by $\mathcal{F}^{(i)}_{\mu\nu} = \partial_\mu \mathcal{A}^{(i)}_\nu - \partial_\nu \mathcal{A}^{(i)}_\mu$. Obstruction to choosing a global potential $\mathcal{A}$ for a band comes from the non-trivial cohomology group H^2 and Eq. (3.63). Numerical evidence of Chern numbers in table 3.2 supports this result. Hence, we observe topological robustness of the band structure in areas of the $(\delta t, \mathcal{B})$–space where the Hamiltonian is gapped. This has been even numerically validated for other parameter adjustments - however, with different Chern number distributions.

Applications to Polariton Kagome Lattice

Characterization of valence Bloch bundles. We combine our numerical results on the Kagome lattice with the statement in Figure 1.4 in order to describe the pullback bundles over the Brillouin zone $\mathbb{T}^2$.

$$\begin{array}{ccc} \mathbb{T}^2 \times U(3) \cong f^{\bullet}_{0.6,0.4}\mathbb{V}_{3,6}(\mathbb{C}) & \xrightarrow{pr_2} & \mathbb{V}_{3,6}(\mathbb{C}) \\ \downarrow{\scriptstyle pr_1} & & \downarrow{\scriptstyle \pi} \\ \mathbb{T}^2 & \xrightarrow[f_{0.6,0.4}]{} & \mathbb{G}_{3,6}(\mathbb{C}) \end{array}$$

(a) Trivial Bloch bundle for $\mathcal{C} = 0$.

$$\begin{array}{ccc} \mathbb{T}^2 \times U(2) \neq f^{\bullet}_{0.2,0.4}\mathbb{V}_{2,6}(\mathbb{C}) & \xrightarrow{pr_2} & \mathbb{V}_{2,6}(\mathbb{C}) \\ \downarrow{\scriptstyle pr_1} & & \downarrow{\scriptstyle \pi} \\ \mathbb{T}^2 & \xrightarrow[f_{0.2,0.4}]{} & \mathbb{G}_{2,6}(\mathbb{C}) \end{array}$$

(b) Non–trivial Bloch bundle for $\mathcal{C} = 2$.

Figure 3.8: Pullback bundle diagrams for polaritonic Kagome configurations. The map is $f_{\delta t,\mathcal{B}} \colon \mathbb{T}^2 \to \mathbb{G}_{m,6}(\mathbb{C}), \mathbf{k} \mapsto \hat{\mathbb{O}}(\mathbf{k})$, given in (3.40). $\pi \circ pr_2 = f_{\delta t,\mathcal{B}} \circ pr_1$. It is sufficient to describe $f_{\delta t,\mathcal{B}}$ up to homotopy, since homotopic maps yield equivalent pullback bundles.

	$\delta t = 0.2$, $\mathcal{B} = 0.4$	$\delta t = 0.6$, $\mathcal{B} = 0.4$
Grassmannian $\mathbb{G}_{m,n+m}(\mathbb{C})$	$\mathbb{G}_{2,6}(\mathbb{C})$	$\mathbb{G}_{3,6}(\mathbb{C})$
Fibre bundle (auxiliary)	$(\mathbb{V}_{2,6}(\mathbb{C}), \mathbb{G}_{2,6}(\mathbb{C}), U(2))$	$(\mathbb{V}_{3,6}(\mathbb{C}), \mathbb{G}_{3,6}(\mathbb{C}), U(3))$
Valence Bloch bundle	$(f^{\bullet}_{0.2,0.4}(\mathbb{V}_{2,6}(\mathbb{C})), \mathbb{T}^2, U(2))$	$(\mathbb{T}^2 \times U(3), \mathbb{T}^2, U(3))$
Valence bands below gap	2	3
Chern number $\mathcal{C}$	2	0
$N_L - N_R$	2	0
$\mathrm{ind}(\hat{\mathbb{P}}) = n - m$	2	0

Table 3.4: Summary: Polariton Insulators on the Kagome lattice. N_L/N_R denote the numbers of left/-right propagating edge mode states on the boundary. Relation $N_L - N_R = \mathcal{C}$ is known from the bulk-boundary correspondence. The principal bundles are written in standard notation as triplets.

We make some comments on the above table 3.4: We observe that the valence Bloch bundle $(f^{\bullet}_{0.2,0.4}(\mathbb{V}_{2,6}(\mathbb{C})), \mathbb{T}^2, U(2))$ cannot be trivial since $\mathcal{C} = 2$, i.e. $f^{\bullet}_{0.2,0.4}(\mathbb{V}_{2,6}(\mathbb{C})) \neq \mathbb{T}^2 \times U(2)$. For both cases, the well known bulk-boundary correspondence predicts $N_L - N_R = \mathcal{C}$. Note that $\mathrm{ind}(\hat{\mathbb{P}}) = n - m$ for $\mathbb{G}_{m,n+m}$ is a purely algebraic result we have presented before. The results indicate the remarkable relation $\mathrm{ind}(\hat{\mathbb{P}}) = \mathcal{C}$, which can be expressed as follows:

Conjecture 42 *(Index Formula) Let $\hat{H}$ be a symmetry class A gapped Hamiltonian on a polaritonic 2D lattice, and let E_g denote the energy surrounding the gap between valence and unoccupied bands. Then, equation $\frac{1}{2\pi}\sum_{\{i:E_i<E_g\}}\int \mathcal{F}^{(i)} = \mathrm{ind}(\hat{\mathbb{P}})$ is a version of an index theorem for the investigated class A Chern insulators.*

This statement is far from being obvious: Why do the Chern numbers of bands below the gap sum up to the analytical index of $\hat{\mathbb{P}}$ for the manifold? The mathematical structure of the conjecture is reminiscent of the *Atiyah-Singer index theorem*. Recall that $\mathrm{ind}(\hat{\mathbb{P}})$ is the difference between zero eigenmodes of $\hat{\mathbb{P}}$ and the zero modes of $\hat{\mathbb{P}}^{\perp}$. From this point of view, the bulk–boundary correspondence

must be interpreted as the manifestation of an index theorem. Attempts for a rigorous proof and development of the topic are deferred to future work. However, there exist already connections to K–theory and non–commutative geometry, and these had been worked out by Bellissard and co-workers [5] - with the purpose of understanding the quantum hall effect.

3.3 Challenges in Polariton Graphs

3.3.1 Discussion - Engineering Chern insulators

Polaritonic lattices offer ideal platforms for nano–fabrication of etched 2D materials with topological properties, such as Chern insulators on the Kagome or honeycomb lattice. The TE-TM and Zeeman splitting term allow for controllable simulation of potential landscapes with a gap opening mechanism. On the Kagome lattice we have demonstrated the existence of a trivial and non–trivial Chern insulator: This corresponds to a topological insulator with 3 bands and 2 bands below the gap, respectively. However, a delicate question is how to obtain Chern insulators as two–dimensional single sheets such that one can systematically manipulate the number m of valence bands, and n of unoccupied bands. This is equivalent to obtaining spectral–flattened Hamiltonians in $\mathbb{G}_{m,n+m}(\mathbb{C})$, with tunable numbers m, n. As an example, consider the projective space $\mathbb{C}P^n = \mathbb{G}_{1,n+1}(\mathbb{C})$ (3.64), which corresponds to a gapped system with one valence band and n empty bands. For the moment, it appears that we do not have a fully systematic approach and absolute control over engineering arbitrary topological insulators. A partial answer could be initiated by the conjectured index formula. Nevertheless, one can investigate various other models: For instance, for a polaritonic Ruby lattice one expects to find 6×2 spectral bands. The SOC analogue gap opening mechanism as well as related topological properties can be investigated by strategies outlined in this work. The implementation could be advanced further by considering different junctions (with two or more hopping amplitudes t_i and TE-TM splitting parame-

ters δt_i) inside the etched microcavity pillar configuration.

We have not touched upon the topic of aperiodic lattices, e.g. *quasicrystals* based on the Ammann-Beenker tiling [36]. From a computational point of view, the lack of translational invariance sets some numerical challenges to the analysis of the bulk spectrum and the definition of topological real–space invariants. In analogy to the concept of the Fredholm operator index, several authors have introduced and investigated a local and global index (Bott index) for this purpose [35, 55].

Supplemental Material

The projective space $\mathbb{C}P^n = \mathbb{G}_{1,n+1}(\mathbb{C})$ has cell decomposition

$$\mathbb{C}P^n = e^0 \cup e^2 \cup e^4 \cup \cdots \cup e^{2n}, \tag{3.64}$$

from which the homology group structure $H_{2k}(\mathbb{C}P^n;\mathbb{Z}) = \mathbb{Z}$ follows. On the cohomological part we obtain $H^{2k}(\mathbb{C}P^n;\mathbb{R}) = \mathbb{R}$. Thus, for a non–degenerate gapped $\mathbb{C}P^n$–space Hamiltonian one may find globally non–trivial abelian Berry curvatures $\mathcal{F}$ such that $[\mathcal{F}] \in H^2(\mathbb{C}P^n)$ with $[\mathcal{F}] \neq [0]$. The analytical index of the $\mathbb{C}P^n$–Hamiltonian is given by $\mathrm{ind}\,\hat{\mathbb{P}} = n-1$ and this would be equal to a $\mathcal{C} = (n-1)$–insulator provided there exists a corresponding gap. The design of this Chern insulator could be achieved by increasing the sites of the unit cell of the lattice - however, this is only feasible to some extent. The crucial problem is to control and manipulate the location of the gap between occupied/unoccupied bands in the spectrum. For that purpose, further mechanisms need to be investigated.

Remark 43 *(Attaching spaces by maps) Let $X_0 \subset X$ and $f\colon X_0 \to Y$ be a map between topological spaces. Then we can create a new topological space $Y \bigcup_f X$ by the attaching map. The space Y is naturally embedded into $Y \bigcup_f X$ through injection, i.e. $Y \hookrightarrow Y \bigcup_f X$. $Y \bigcup_f X := X + Y/\sim$, $x_0 \sim f(x_0)$ by identification.*

Attaching an n–cell e^n to a (path–connected) space Y to get $Y \cup e^n$ is given by $f\colon S^{n-1} \to Y$, where $S^{n-1} \approx \partial e^n$ (boundary of n-cell is $(n-1)$–dimensional sphere which is glued to space Y via the mapping).

The momentum space perspective yields a map $\mathbb{T}^2 \to \mathbb{C}P^n$, $\mathbf{k} \mapsto \hat{H}(\mathbf{k})$. It can be transformed into a homotopic (cellular) map g such that $g(\mathbb{T}^2) \subseteq X^2$ holds, where X^2 is the two-skeleton of the projective space. X^2 is readily determined by (3.64): $X^2 = e^0 \cup e^2 = \mathbb{S}^2$.

Chapter 4

Novel Topological Design in Ultracold Atoms

In this chapter we analyse some ultra cold atom systems and we elaborate on recently done experimental work by enriching its theoretical interpretation. Along these lines, we compare the proposals with the numerically and analytically obtained results.

4.1 Abelian monopoles in spin–1 ultracold atoms

4.1.1 Experimental setup scheme

The method consists of coupling the 3 hyperfine states (spin 1) of ultracold Rubidium atoms ^{87}Rb by two independent rf fields (radio–frequency) [23]. Production of Bose-Einstein condensates (BECs) follows closely methods proposed in [4, 13] and the recent direct laser cooling technique [56]. The formed BEC of rubidium atoms is subject to a dipole trap. We use the fact that ^{87}Rb alkali atoms have a ground state with a hyperfine level splitting, i.e. $S = 1$ and $S = 2$. This is due to the fact that ^{87}Rb atoms have nuclear spin $I = 3/2$ and ground state with $J = 1/2$. Therefore, hyperfine levels are described via $\mathbf{3/2} \otimes \mathbf{1/2} = \mathbf{2} \oplus \mathbf{1}$. The splitting

of these levels corresponds to a frequency of 6.8 GHz.[1] Focusing on the $S = 1$ hyperfine level structure and applying a combination of rf fields, one can generate couplings between the states, as is depicted in the level diagram 4.1.

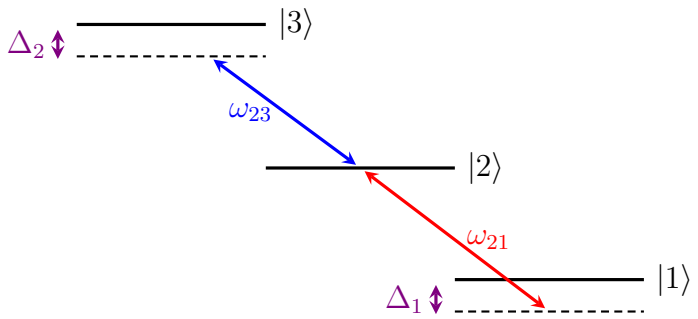

Figure 4.1: Rf–induced coupling of three $S = 1$ hyperfine states in ^{87}Rb (drawn in TikZ). The detunings Δ_1 and Δ_2 have been chosen according to $E_3 - E_2 = \hbar\omega_{23} + \Delta_2$ and $E_2 - E_1 = \hbar\omega_{21} - \Delta_1$, respectively. ω_{21} and ω_{23} are the corresponding frequencies of the coupled rf fields.

Effective Hamiltonian and properties

We write $|1,1\rangle = |1\rangle$, $|1,0\rangle = |2\rangle$, $|1,-1\rangle = |3\rangle$ in order to abbreviate notation for the coupled hyperfine states. Taking into account the detunings, coupling strengths (amplitudes) and relative phases, the effective hyperfine-coupling Hamiltonian can be constructed from Figure 4.1:

$$\hat{H} = \Delta_1 |1\rangle\langle 1| + \Delta_2 |3\rangle\langle 3| + \left(\Theta_{12} e^{i\varphi_{12}} |1\rangle\langle 2| + \Theta_{23} e^{i\varphi_{23}} |2\rangle\langle 3| + h.c.\right) \tag{4.1}$$

The matrix form version is given by

$$H_{eff} = \begin{pmatrix} \Delta_1 & \Theta_{12} e^{i\varphi_{12}} & 0 \\ \Theta_{12} e^{-i\varphi_{12}} & 0 & \Theta_{23} e^{i\varphi_{23}} \\ 0 & \Theta_{23} e^{-i\varphi_{23}} & \Delta_2 \end{pmatrix}, \tag{4.2}$$

[1] Precise measurements yield 6834.7 MHz.

and it consists of six parameters (forming a 6–dim. parameter space). The amplitudes Θ_{ij}, frequencies ω_{ij} and phases φ_{ij} of the driving fields can all be controlled to a sufficiently high degree.

Since we are dealing with a spin–1–representation, we can use a basis of hermitian spin–1 operators $\hat{\mathcal{S}} = (\hat{S}_x, \hat{S}_y, \hat{S}_z)$ (section D.1), $\mathbf{m} = (m_x, m_y, m_z)$ and rewrite the effective Hamiltonian

$$H_{eff} = \mathbf{m} \cdot \hat{\mathcal{S}} + \hat{\mathcal{O}}. \tag{4.3}$$

The rest of the basis, represented by operator $\hat{\mathcal{O}}$, can be constructed from the enveloping algebra by employing the following *ansatz*

$$\hat{\mathcal{O}} = \sum_{i,j} t_{ij} \hat{O}_{ij} = t_{zz}\hat{O}_{zz} + t_{yz}\hat{O}_{yz} + t_{xz}\hat{O}_{xz}, \tag{4.4}$$

$$\hat{O}_{ij} = \frac{1}{2}(\hat{S}_i\hat{S}_j + \hat{S}_j\hat{S}_i). \tag{4.5}$$

$$\hat{\mathcal{O}} = \begin{pmatrix} t_{zz} & \frac{1}{\sqrt{2}}(t_{xz} - it_{yz}) & 0 \\ \frac{1}{\sqrt{2}}(t_{xz} + it_{yz}) & 0 & \frac{1}{\sqrt{2}}(-t_{xz} + it_{yz}) \\ 0 & -\frac{1}{\sqrt{2}}(t_{xz} + it_{yz}) & t_{zz} \end{pmatrix} \tag{4.6}$$

From a physical point of view the rf couplings generate an effective magnetic field $\mathbf{m}$. The operators $\hat{\mathcal{O}}_{ij}$ are coupled to spin–tensors t_{ij}. Note that the couplings m_i and t_{ij} are functions of the tunable parameters φ_{kl}, Θ_{kl} and Δ_i. The transformations are

$$m_x = \frac{1}{\sqrt{2}}(\Theta_{12}\cos\varphi_{12} + \Theta_{23}\cos\varphi_{23}) = r\sin\vartheta\cos\phi \tag{4.7}$$

$$m_y = -\frac{1}{\sqrt{2}}(\Theta_{12}\sin\varphi_{12} + \Theta_{23}\sin\varphi_{23}) = r\sin\vartheta\sin\phi \tag{4.8}$$

$$m_z = \frac{1}{2}(\Delta_1 - \Delta_2) = r\cos\vartheta \tag{4.9}$$

$$t_{xz} = \sqrt{2}(\Theta_{12}\cos\varphi_{12} - \Theta_{23}\cos\varphi_{23}) \tag{4.10}$$

$$t_{yz} = \sqrt{2}(-\Theta_{12}\sin\varphi_{12} + \Theta_{23}\sin\varphi_{23}) \tag{4.11}$$

$$t_{zz} = \frac{1}{2}(\Delta_1 + \Delta_2) \tag{4.12}$$

This can be derived by comparing Equation (4.2) with (4.3).

Prerequisites for numerical computation

We perform an analysis of three different forms of the Hamiltonian structure, in accordance with the vector and tensor–like couplings.

1. $\hat{H} = \mathbf{m} \cdot \hat{\mathcal{S}}$ (only spin–vector coupling). This can be achieved by setting $\Delta_1 = -\Delta_2$, $\Theta_{12} = \Theta_{23}$ and $\varphi_{12} = \varphi_{23}$.

2. $\hat{H} = \mathbf{m} \cdot \hat{\mathcal{S}} + \alpha m_z \hat{S}_z^2$ (z spin–tensor coupling). Here, we set the amplitudes Θ_{12}, Θ_{23} and phases $\varphi_{12}, \varphi_{23}$ as in 1. The detunings are $\Delta_1 = r(\alpha + 1)\cos\vartheta$ and $\Delta_2 = r(\alpha - 1)\cos\vartheta$.

3. $\hat{H} = \mathbf{m} \cdot \hat{\mathcal{S}} + \beta m_x \hat{O}_{xz}$ (xz spin–tensor coupling; yz analogue). For this Hamiltonian, we set $\Delta_1 = -\Delta_2$, $t_{xz} = \beta m_x$.

In all three cases the base manifold is parametrized by $\mathbf{m} \neq 0$, which is equivalent to saying $\mathbb{R}^3 - \{0\} \simeq \mathbb{S}^2$. Therefore, it is assumed that we will be dealing with a fibre bundle structure over $\mathbb{S}^2$. The expected fibre can be determined by the characteristic polynomial (of the energy levels)

$$0 = \det(H_{eff} - E\hat{1}) = \begin{vmatrix} \Delta_1 - E & \Theta_{12}e^{i\varphi_{12}} & 0 \\ \Theta_{12}e^{-i\varphi_{12}} & -E & \Theta_{23}e^{i\varphi_{23}} \\ 0 & \Theta_{23}e^{-i\varphi_{23}} & \Delta_2 - E \end{vmatrix} \tag{4.13}$$

$$= -E(\Delta_1 - E)(\Delta_2 - E) - (\Delta_1 - E)\Theta_{23}^2 - \Theta_{12}^2(\Delta_2 - E), \tag{4.14}$$

which shows $E = E(\Delta_1, \Delta_2, \Theta_{12}, \Theta_{23})$ and independence of the phases φ_{ij}. One can show that the energy bands remain non–degenerate during possible (non–vanishing) parameter tunings. The non–degeneracy condition ensures that states are only allowed to acquire a phase change during an adiabatic evolution. And, this is crucial for having a $U(1)$–bundle, where gauge transformations are represented by $U(1)$–factors (Berry phase). In order to show this, we recall from [27]: The discriminant δ of a third degree polynomial $p(x) = x^3 + bx^2 + cx + d$ is given by $\delta = b^2c^2 - 4c^3 - 4b^3d + 18bcd - 27d^2$. For our system, the possibilities are reduced to

1. $\delta > 0$: 3 simple real roots.

2. $\delta = 0$: either 1 simple and 1 double real root, or a triple real root.

Consider tuning the system in such a way that $\Theta = \Theta_{12} = \Theta_{23}$ and $\Delta = \Delta_1 = -\Delta_2$. Then the distinct eigenvalues are $E_1 = 0$ and $E_{2/3} = \pm\sqrt{\Delta^2 + 2\Theta^2}$. The existing non–vanishing gaps between the levels indicate the non–degeneracy of the spectrum and we can therefore expect to find $U(1)$–bundles over the parameter space. This can be verified for all of the cases which we consider for our numerical analysis.

4.1.2 Chern numbers, phase transitions, spin textures

In this section we report on phase transitions of spin 1 monopoles with Chern numbers $\mathcal{C} = 1, 2, 0$. It is due to the highly tunable 6D parameter space that we can effectively reduce dimensions and change the manifold to our preference and allow it to host topologically different monopoles, i.e. carrying different topological charge inherited by the engineered bundle structure.

Numerical Results

Numerical implementation of the algorithm *CHN-AL*[2] for the computation of Chern numbers into a Python code reveals topological phase transitions of ground states. We study the phenomenon by covering the parameter space of $\mathbb{S}^2$ with a grid of 50×50 sites, hence, allowing for a good resolution and fast performance.

Case 1: transition $\mathcal{C} = 2 \to \mathcal{C} = 1$ for $\mathbb{S}^2$-submanifold. We use

$$\hat{H} = \mathbf{m} \cdot \hat{\mathcal{S}} + \alpha m_z \hat{S}_z^2. \tag{4.15}$$

For the numerical analysis, we vary the parameter α within the interval $[0, 10]$, and observe a topological phase transition at $\alpha = 1$. This is indicated by an abrupt change of $\mathcal{C}$ from 2 to 1 as the parameter value increases (Figure 4.2 a).

[2] See chapter 2 for the definition and details.

Case 2: transition $\mathcal{C} = 2 \to \mathcal{C} = 0$ for $\mathbb{S}^2$-submanifold. For this case, we make use of

$$\hat{H} = \mathbf{m} \cdot \hat{\mathcal{S}} + \beta m_x \hat{O}_{xz}, \tag{4.16}$$

and increase the β parameter within the interval $[0, 10]$. We observe a topological phase transition at $\beta = 2$, where the Chern number changes from 2 to 0 (Figure 4.2 b).

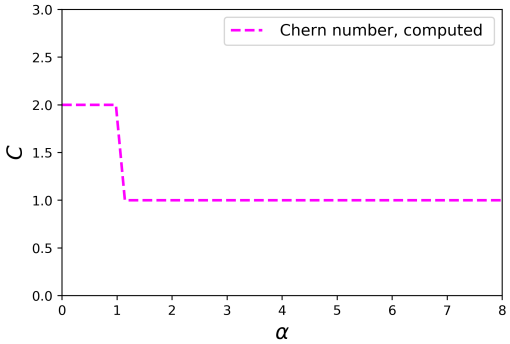

(a) Transition of the Chern number from 2 to 1; the parameter α is increased. $\mathcal{C} = 1$ is assumed to correspond to a Hopf bundle $(\mathbb{S}^3, \pi, \mathbb{S}^2, U(1))$.

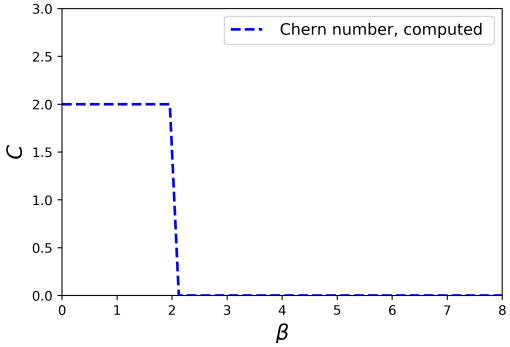

(b) Transition of the Chern number from 2 to 0 by increasing the parameter β. $\mathcal{C} = 0$ characterizes the trivial bundle $(\mathbb{S}^2 \times U(1), \pi, \mathbb{S}^2, U(1))$.

Figure 4.2: Results of the numerical simulation of the topological phase transition, indicated by the Chern number $\mathcal{C}$. We suggest that the phase transitions occur due to a topology change in the total space of the bundle.

Topological Analysis

We are now going to determine the fibre bundles associated with the ground state $|\psi_g\rangle$ of the effective Hamiltonian $\hat{H}$ in more detail.

Alternative mapping. The gauge connection (defined in Chap. 2) is given by $\mathcal{A} = i \langle\psi_g| \nabla_{\mathbf{m}} |\psi_g\rangle$, with the effective magnetic field $\mathbf{m}$ taking values in the synthetic space $\mathbb{R}^3 - \{0\}$. In the chosen spin-1 basis we can write $|\psi_g\rangle = \sum_i \alpha_i |i\rangle$, where the coefficients $\alpha_i = \alpha_i(\vartheta, \phi)$ are functions of coordinates (ϑ, ϕ) on the synthetic sphere $\mathbb{S}^2$. The spin-1 Hilbert space $\mathfrak{H}_\mathbf{1}$ can be obtained from a Clebsch–Gordan decomposition (CGD), $\mathfrak{H}_\mathbf{1/2} \otimes \mathfrak{H}_\mathbf{1/2} = \mathfrak{H}_\mathbf{1} \otimes \mathfrak{H}_\mathbf{0}$. For $|i\rangle \in \mathfrak{H}_\mathbf{1}$:

$$|1\rangle = |\uparrow\rangle \otimes |\uparrow\rangle\,, \quad |2\rangle = \frac{1}{\sqrt{2}}(|\uparrow\rangle \otimes |\downarrow\rangle + |\downarrow\rangle \otimes |\uparrow\rangle), \quad |3\rangle = |\downarrow\rangle \otimes |\downarrow\rangle \tag{4.17}$$

From the above representation we can recover the coefficient matrix $C = (c_{mn})$ for $|\psi_g\rangle \in \mathfrak{H}_\mathbf{1} = (\mathfrak{H}_\mathbf{1/2} \otimes \mathfrak{H}_\mathbf{1/2})_s$, after which a Singular Value decomposition (SVD) can be performed

$$C = \begin{pmatrix} \alpha_1 & \frac{1}{\sqrt{2}}\alpha_2 \\ \frac{1}{\sqrt{2}}\alpha_2 & \alpha_3 \end{pmatrix} \xrightarrow{SVD} VCW^\dagger = \begin{pmatrix} \tilde{c}_\uparrow & 0 \\ 0 & \tilde{c}_\downarrow \end{pmatrix}, \quad \tilde{c}_\uparrow, \tilde{c}_\downarrow \in \mathbb{R}^{\geq 0}. \tag{4.18}$$

Consequently, the ground state can be written as[3]

$$|\psi_g\rangle = \tilde{c}_\uparrow |\widetilde{1\uparrow}\rangle \otimes |\widetilde{2\uparrow}\rangle + \tilde{c}_\downarrow |\widetilde{1\downarrow}\rangle \otimes |\widetilde{2\downarrow}\rangle\,. \tag{4.19}$$

Equation (4.19) consists of the bi–orthogonal basis $\{|\widetilde{1\uparrow}\rangle \otimes |\widetilde{2\uparrow}\rangle\,, |\widetilde{1\downarrow}\rangle \otimes |\widetilde{2\downarrow}\rangle\}$ in $\mathfrak{H}_\mathbf{1/2} \otimes \mathfrak{H}_\mathbf{1/2}$. Thus, it is possible to obtain a two-mode representation for the spin 1 state. However, standard projectors $\hat{\Pi}_{\uparrow,\downarrow}$ map the ground state onto coordinates $(\tilde{c}_\uparrow, \tilde{c}_\downarrow)$ of a circle, since $\tilde{c}_\uparrow^2 + \tilde{c}_\downarrow^2 = 1$ holds. Such a decomposition may facilitate state tomography for visualizing the onset of a topological phase transition on $\mathbb{S}^2$ while driving parameters α, β related to Hamiltonians $\hat{H} = \mathbf{m} \cdot \hat{\mathcal{S}} + \alpha m_z \hat{S}_z^2$ and $\hat{H} = \mathbf{m} \cdot \hat{\mathcal{S}} + \beta m_x \hat{O}_{xz}$ respectively.

[3] In general, states of higher tensor product spaces $\mathfrak{H}_1 \otimes \mathfrak{H}_2 \otimes \cdots \otimes \mathfrak{H}_N$ do not admit simple decompositions with one-index summation for $N \geq 3$, unless specific symmetries exist. For general tensors of the type $c_{m_1 m_2 \ldots m_N}$ one has to deploy higher order forms of SVD (HOSVD), and these algorithms would still include multi-index summations.

Transition functions, Chern and winding numbers. We discuss now the role of transition functions related to gauge transformations. Due to the effective magnetic field $\mathbf{m} \in \mathbb{R}^3 - \{0\}$ and the homotopy equivalence $\mathbb{R}^3 - \{0\} \sim \mathbb{S}^2$, the gauge field $\mathcal{A}$ is completely determined on $\mathbb{S}^2$. We cover the sphere by two open sets (charts) U_1, U_2: $\mathbb{S}^2 = U_1 \cup U_2$; $U_1 = \mathbb{S}^2 - (\vartheta = \pi, 0)$ and $U_2 = \mathbb{S}^2 - (\vartheta = 0, 0)$. The intersection is homotopic to a circle, i.e. $U_1 \cap U_2 \sim \mathbb{S}^1$. We now specify two connection 1-forms $\mathcal{A}^{(1)}$ and $\mathcal{A}^{(2)}$ on each of the two charts. Along the circle $(\vartheta, \phi) \in \mathbb{S}^1$ (parametrized by ϕ) the fields must be related by a gauge transformation:

$$\mathcal{A}^{(2)}(\vartheta, \phi) = g_{12}(\phi)\mathcal{A}^{(1)}(\vartheta, \phi)g_{12}^{-1}(\phi) + ig_{12}(\phi)dg_{12}^{-1}(\phi). \tag{4.20}$$

A $U(1)$–bundle implies that $g_{12} \in U(1)$ and this defines a map $g_{12}\colon \mathbb{S}^1 \to \mathbb{S}^1$, where g_{12} is the so called *transition function*. This map is given by $g_{12}(\phi) = \exp(in\phi)$, with $n \in \pi_1(\mathbb{S}^1)$. Therefore, above equation is written as

$$\mathcal{A}^{(2)}(\vartheta, \phi) = \mathcal{A}^{(1)}(\vartheta, \phi) + nd\phi. \tag{4.21}$$

It follows that all $U(1)$–bundles over $\mathbb{S}^2$ can be classified by $\pi_1(\mathbb{S}^1) = \mathbb{Z}$.[4] We compute the Chern number $\mathcal{C}$ in the following way

$$\begin{aligned} 2\pi\mathcal{C} = \int_{\mathbb{S}^2} \mathcal{F} = \int_{U_1} d\mathcal{A}^{(1)} + \int_{U_2} d\mathcal{A}^{(2)} &= \int_{\partial U_1} \mathcal{A}^{(1)} + \int_{\partial U_2} \mathcal{A}^{(2)} \\ &= -\int_{\mathbb{S}^1} \mathcal{A}^{(1)} + \int_{\mathbb{S}^1} \mathcal{A}^{(2)} \\ &= \int_{\mathbb{S}^1} nd\phi = 2\pi n, \end{aligned} \tag{4.22}$$

where we used Stokes theorem and took into account that U_1, U_2 are both homeomorphic to an open disc with boundary $\mathbb{S}^1$. This proves unequivocally that the Chern number $\mathcal{C}$ is equal to the winding number n appearing in the transition function, i.e. $\mathcal{C} = n$ with $n \in \pi_1(\mathbb{S}^1)$.

Total space E models. We are now in the position to determine the total space E for each bundle $(E, \pi, \mathbb{S}^2, \mathbb{S}^1)$ associated with the observed values $\mathcal{C} = 0, 1, 2$.

[4] In fact, the generalization of this statement is that principal G–bundles over $\mathbb{S}^n$ are in one–to one correspondence with the group $\pi_{n-1}(G)$, i.e. $(E, \pi, \mathbb{S}^n, G) \rightleftharpoons \pi_{n-1}(G)$.

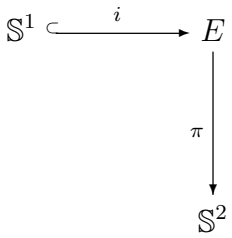

Figure 4.3: Diagram of the fibre bundle structure.

We see from the preceding discussion and the diagram that E is a 3-dimensional, $\mathbb{S}^1$–fibred space, which is locally homeomorphic to $\mathbb{S}^2 \times \mathbb{S}^1$. However, having three different Chern numbers we must obtain three globally distinct spaces E.

- $\mathcal{C} = n = 0$: The transition function is $g_{12}(\phi) \equiv 1$ and thus constant. This implies compatibility with a globally trivial bundle; $E \cong \mathbb{S}^2 \times \mathbb{S}^1$.

- $\mathcal{C} = n = 1$: $g_{12}(\phi) = \exp(i\phi)$. From this result we can define a natural action $U(1) \times \mathbb{S}^3 \to \mathbb{S}^3$ which partitions the 3-sphere into orbits of circles, such that the coset space is $\mathbb{S}^3/\mathbb{S}^1 \cong \mathbb{S}^2$. This implies $E \cong \mathbb{S}^3$ with a similar Hopf fibration as in Chap. 2, where the same Chern number was found.

- $\mathcal{C} = n = 2$: $g_{12}(\phi) = \exp(i2\phi)$. Going along one fibre, parametrized by ϕ in the space $\mathbb{S}^3$, we obtain the following picture: Doubling the winding number identifies antipodal points of the sphere $\mathbb{S}^3$. In other words, this gives rise to an action $\mathbb{Z}_2 \times \mathbb{S}^3 \to \mathbb{S}^3$. The total space E is derived as the coset $\mathbb{S}^3/\mathbb{Z}_2$, and it describes the set of $\mathbb{Z}_2$-orbits covering $\mathbb{S}^3$. Thus, E is the real 3D projective space, $E \cong \mathbb{S}^3/\mathbb{Z}_2 = \mathbb{R}P^3$.

Principal $U(1)$–bundles over $\mathbb{S}^2$ with higher Chern numbers may be constructed by an analogous procedure, e.g. by considering the action $\mathbb{Z}_n \times \mathbb{S}^3 \to \mathbb{S}^3$ and forming the quotient, which yields a lens space structure via transformation $(z_1, z_2) \to (e^{i2\pi p/n} z_1, e^{i2\pi p/n} z_2)$, $p = 0, \cdots, n-1$.

Spin textures. We claim that the above phase transitions are accompanied by significant spin texture changes, alongside expected Berry curvature manifestations. The spin operators are

$$\hat{S}_i = \sum_{\mathbf{k},\sigma;\mathbf{k}',\sigma'} \langle \mathbf{k},\sigma|\, \hat{S}_i\, |\mathbf{k}',\sigma'\rangle\, \hat{a}^\dagger_{\mathbf{k},\sigma}\hat{a}_{\mathbf{k}',\sigma'} = \sum_{\mathbf{k};\sigma,\sigma'} \langle \sigma|\, \hat{S}_i\, |\sigma'\rangle\, \hat{a}^\dagger_{\mathbf{k},\sigma}\hat{a}_{\mathbf{k},\sigma'}, \quad i = x,y,z, \tag{4.23}$$

where $\hat{a}_{\mathbf{k},\sigma}$ and $a^\dagger_{\mathbf{k},\sigma'}$ are the annihilation and creation operators of atoms with possible momentum $\mathbf{k}$ and hyperfine state $\sigma = 1,2,3$, as defined before. For demonstration purposes, consider $\hat{S}_z$ (D.16):

$$\hat{S}_z = \sum_{\mathbf{k};\sigma,\sigma'} \underbrace{\langle \sigma|\, \hat{S}_z\, |\sigma'\rangle}_{\pm\delta_{\sigma\sigma'}}\, \hat{a}^\dagger_{\mathbf{k},\sigma}\hat{a}_{\mathbf{k},\sigma'} = \sum_{\mathbf{k}}(\hat{a}^\dagger_{\mathbf{k},1}\hat{a}_{\mathbf{k},1} - \hat{a}^\dagger_{\mathbf{k},3}\hat{a}_{\mathbf{k},3}) = \sum_{\mathbf{k}}(\hat{n}_{\mathbf{k},1} - \hat{n}_{\mathbf{k},3}) \simeq \hat{n}_{0,1} - \hat{n}_{0,3}. \tag{4.24}$$

$\hat{n}_{\mathbf{k},i}$ denotes the corresponding atom number operator. The last step (approximation) in (4.24) can be confirmed with respect to a BEC. According to (4.23) and (D.16), we can represent the remaining spin operators as

$$\hat{S}_x = \frac{1}{\sqrt{2}} \sum_{\mathbf{k}} \hat{a}^\dagger_{\mathbf{k},1}\hat{a}_{\mathbf{k},2} + a^\dagger_{\mathbf{k},2}\hat{a}_{\mathbf{k},1} + a^\dagger_{\mathbf{k},2}\hat{a}_{\mathbf{k},3} + a^\dagger_{\mathbf{k},3}\hat{a}_{\mathbf{k},2} \tag{4.25}$$

$$\hat{S}_y = \frac{-i}{\sqrt{2}} \sum_{\mathbf{k}} \hat{a}^\dagger_{\mathbf{k},1}\hat{a}_{\mathbf{k},2} - a^\dagger_{\mathbf{k},2}\hat{a}_{\mathbf{k},1} + a^\dagger_{\mathbf{k},2}\hat{a}_{\mathbf{k},3} - a^\dagger_{\mathbf{k},3}\hat{a}_{\mathbf{k},2} \tag{4.26}$$

For states $|\psi\rangle$ of the system with Hamiltonian H_{eff}, we have

$$|\psi\rangle = \alpha_1 |1\rangle + \alpha_2 |2\rangle + \alpha_3 |3\rangle\,, \tag{4.27}$$

$$\hat{n}_{0,i}\, |\psi\rangle = \alpha_i\, |i\rangle\,, \tag{4.28}$$

$$\frac{N_i}{N_1+N_2+N_3} = \langle \hat{n}_{0,i}\rangle = \frac{\langle\psi|\, \hat{n}_{0,i}\, |\psi\rangle}{\langle\psi|\psi\rangle} = \frac{|\alpha_i|^2}{|\alpha_1|^2+|\alpha_2|^2+|\alpha_3|^2}. \tag{4.29}$$

Within the BEC cloud, the total number of atoms will split according to the fractions populating the hyperfine levels. N_i is the atomic population number for the hyperfine state i. In equation (4.29) we have calculated the relative atomic population number $N_i/(N_1+N_2+N_3)$. The spin expectation value along z is then given by

$$\langle \hat{S}_z\rangle = \frac{\langle\psi|\, \hat{S}_z\, |\psi\rangle}{\langle\psi|\psi\rangle} = \frac{|\alpha_1|^2 - |\alpha_3|^2}{|\alpha_1|^2+|\alpha_2|^2+|\alpha_3|^2} = \frac{N_1 - N_3}{N_1+N_2+N_3}. \tag{4.30}$$

This means that we can reconstruct the spin texture configuration over the whole manifold by measuring the population numbers N_1, N_2, N_3 or their associated fractions. The measurement can be done experimentally via a resolution mechanism after releasing the atoms from the trap.

In order to describe the detection of the aforementioned phase transitions, we numerically compute the resulting spin texture profiles $\langle \hat{S}_z \rangle (\phi, \vartheta)$ over the whole manifold. The corresponding spin textures are shown in Figure 4.4 and we emphasize some properties: The invariance $\langle \hat{S}_z \rangle (\phi, \vartheta) = \langle \hat{S}_z \rangle (\phi + \Delta\phi, \vartheta)$ is a consequence of the cylinder symmetry of $\hat{H}$. Increasing the parameter α reflects the non–uniform distribution of $\langle \hat{S}_z \rangle$ with respect to ϑ, which is caused by the inclusion of the spin–tensor, see Figure 4.4 b)-c). Moreover, the phase transition can be easily measured by the values of $\langle \hat{S}_z \rangle$ on the north and south pole, respectively. For $\alpha < 1$ ($\mathcal{C} = 2$ monopole), we compute $\langle \hat{S}_z \rangle (\phi, \vartheta = 0) = - \langle \hat{S}_z \rangle (\phi, \vartheta = \pi) = -1$. Whereas, for $\alpha > 1$ ($\mathcal{C} = 1$ monopole), $\langle \hat{S}_z \rangle (\phi, \vartheta = 0) = 0$ and $\langle \hat{S}_z \rangle (\phi, \vartheta = \pi) = 1$. This discontinuity of the spin expectation value on the north pole $(\phi, \vartheta = 0)$ marks the phase transition at $\alpha = 1$.

The spin textures in Figure 4.5 are no longer invariant under arbitrary translations $\phi \to \phi + \Delta\phi$. The rotational invariance is obviously broken due to the influence of the spin-tensor operator $\hat{O}_{xz}$. However, the structure suggests that $\langle \hat{S}_z \rangle$ remains invariant for specifically chosen periods of ϕ - hence, there is a proper discrete subgroup $G \subset SO(2)$ which leaves the spin texture invariant. In contrast to Figure 4.4 for $\mathcal{C} = 2 \to \mathcal{C} = 1$, it is not possible to simply measure the spin polarization on the north/south pole to detect the phase transition, since these specific values remain constant during the $\mathcal{C} = 2 \to \mathcal{C} = 0$–transition process. Therefore, one would have to pick another significant manifold point and corresponding spin expectation value to highlight the transition.

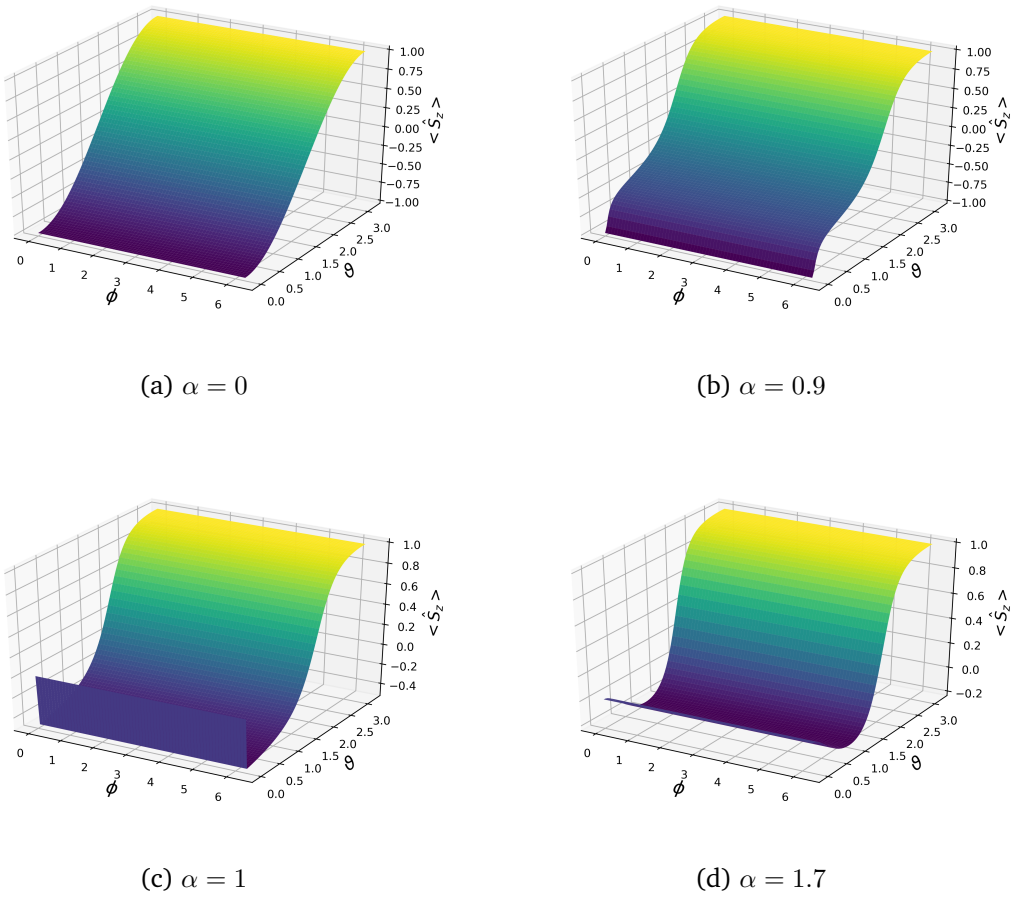

(a) $\alpha = 0$

(b) $\alpha = 0.9$

(c) $\alpha = 1$

(d) $\alpha = 1.7$

Figure 4.4: Numerical simulation of the spin texture profile $\langle \hat{S}_z \rangle (\phi, \vartheta)$ (in units of $\hbar$) for different parameter values α, with respect to $\hat{H} = \mathbf{m} \cdot \hat{\mathcal{S}} + \alpha m_z \hat{S}_z^2$. The emergent kink in the spin texture c) is associated with the phase transition $\mathcal{C} = 2 \rightarrow \mathcal{C} = 1$.

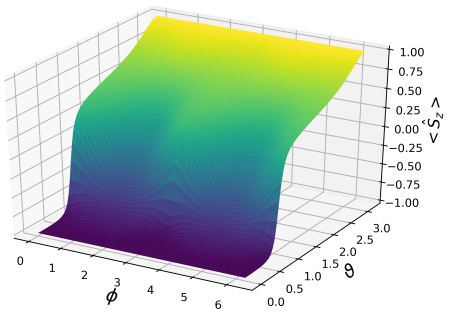

(a) $\beta = 1.5$

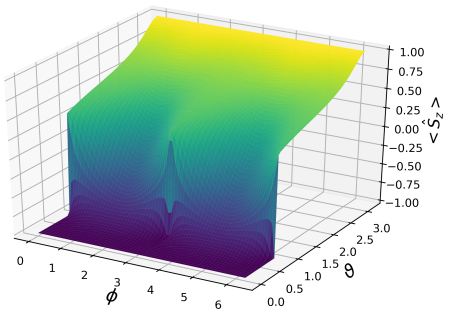

(b) $\beta = 2$

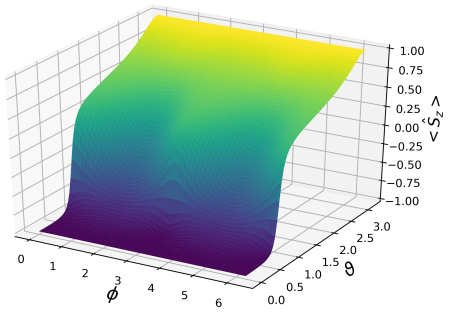

(c) $\beta = 2.5$

Figure 4.5: Numerical simulation of the spin texture profile $\langle \hat{S}_z \rangle (\phi, \vartheta)$ (in units of $\hbar$) for different values β, with respect to $\hat{H} = \mathbf{m} \cdot \hat{\mathcal{S}} + \beta m_x \hat{O}_{xz}$. $\beta = 2$ corresponds to the phase transition $\mathcal{C} = 2 \rightarrow \mathcal{C} = 0$, note the emergent patterns within each profile.

4.1.3 Discussion of Results

The previous results confirm the existence of spin 1 abelian monopoles having three different Chern numbers (i.e. $\mathcal{C} = 0, 1, 2$) with respect to the ground state of the effective Hamiltonian. A 6–dimensional (synthetic) parameter space has been engineered through the coupling of $S = 1$–hyperfine states of ^{87}Rb atoms. A clever tuning of the lasers reduces the space to a $\mathbb{S}^2$–base manifold. The non–degenerate eigenstates of the Hamiltonian only allow for a Berry type phase change during a cyclic evolution. Thus, we are immediately led to $U(1)$–bundles over $\mathbb{S}^2$, and the bundle types are characterized by different Chern numbers. $\mathcal{C} = 0$ indicates a trivial $U(1)$–bundle: $\mathbb{S}^2 \times U(1)$. ($\mathcal{C} = 1$)–ground state can be modelled via a Hopf bundle $(\mathbb{S}^3, \pi, \mathbb{S}^2, U(1))$, similar to our initial example, but now for a system with 3 states. These phenomena are clearly beyond Landau's standard theory of phase transitions. To understand that we have a non–Landau phase transition, take the $\mathcal{C} = 2 \to \mathcal{C} = 1$–transition which occurs by adding the term $\alpha m_z \hat{S}_z^2$ and driving the system to the point $\alpha = 1$. The Hamiltonian and ground state symmetry each remain the same for values $0 < \alpha < 1$ and $\alpha > 1$, such that classical symmetry breaking cannot explain the observed topological transition at $\alpha = 1$ (level crossing). However, one possible way of understanding comes from the fibre bundle perspective. The base space $\mathbb{S}^2$ and the fibre $U(1)$, regarded as topological spaces, remain invariant before and after the transition - it is the total space E of the bundle which undergoes a topology change after the level crossing, and this is measured by the Chern number. $\mathcal{C} = 2 \to \mathcal{C} = 1$–transition is associated with a topology change $\mathbb{R}P^3 \rightsquigarrow \mathbb{S}^3$ of E in the bundle $(E, \mathbb{S}^2, \mathbb{S}^1)$. Similarly, $\mathcal{C} = 2 \to \mathcal{C} = 0$–phase transition is related to $\mathbb{R}P^3 \rightsquigarrow \mathbb{S}^2 \times U(1)$, which represents a full untwisting of the bundle. From the topological analysis we learn that these phase transitions are accompanied by a decreasing degree of bundle twisting, given by $\mathcal{C}$. At the same time, the reduction of $\mathcal{C}$ happens at the cost of a considerably changing spin-vorticity, measured by $\langle \hat{S}_z \rangle$ on the sphere manifold.

4.2 Non–abelian monopole in spin–3/2 cold atoms

Recent experimental progress in the simulation with ultracold Rubidium atoms has allowed to verify the existence of a non–abelian monopole in a synthetic high–dimensional space [53]. This monopole is characterized by a non–vanishing second Chern number. We attempt to supplement the experimental work from a theoretical point of view: In particular, I will describe the non–trivial principal G–bundle $(E, \pi, \mathcal{M}, G)$ which encompasses the experimental results. The bundle turns out to have a non–abelian Lie group G as its fibre. Moreover, one finds $\pi_2(\mathcal{M}) = 0$ and $\pi_4(\mathcal{M}) \neq 0$ for the parameter space of the Hamiltonian, which, together with the non–abelian fibre, emphasizes the existence of a non–abelian monopole.

4.2.1 Experimental setup scheme

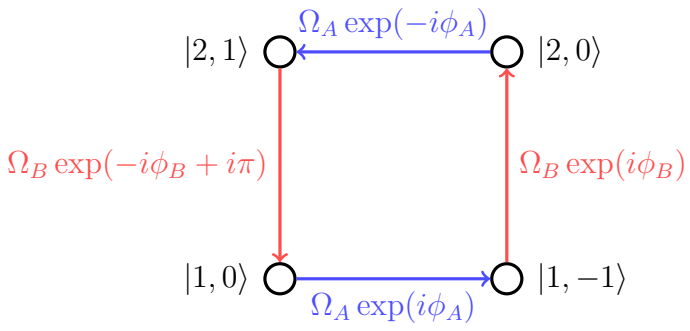

Figure 4.6: Scheme for the coupling of hyperfine states of ^{87}Rb atoms with rf (blue) and μ-waves (red); taken from the experimental arrangement by Sugawa, Spielman et al. [53]. Ω_A/Ω_B and ϕ_A/ϕ_B denote the amplitudes and phases of the driving electromagnetic fields, respectively. The atomic BEC has been produced by standard laser cooling and evaporation techniques in a dipole trap. The system has four states and TR symmetry of the fermionic type $\hat{\mathcal{T}}^2 = -\hat{\mathbb{1}}$. Therefore, the setup simulates a specific (pseudo)-spin 3/2 type of system. The total phase flux inside the plaquette is $\Phi = \pi$.

Basic properties

The model Hamiltonian of the four level system in Fig. 4.6 can be cast into the form

$$\hat{H} = -\frac{1}{2}\mathbf{r}\cdot\hat{\Gamma} = -\frac{1}{2}\sum_{i=1}^{5} r_i\Gamma_i,^{5} \tag{4.31}$$

with 4×4- Dirac matrices as the generators of a Clifford algebra:

$$\{\Gamma_i,\Gamma_j\} = 2\delta_{ij}\mathbb{1}_4; \quad i,j=1,\ldots,4. \tag{4.32}$$

The full derivation of the Hamiltonian from the coupling of the states is found in the supplements of [53]. The 5-dimensional $\mathbb{R}$–vector space in which Hamiltonians of the above form are generated is given by

Notation 44

$$\mathcal{M}_H := \left\{ \sum_{i=1}^{5} r_i\Gamma_i \,|\, \|\boldsymbol{r}\| \neq 0 \right\} \subset Mat(4,\mathbb{C})$$

The last gamma matrix Γ_5 can be represented as a product of the other four generators - the algebraic construction being in analogy to relativistic field theory formulations. In even dimensions the Clifford algebra can be reconstructed via tensor products of Pauli matrices $\sigma_i\otimes\sigma_j$:

$$\Gamma_1 = \sigma_y\otimes\sigma_y \tag{4.33}$$

$$\Gamma_2 = \mathbb{1}_2\otimes\sigma_x \tag{4.34}$$

$$\Gamma_3 = -\sigma_z\otimes\sigma_y \tag{4.35}$$

$$\Gamma_4 = \mathbb{1}_2\otimes\sigma_z \tag{4.36}$$

$$\Gamma_5 = \prod_i \Gamma_i = -\sigma_y\sigma_z\otimes\sigma_y\sigma_x\sigma_y\sigma_z = \sigma_x\otimes\sigma_y \tag{4.37}$$

The five vector $\mathbf{r}$ is determined by the amplitudes $\Omega_{A/B}$, phases $\phi_{A/B}$ and detuning δ of the coupled driving fields

$$\mathbf{r} = (-\Omega_B\cos\phi_B, -\Omega_A\cos\phi_A, -\Omega_A\sin\phi_A, \delta, -\Omega_B\sin\phi_B). \tag{4.38}$$

[5] We have chosen the scaling $\hat{H}\mapsto\frac{1}{\hbar}\hat{H}$.

Before describing the topology which is attached to parameter space $\mathcal{M}$, we derive further useful results. Regard the eigenvalue equation $\hat{H}\,|\Psi\rangle = E\,|\Psi\rangle$, then

$$\hat{H}^2 = \frac{1}{4}\sum_{i,j} r_i r_j \Gamma_i \Gamma_j = \frac{1}{4}\sum_{i=1}^{5} r_i^2 = \frac{1}{4}\|\mathbf{r}\|^2 \tag{4.39}$$

$$= \frac{1}{4}(\Omega_A^2 + \Omega_B^2 + \delta^2). \tag{4.40}$$

It follows for the eigenvalues

$$E_{1,2} = \pm\frac{1}{2}\|\mathbf{r}\| = \pm\frac{1}{2}\sqrt{\Omega_A^2 + \Omega_B^2 + \delta^2}. \tag{4.41}$$

The operator $\hat{\mathcal{T}} = \hat{U}_{\mathsf{T}} K$, with $\hat{U}_{\mathsf{T}} = i\sigma_y \otimes \mathbb{1}_2$ and K acting as complex conjugation operation, describes time–reversal symmetry as in Eq. (C.1). Because of TR symmetry $[\hat{H}, \hat{\mathcal{T}}] = 0$ and relation $\hat{\mathcal{T}}^2 = -\mathbb{1}_4$ each energy eigenvalue will be degenerate due to Kramer's theorem (C.6), thus mimicking a fermionic system. The eigenstates belonging to each of the 2-D subspaces $\mathfrak{H}_{\pm E}$ are

$$|u_+^{\uparrow\downarrow}(\mathbf{r})\rangle\,, \quad |u_-^{\uparrow\downarrow}(\mathbf{r})\rangle\,, \tag{4.42}$$

such that $\hat{\mathcal{T}}\,|u_+^{\uparrow}(\mathbf{r})\rangle = |u_+^{\downarrow}(\mathbf{r})\rangle$, $\hat{\mathcal{T}}\,|u_-^{\uparrow}(\mathbf{r})\rangle = |u_-^{\downarrow}(\mathbf{r})\rangle$. The full Hilbert space $\mathfrak{H}$ has the spectral resolution

$$\mathfrak{H} = \mathfrak{H}_E \oplus \mathfrak{H}_{-E}. \tag{4.43}$$

We observe immediately the signature of a potential singularity in the origin which stems from a non–trivial coupling to the laser fields. Let us fix an $\mathbf{r} \neq 0$ and diagonalize $\hat{H}$ according to the subspaces:

$$\hat{H}'(\mathbf{r}) = \mathcal{U}\hat{H}(\mathbf{r})\mathcal{U}^\dagger = \frac{1}{2}\|\mathbf{r}\|\left(|u_+^{\uparrow}(\mathbf{r})\rangle\langle u_+^{\uparrow}(\mathbf{r})| + |u_+^{\downarrow}(\mathbf{r})\rangle\langle u_+^{\downarrow}(\mathbf{r})|\right)$$
$$- \frac{1}{2}\|\mathbf{r}\|\left(|u_-^{\uparrow}(\mathbf{r})\rangle\langle u_-^{\uparrow}(\mathbf{r})| + |u_-^{\downarrow}(\mathbf{r})\rangle\langle u_-^{\downarrow}(\mathbf{r})|\right). \tag{4.44}$$

4.2.2 Approach to a topological bundle model

As before, we can proceed by describing the base space (parameter space of the Hamiltonian) up to homotopy:

$$\mathcal{M}_H = \mathbb{R}^5 - \{0\} \simeq \mathbb{S}^4 \quad \text{homotopy} \tag{4.45}$$

The above relation is a deformation retract and the parameter space is homotopic to $\mathbb{S}^4$. Hence, we can use 4–D spheres to detect any point like defects in our parameter space - i.e.

$$\pi_k(\mathbb{S}^4) = 0, \quad 0 \leq k \leq 3, \tag{4.46}$$

$$\pi_4(\mathbb{S}^4) = \mathbb{Z}. \tag{4.47}$$

It will be demonstrated that there exists a $\mathbb{Z}$–valued invariant (*2nd Chern number*) which can be obtained by integration over the 4–D hypersphere, whereas the first Chern number vanishes.

A suitable bundle structure

Having identified the base space is not sufficient, however, since we lack further data which constitutes a full fibre bundle. Now let us interpret each Hamiltonian of the space $\mathcal{M}_H$ as a point on $\mathbb{S}^4$: If $\hat{H}_1, \hat{H}_2 \in \mathcal{M}_H$ and $\mathrm{Spec}(\hat{H}_1) = \mathrm{Spec}(\hat{H}_2)$, then there exists a $SO(5)$–transformation R which connects both Hamiltonians by transforming the corresponding vectors via $\mathbf{r}_2 = R \cdot \mathbf{r}_1$. This view gives us a natural action of $SO(5)$ on $\mathbb{S}^4$ and we know that spheres can be represented as homogeneous spaces, i.e. $\mathbb{S}^4 = SO(5)/SO(4)$. So, we can propose first the following fibre bundle

$$(SO(5), \pi, \mathbb{S}^4, SO(4)), \quad \pi \colon SO(5) \to \mathbb{S}^4 \quad \text{projection}. \tag{4.48}$$

Although this seems as an acceptable fibre bundle at first, there are some problems: The experimental setup suggests a structure group which can be represented by unitary 2×2–matrices, related to the degenerate 2–dimensional subspaces. Moreover, we have to account for the time–reversal symmetry of the system. Hence, we propose

$$U(4) \times \mathcal{M}_H \to \mathcal{M}_H, \quad (\mathcal{U}, \hat{H}) \mapsto \mathcal{U}\hat{H}\mathcal{U}^\dagger \tag{4.49}$$

$$\Gamma_i \mapsto \Gamma_i' := \mathcal{U}\Gamma_i\mathcal{U}^\dagger, \quad \mathcal{U} \in U(4). \tag{4.50}$$

The new set of generators $\{\Gamma'_i\}$ is admissible as it fulfills the defining relation (4.32) which can be readily verified. Introducing a matrix $\Lambda(\mathcal{U})$, we must have

$$\Gamma'_i := \mathcal{U}\Gamma_i\mathcal{U}^\dagger = \Lambda(\mathcal{U})^k{}_i\Gamma_k, \tag{4.51}$$

$$\mathcal{U}\hat{H}(\mathbf{r})\mathcal{U}^\dagger = -\frac{1}{2}\sum_i r^i\Lambda(\mathcal{U})^k{}_i\Gamma_k = -\frac{1}{2}\left(\Lambda(\mathcal{U})\mathbf{r}\right)^k\Gamma_k = \hat{H}(\Lambda(\mathcal{U})\mathbf{r}). \tag{4.52}$$

We define a scalar product $(\cdot|\cdot)$ on $\mathcal{M}_H$ and draw a connection to conventional euclidean space $(\mathbb{R}^5, \langle\cdot|\cdot\rangle)$.

Definition 45 $(\hat{H}(\boldsymbol{r}_1)|\hat{H}(\boldsymbol{r}_2)) := \mathrm{Tr}(\hat{H}(\boldsymbol{r}_1)\hat{H}(\boldsymbol{r}_2))$

Note that $\mathrm{Tr}(\hat{H}(\mathbf{r}_1)\hat{H}(\mathbf{r}_2)) = \langle\mathbf{r}_1|\mathbf{r}_2\rangle$ and take $\hat{H}' = \mathcal{U}\hat{H}\mathcal{U}^\dagger$, then

$$(\hat{H}'(\mathbf{r}_1)|\hat{H}'(\mathbf{r}_2)) = \langle\Lambda(\mathcal{U})\mathbf{r}_1|\Lambda(\mathcal{U})\mathbf{r}_2\rangle = (\hat{H}(\mathbf{r}_1)|\hat{H}(\mathbf{r}_2)) = \langle\mathbf{r}_1|\mathbf{r}_2\rangle \tag{4.53}$$

$$\Rightarrow \Lambda(\mathcal{U})^t\Lambda(\mathcal{U}) = \mathbb{1}_5. \tag{4.54}$$

This yields a surjective homomorphism

$$\Lambda\colon U(4) \to SO(5). \tag{4.55}$$

It is actually necessary to restrict the map to the symplectic group $Sp(2) := U(4) \cap \{\mathcal{U}\mathcal{J}\mathcal{U}^t = \mathcal{J}\}$ due to TR symmetry: $[\hat{H}(\mathbf{r}), \hat{\mathcal{T}}] = 0, \forall\mathbf{r}$ implies $\mathcal{U}[\hat{H}(\mathbf{r}), \hat{\mathcal{T}}]\mathcal{U}^\dagger = 0$ or $[\hat{H}(\mathbf{r}'), \mathcal{U}\hat{\mathcal{T}}\mathcal{U}^\dagger] = 0$. Uniqueness of the TR operator imposes condition $\mathcal{U}\hat{\mathcal{T}}\mathcal{U}^\dagger = \hat{\mathcal{T}}$, and by acting on a state $|\psi\rangle$: $\mathcal{U}\hat{U}_\mathsf{T}K\mathcal{U}^\dagger|\psi\rangle = \mathcal{U}\hat{U}_\mathsf{T}\mathcal{U}^t|\psi\rangle^* = \hat{U}_\mathsf{T}|\psi\rangle^*$. Finally, we obtain the restriction $\mathcal{U}\hat{U}_\mathsf{T}\mathcal{U}^t = \hat{U}_\mathsf{T}$ for $\mathcal{U} \in U(4)$ with $\hat{U}_\mathsf{T} = i\sigma_y \otimes \mathbb{1}_2$

$$\hat{U}_\mathsf{T} = i\sigma_y \otimes \mathbb{1}_2 = \begin{pmatrix} 0_2 & \mathbb{1}_2 \\ -\mathbb{1}_2 & 0_2 \end{pmatrix} = \mathcal{J}, \tag{4.56}$$

which is the symplectic form $\mathcal{J}$ with respect to $Sp(2)$. In other words, time–reversal invariance of the fermionic type $\hat{\mathcal{T}}^2 = -\mathbb{1}$ implies a symplectic group structure. Both Lie algebras are isomorphic, i.e. $\mathfrak{sp}(2) \cong \mathfrak{so}(5)$[6]. Via the universal covering of Lie groups we get

$$Sp(2)/H \cong SO(5), \quad \pi_1(Sp(2)) = 0. \tag{4.57}$$

[6]This can be seen through the corresponding Dynkin diagrams of the Lie algebras.

A similar analysis can be applied to $SO(4)$ since we have for its Lie algebra $\mathfrak{so}(4) \cong \mathfrak{sp}(1) \oplus \mathfrak{sp}(1) \cong \mathfrak{su}(2) \oplus \mathfrak{su}(2)$ (see corresponding Dynkin diagrams).

$$(Sp(1) \times Sp(1))/H' \cong SO(4), \tag{4.58}$$

$$\pi_1(Sp(1) \times Sp(1)) = \pi_1(\mathbb{S}^3) \oplus \pi_1(\mathbb{S}^3) = 0. \tag{4.59}$$

It is known that $H = H'$ and more generally $H = \mathbb{Z}/2\mathbb{Z} = \pi_1(SO(n))$. We rewrite the fibre bundle and then reduce it through group isomorphisms

$$(SO(5), \pi, \mathbb{S}^4, SO(4)) = (Sp(2)/H, \pi, \mathbb{S}^4, (Sp(1) \times Sp(1))/H) \tag{4.60}$$

$$\longrightarrow (Sp(2), \pi, \mathbb{S}^4, Sp(1) \times Sp(1)) \tag{4.61}$$

4.2.3 Gauge field(s), Berry curvature, Topological number

The *structure group* of the bundle (4.61) is identified with the fibre $Sp(1) \times Sp(1)$ and it determines the Berry or gauge connection $\mathcal{A}$ from which one can calculate the observable Berry curvature or field strength $\mathcal{F}$. This reasoning amounts of constructing the gauge connection as a vector–valued matrix of the form (2.39)

$$\mathcal{A}^{\pm}(\mathbf{r}) = i \begin{pmatrix} \langle u^{\uparrow}_{\pm}(\mathbf{r})| \nabla_{\mathbf{r}} |u^{\uparrow}_{\pm}(\mathbf{r})\rangle & \langle u^{\uparrow}_{\pm}(\mathbf{r})| \nabla_{\mathbf{r}} |u^{\downarrow}_{\pm}(\mathbf{r})\rangle \\ \langle u^{\downarrow}_{\pm}(\mathbf{r})| \nabla_{\mathbf{r}} |u^{\uparrow}_{\pm}(\mathbf{r})\rangle & \langle u^{\downarrow}_{\pm}(\mathbf{r})| \nabla_{\mathbf{r}} |u^{\downarrow}_{\pm}(\mathbf{r})\rangle \end{pmatrix}, \tag{4.62}$$

$$\mathcal{A}(\mathbf{r}) = \mathcal{A}^{+}(\mathbf{r}) \oplus \mathcal{A}^{-}(\mathbf{r}). \tag{4.63}$$

The direct sum means we have two independent spaces. The connection one-form can be written as $\mathcal{A} = \mathcal{A}_\mu dr^\mu = \mathcal{A}^+_\mu dr^\mu + \mathcal{A}^-_\mu dr^\mu \in (\mathfrak{sp}(1) \oplus \mathfrak{sp}(1)) \otimes \Omega^1(\mathbb{S}^4)$. In fact, because of the isomorphism $\mathfrak{sp}(1) \cong \mathfrak{su}(2)$ we have two independent $SU(2)$ gauge fields $\mathcal{A}^{\pm}$ referring to one of the energy levels of $\hat{H}$. For the non–abelian Berry curvature 2–form we use the fact $\mathcal{F} = d_{\mathcal{A}}\mathcal{A} = d\mathcal{A} + \mathcal{A} \wedge \mathcal{A} \in (\mathfrak{sp}(1) \oplus \mathfrak{sp}(1)) \otimes \Omega^2(\mathbb{S}^4)$, hence

$$\mathcal{F} = d(\mathcal{A}^+ + \mathcal{A}^-) + (\mathcal{A}^+ + \mathcal{A}^-) \wedge (\mathcal{A}^+ + \mathcal{A}^-) \tag{4.64}$$

$$= (d\mathcal{A}^+ + \mathcal{A}^+ \wedge \mathcal{A}^+) + (d\mathcal{A}^- + \mathcal{A}^- \wedge \mathcal{A}^-) = \mathcal{F}^+ + \mathcal{F}^-, \tag{4.65}$$

where $\mathcal{A}^+ \wedge \mathcal{A}^- = \mathcal{A}^- \wedge \mathcal{A}^+ = 0$ was employed due to the commutation relation $[\mathcal{A}^+_\mu, \mathcal{A}^-_\nu] = 0$. It is justified to write $\mathcal{F} = \mathcal{F}^+ \oplus \mathcal{F}^-$ for the complete Berry curvature.

Geometric construction of a characteristic form

The next problem we need to solve is related to the available quantities which can describe the topological features of a non–abelian monopole. The second cohomology group is trivial, i.e. $H^2(\mathbb{S}^4) = H_2(\mathbb{S}^4) = 0$. This means that an $\mathbb{R}$–valued closed 2–form, constructed from $\mathcal{F}$, must be the global derivative of a one–form and this yields a vanishing (first) Chern number. However, the relation $H^4(\mathbb{S}^4, \mathbb{R}) = H_4(\mathbb{S}^4, \mathbb{R}) = \mathbb{R}$ tells us that we can produce a non–trivial, closed $\mathbb{R}$–valued 4–form from the Berry curvature $\mathcal{F}$. From now on, we omit the superscripts $\pm$ and use the mathematical convention (B.13) introduced in the appendix.

Let $\mathcal{F} \in \mathfrak{g} \otimes \Omega^2(\mathcal{M})$ be the Berry curvature and introduce an Ad_g–invariant scalar product $\langle \cdot, \cdot \rangle : \mathfrak{g} \times \mathfrak{g} \to \mathbb{R}$ on the Lie–algebra $\mathfrak{g}$ of the group G. Forming the exterior tensor product

$$\mathcal{F} \hat{\otimes} \mathcal{F} \in (\mathfrak{g} \otimes \mathfrak{g}) \otimes \Omega^4(\mathcal{M}), \tag{4.66}$$

we obtain a $\mathfrak{g} \otimes \mathfrak{g}$–valued 4-form. Inserting this into the scalar product yields

$$\langle \mathcal{F} \hat{\otimes} \mathcal{F} \rangle \in \mathbb{R} \otimes \Omega^4(\mathcal{M}). \tag{4.67}$$

To see this we can write $\mathcal{F} = \mathcal{F}^a T_a$ with real–valued 2-forms $\mathcal{F}^a$ and T_a being the generators of $\mathfrak{g}$, possibly expressed in a specific representation. Then, $\mathcal{F} \hat{\otimes} \mathcal{F} = \mathcal{F}^a \wedge \mathcal{F}^b (T_a \otimes T_b)$ and $\langle \mathcal{F} \hat{\otimes} \mathcal{F} \rangle = \mathcal{F}^a \wedge \mathcal{F}^b \langle T_a, T_b \rangle$. The form in (4.67) is our fundamental object of investigation.

Definition 46 *Referring to a gauge field $\mathcal{A}$ on a closed 4-dimensional manifold $\mathcal{M}$ we define a number assigned to $\mathcal{A}$ by the integral*

$$N(\mathcal{A}) := \int_{\mathcal{M}} \langle \mathcal{F} \hat{\otimes} \mathcal{F} \rangle \,, \quad \mathcal{F} = d_{\mathcal{A}} \mathcal{A} = d\mathcal{A} + \mathcal{A} \wedge \mathcal{A}. \tag{4.68}$$

First, we observe that (4.67) is gauge–invariant: Consider the transformation $\mathcal{F} \to \mathcal{F}^g := Ad_g \mathcal{F} = g \mathcal{F} g^{-1}$ with $g \in G$. Then, we compute $\langle \mathcal{F}^g \hat{\otimes} \mathcal{F}^g \rangle = \langle \mathcal{F} \hat{\otimes} \mathcal{F} \rangle$ due to Ad_g–invariance of the scalar product. Moreover, we calculate the exterior derivative

$$d \langle \mathcal{F} \hat{\otimes} \mathcal{F} \rangle = \langle \underbrace{(d_{\mathcal{A}} \mathcal{F})}_{0} \hat{\otimes} \mathcal{F} \rangle + \langle (-1)^2 \mathcal{F} \hat{\otimes} \underbrace{(d_{\mathcal{A}} \mathcal{F})}_{0} \rangle = 0, \tag{4.69}$$

which follows from the well-known Bianchi identity $d_{\mathcal{A}}\mathcal{F} = 0$ in its differential form notation. Consequently, $\langle \mathcal{F}\hat{\otimes}\mathcal{F}\rangle$ is a closed 4-form or a co–cycle in the cohomology group $H^4(\mathcal{M})$, i.e. one maps

$$\langle \mathcal{F}\hat{\otimes}\mathcal{F}\rangle \to [\langle \mathcal{F}\hat{\otimes}\mathcal{F}\rangle] \in H^4(\mathcal{M}). \tag{4.70}$$

By virtue of this result and Stokes theorem the integral in Eq. (4.68) depends only on the corresponding homology and cohomology classes, so we can rewrite it taking advantage of the the pairing $(\cdot,\cdot)\colon H^4(\mathcal{M}) \times H_4(\mathcal{M}) \to \mathbb{R}$ from de Rham's theory

$$N(\mathcal{A}) = \left([\langle \mathcal{F}\hat{\otimes}\mathcal{F}\rangle], [\mathcal{M}]\right), \quad [\mathcal{M}] \in H_4(\mathcal{M}), [\langle \mathcal{F}\hat{\otimes}\mathcal{F}\rangle] \in H^4(\mathcal{M}). \quad \square \tag{4.71}$$

Variation $\mathcal{A} \to \mathcal{A} + \delta\mathcal{A}$. The purpose of this paragraph is to examine the behaviour of $N(\mathcal{A})$ under continuous deformations of $\mathcal{A}$. The derivations are carried out following a variational scheme

$$\mathcal{A} \to \mathcal{A} + \delta\mathcal{A} \tag{4.72}$$

$$\Rightarrow \mathcal{F} \to \mathcal{F} + \delta\mathcal{F} = d_{\mathcal{A}}(\mathcal{A} + \delta\mathcal{A}) = \mathcal{F} + d_{\mathcal{A}}\delta\mathcal{A}, \tag{4.73}$$

$$\Rightarrow \delta\mathcal{F} = d_{\mathcal{A}}\delta\mathcal{A}. \tag{4.74}$$

The variation of N is

$$\delta N = \int_{\mathcal{M}} \delta \langle \mathcal{F}\hat{\otimes}\mathcal{F}\rangle = \int_{\mathcal{M}} \langle \delta\mathcal{F}\hat{\otimes}\mathcal{F}\rangle + \langle \mathcal{F}\hat{\otimes}\delta\mathcal{F}\rangle = 2\int_{\mathcal{M}} \langle \delta\mathcal{F}\hat{\otimes}\mathcal{F}\rangle . \tag{4.75}$$

In detail, we see that

$$\delta \langle \mathcal{F}\hat{\otimes}\mathcal{F}\rangle = 2\langle \delta\mathcal{F}\hat{\otimes}\mathcal{F}\rangle = 2\langle d_{\mathcal{A}}\delta\mathcal{A}\hat{\otimes}\mathcal{F}\rangle , \tag{4.76}$$

by using the Bianchi identity $d_{\mathcal{A}}\mathcal{F} = 0$ and relation

$$2d\langle \delta\mathcal{A}\hat{\otimes}\mathcal{F}\rangle = 2\langle d_{\mathcal{A}}\delta\mathcal{A}\hat{\otimes}\mathcal{F}\rangle - 2\langle \delta\mathcal{A}\hat{\otimes}d_{\mathcal{A}}\mathcal{F}\rangle = 2\langle d_{\mathcal{A}}\delta\mathcal{A}\hat{\otimes}\mathcal{F}\rangle . \tag{4.77}$$

This means that the variation is a total derivative, i.e. $\delta\langle \mathcal{F}\hat{\otimes}\mathcal{F}\rangle = 2d\langle \delta\mathcal{A}\hat{\otimes}\mathcal{F}\rangle$. Hence,

$$\delta N = 2\int_{\mathcal{M}} d\langle \delta\mathcal{A}\hat{\otimes}\mathcal{F}\rangle = 0, \tag{4.78}$$

which proves that $N(\mathcal{A})$ remains constant for continuous variations of $\mathcal{A}$. Thus, $N(\mathcal{A})$ can be regarded as a homotopy invariant of $\mathcal{A}$.

Local form of $\langle \mathcal{F} \hat{\otimes} \mathcal{F} \rangle$. According to Poincare's Lemma every closed n–form is locally exact and so, it can be locally represented as a derivative of a $(n-1)$–form. However, this is not true globally. We are going to find the 3–form for our problem. For a local neighbourhood $U_i \cong \mathbb{R}^n$ we may choose a family $\{\mathcal{A}_t\}$ with $\mathcal{A}_t := t\mathcal{A}$, which mediates between the zero gauge field and $\mathcal{A}$. So,

$$\mathcal{F}_t = td\mathcal{A} + t^2 \mathcal{A} \wedge \mathcal{A} = t\mathcal{F} + (t^2 - t)\mathcal{A} \wedge \mathcal{A}. \tag{4.79}$$

Then, integrating $\frac{d}{dt} \langle \mathcal{F}_t \hat{\otimes} \mathcal{F}_t \rangle = 2d \langle (\frac{d}{dt} \mathcal{A}_t) \hat{\otimes} \mathcal{F}_t \rangle$ with respect to parameter t over $[0, 1]$ one obtains

$$\begin{aligned}
\langle \mathcal{F} \hat{\otimes} \mathcal{F} \rangle &= 2d \int_0^1 \langle \left(\frac{d}{dt} \mathcal{A}_t \right) \hat{\otimes} \mathcal{F}_t \rangle \, dt && (4.80)\\
&= 2d \int_0^1 \langle \mathcal{A} \hat{\otimes} (t\mathcal{F} + (t^2 - t)\mathcal{A} \wedge \mathcal{A}) \rangle \, dt && (4.81)\\
&= 2d \int_0^1 t \langle \mathcal{A} \hat{\otimes} \mathcal{F} \rangle + (t^2 - t) \langle \mathcal{A} \hat{\otimes} (\mathcal{A} \wedge \mathcal{A}) \rangle \, dt && (4.82)\\
&= d(\langle \mathcal{A} \hat{\otimes} \mathcal{F} \rangle - \frac{1}{3} \langle \mathcal{A} \hat{\otimes} (\mathcal{A} \wedge \mathcal{A}) \rangle . \quad \square && (4.83)
\end{aligned}$$

According to appendix B we can write $\int_{\mathbb{S}^4} \langle \mathcal{F} \hat{\otimes} \mathcal{F} \rangle = \int_{\mathbb{R}^4} \langle \mathcal{F} \hat{\otimes} \mathcal{F} \rangle$ with $\mathcal{F} \to 0$ for $\|r\| \to \infty$. However, this can be interpreted as an integral over $\mathbb{D}^4$ such that $\mathcal{F}|\partial \mathbb{D}^4 = \mathcal{F}|\mathbb{S}^3 = 0$ holds, which is supported via the identification $\mathbb{S}^4 \cong \mathbb{D}^4 / \mathbb{S}^3$. Since $\mathbb{D}^4$ is contractible, one can use (4.83) to obtain

$$\begin{aligned}
N(\mathcal{A}) = \int_{\mathbb{S}^4} \langle \mathcal{F} \hat{\otimes} \mathcal{F} \rangle &= \int_{\mathbb{D}^4} \langle \mathcal{F} \hat{\otimes} \mathcal{F} \rangle , \quad \mathcal{F}|\mathbb{S}^3 = 0 && (4.84)\\
&= \int_{\mathbb{D}^4} d(\langle \mathcal{A} \hat{\otimes} \mathcal{F} \rangle - \frac{1}{3} \langle \mathcal{A} \hat{\otimes} (\mathcal{A} \wedge \mathcal{A}) \rangle && (4.85)\\
&= \int_{\mathbb{S}^3} \langle \mathcal{A} \hat{\otimes} \mathcal{F} \rangle - \frac{1}{3} \langle \mathcal{A} \hat{\otimes} (\mathcal{A} \wedge \mathcal{A}) \rangle && (4.86)\\
&= -\frac{1}{3} \int_{\mathbb{S}^3} \langle \mathcal{A} \hat{\otimes} (\mathcal{A} \wedge \mathcal{A}) \rangle . \quad \square && (4.87)
\end{aligned}$$

Because of the discussion in appendix B.1.2 $\mathcal{A}$ must be pure–gauge on $\mathbb{S}^3$- that is $\mathcal{A}(x) = g(x) dg^{-1}(x)$ with $SU(2)$–parametrization

$$g \colon \mathbb{S}^3 \to \mathbb{S}^3, x \mapsto g(x) = \frac{1}{\|x\|} \begin{pmatrix} x^0 + ix^3 & x^2 + ix^1 \\ -(x^2 - ix^1) & x^0 - ix^3 \end{pmatrix} = \frac{1}{\|x\|} (x^0 \mathbb{1} + ix^k \sigma_k). \tag{4.88}$$

So, the 3–form can be represented as $\langle g dg^{-1} \hat{\otimes} g dg^{-1} \wedge g dg^{-1} \rangle$.

4.2.4 First Principle Computation - Ground state 2nd Chern number

We need to evaluate (4.87) for the ground state configuration of the gauge field $\mathcal{A} = \mathcal{A}^-$ in Eq. (4.62). For the following computation we set $(T_\mu) = (\mathbb{1}, -i\sigma_k)$

$$\mathcal{A}(x) = g(x)dg^{-1}(x) = \frac{1}{\|x\|}(x^0\mathbb{1} + ix^k\sigma_k)d\left(\frac{1}{\|x\|}(x^0\mathbb{1} - ix^k\sigma_k)\right) \tag{4.89}$$

$$= \frac{1}{\|x\|}(x^0\mathbb{1} + ix^k\sigma_k)T_\mu\left(\frac{1}{\|x\|}\delta^\mu_\nu dx^\nu - \frac{x_\nu x^\mu}{\|x\|^3}dx^\nu\right) \tag{4.90}$$

$$= \frac{1}{\|x\|^2}(x^0\mathbb{1} + ix^k\sigma_k)\left(T_\nu dx^\nu - T_\mu\frac{x^\mu x_\nu}{\|x\|^2}dx^\nu\right) \tag{4.91}$$

Due to the symmetry of $\mathcal{A}(x)$ on the whole manifold $\mathbb{S}^3$ we are able to set $x = (x^0 = 1, \mathbf{x} = 0)$ which gives the answer

$$\mathcal{A}(x) = \mathbb{1}(T_\nu dx^\nu - T_0 dx^0) = -i\sigma_k dx^k. \tag{4.92}$$

We can now recast the 3–form in a more compact form

$$\langle\mathcal{A}\hat{\otimes}(\mathcal{A}\wedge\mathcal{A})\rangle = \langle\mathcal{A}_\mu dx^\mu\hat{\otimes}\frac{1}{2}[\mathcal{A}_\nu,\mathcal{A}_\lambda]dx^\nu\wedge dx^\lambda\rangle \tag{4.93}$$

$$= \frac{1}{2}\langle\mathcal{A}_\mu,[\mathcal{A}_\nu,\mathcal{A}_\lambda]\rangle\, dx^\mu\wedge dx^\nu\wedge dx^\lambda \tag{4.94}$$

$$= (-i)^3\frac{1}{2}\langle\sigma_\mu,\underbrace{[\sigma_\nu,\sigma_\lambda]}_{2i\epsilon_{\nu\lambda k}\sigma_k}\rangle\, dx^\mu\wedge dx^\nu\wedge dx^\lambda \tag{4.95}$$

$$= (-i)^3 i\epsilon_{\nu\lambda k}\langle\sigma_\mu,\sigma_k\rangle\, dx^\mu\wedge dx^\nu\wedge dx^\lambda \tag{4.96}$$

Note that the G–invariant bilinear form $\langle\cdot,\cdot\rangle$ is related to the trace on the Lie–algebra by $\langle\cdot,\cdot\rangle = -2\,\mathrm{Tr}(\cdot,\cdot)$. Therefore, we have $\langle\sigma_\mu,\sigma_k\rangle = -2\,\mathrm{Tr}(\sigma_\mu\sigma_k) = -4\delta_{\mu k}$ since $\{\sigma_i,\sigma_j\} = 2\delta_{ij}\mathbb{1}_2$.

$$\langle\mathcal{A}\hat{\otimes}(\mathcal{A}\wedge\mathcal{A})\rangle = -4\delta_{\mu k}\epsilon_{\nu\lambda k}dx^\mu\wedge dx^\nu\wedge dx^\lambda = -4\epsilon_{\nu\lambda\mu}dx^\mu\wedge dx^\nu\wedge dx^\lambda \tag{4.97}$$

Recall now the identities $\epsilon_{\nu\lambda\mu} = \epsilon_{\mu\nu\lambda}$ and $\epsilon_{\mu\nu\lambda}dx^\mu\wedge dx^\nu\wedge dx^\lambda = 3!dx^1\wedge dx^2\wedge dx^3$. Altogether, we come to the final expression

$$\langle\mathcal{A}\hat{\otimes}(\mathcal{A}\wedge\mathcal{A})\rangle = -24dx^1\wedge dx^2\wedge dx^3. \tag{4.98}$$

Inserting Eq. (4.98) into (4.87) reveals the following relation

$$N(\mathcal{A}) = \frac{24}{3}\int_{\mathbb{S}^3} dx^1 \wedge dx^2 \wedge dx^3 = 8\,\mathrm{vol}(\mathbb{S}^3) = 16\pi^2. \quad [7] \tag{4.99}$$

By comparing the standard definition of the second Chern number in the theory of characteristic classes we see that there is a normalization factor of $16\pi^2$. Thus, we derive

$$\mathcal{C}_2 = \frac{1}{16\pi^2} N(\mathcal{A}) = 1. \tag{4.100}$$

The experimental value $\mathcal{C}_2 = 0.97(6)$ from the work of Sugawa et al. agrees well with our precise first principle computation. Usually, integrals for higher Chern numbers are numerically difficult to deal with, as indicated in the work of Kolodrubetz [32]. However, I have been able to present a fully analytical solution by deploying all the symmetries of the gauge field geometry. Moreover, the strong connection to the area of high energy physics becomes obvious: In its ground state configuration the cold atom system in Figure 4.6 simulates an $SU(2)$–gauge field defined over $\mathbb{S}^4$. The concrete type of the principal bundle model is revealed by looking at the adiabatic state evolution.

4.2.5 Adiabatic state evolution

Consider a cyclic adiabatic evolution of a ground state $|\Phi_0\rangle$ of the system. The evolution of this state is determined by

$$|\Psi(T)\rangle = e^{\frac{i}{2}\int_0^T \|\mathbf{r}(t')\|\,dt'} \hat{\mathcal{W}}^{(-)}(\mathcal{C})\,|\Phi_0\rangle\,, \quad \hat{\mathcal{W}}^{(-)}(\mathcal{C}) \in SU(2), \tag{4.101}$$

such that $\mathbf{r}(0) = \mathbf{r}(T)$ holds for a time cycle of length T. The $(\Phi_0\Phi_0)$–transition amplitude and probability can be computed by

$$\langle\Phi_0|\Psi(T)\rangle = e^{\frac{i}{2}\int_0^T \|\mathbf{r}(t')\|\,dt'} \langle\Phi_0|\,\hat{\mathcal{W}}^{(-)}(\mathcal{C})\,|\Phi_0\rangle\,, \tag{4.102}$$

$$\mathcal{P}(\Phi_0 \to \Phi_0) = |\,\langle\Phi_0|\,\hat{\mathcal{W}}^{(-)}(\mathcal{C})\,|\Phi_0\rangle\,|^2. \tag{4.103}$$

It is striking to observe that the magnitude of the transition amplitude is given by the expectation value $\langle\hat{\mathcal{W}}^{(-)}(\mathcal{C})\rangle = \langle\Phi_0|\,\hat{\mathcal{W}}^{(-)}(\mathcal{C})\,|\Phi_0\rangle$ of the corresponding Wilson

[7] $\mathrm{vol}(\mathbb{S}^{n-1}) = \frac{2\pi^{n/2}}{\Gamma(\frac{n}{2})}$, Gamma function $\Gamma(x) = (x-1)\Gamma(x-1)$. For $n=4$ we get $\mathrm{vol}(\mathbb{S}^3) = 2\pi^2$.

loop configuration, where $\mathcal{C}$ is the loop traced out in the parameter space. One can suggest the following idea: Imposing an adiabatic cyclic evolution of the state restricts the fibre bundle (4.61) in a specific way. Since $\hat{\mathcal{W}}^{(-)}(\mathcal{C}) \in Sp(1)$, the fibre must be reduced to $(Sp(1) \times Sp(1))/(Sp(1) \times \{1\}) = Sp(1)$. Starting from (4.61) and exploiting group theoretical equivalence relations we write

$$\mathbb{S}^4 = Sp(2)/(Sp(1) \times Sp(1)) \tag{4.104}$$

$$= (Sp(2)/Sp(1))/[(Sp(1) \times Sp(1))/(Sp(1) \times \{1\})] \tag{4.105}$$

$$= (Sp(2)/Sp(1))/Sp(1) \tag{4.106}$$

Note the general claim $Sp(n)/Sp(n-1) \cong \mathbb{S}^{4n-1}$. Thus,

$$\longrightarrow (Sp(2)/Sp(1), \tilde{\pi}, \mathbb{S}^4, Sp(1)) = (\mathbb{S}^7, \tilde{\pi}, \mathbb{S}^4, \mathbb{S}^3). \tag{4.107}$$

This is a *quaternionic Hopf bundle* with projection map $\tilde{\pi}\colon \mathbb{S}^7 \to \mathbb{S}^4$ and $\mathbb{S}^3$–fibres. Remarkably, the instanton bundle in high energy physics has the same structure, and one of its field configurations has an instanton number which agrees with the calculated Chern number for the (pseudo-)spin–3/2 system.

Final Remarks and Statistical Interpretation. The quantum statistical point of view on the expectation value of a Wilson loop is given by $\langle \hat{\mathcal{W}}^{(-)}(\mathcal{C}) \rangle = \mathrm{Tr}\left(\hat{\rho}\hat{\mathcal{W}}^{(-)}(\mathcal{C})\right)$ with an appropriate system density matrix $\hat{\rho}$. The path integral representation offers another perspective on the expectation value

$$\langle \hat{\mathcal{W}}^{(-)}(\mathcal{C}) \rangle = \frac{\int \mathcal{D}[\mathcal{A}]\, \mathrm{Tr}\left(\mathcal{W}^{(-)}(\mathcal{C})\right) e^{-\frac{1}{\hbar}S_E[\mathcal{A}]}}{\int \mathcal{D}[\mathcal{A}] e^{-\frac{1}{\hbar}S_E[\mathcal{A}]}}, \tag{4.108}$$

$\mathcal{D}\mathcal{A}$ is a measure on gauge field configurations and S_E is the euclidean action. Linear response theory predicts that deviations from the adiabatic regime will be accounted in terms of a geometric force M exerted on the system; the equation is $M_\mu = v^\lambda \langle F_{\mu\lambda} \rangle = v^\lambda \,\mathrm{Tr}(\hat{\rho}\mathcal{F}_{\mu\lambda})$, where v^λ describes the velocity for changing system parameters r^λ [45]. Thus, the Berry curvature components can be reconstructed from measurements of the deflection or geometric force while driving

the coupled laser fields of the system; this was done by Sugawa et al. in their work. Another interesting theoretical proposal made by Kolodrubetz is based on a stochastic measurement protocol of the 2nd Chern number [32]. This approach could prove useful for tackling aforementioned observables such as Wilson loops etc.

Appendix A

Review of Group theory approach to Diagonalization

Translational invariant Hamilton operators based on lattice systems can be all diagonalized in a similar way. We focus on the group theoretical approach by examining the SSH ring as an instructive example. The computational details and underlying ideas are included for the convenience of the reader only.

A.1 Basic Principles

The eigenvalue equation in momentum space is

$$\hat{H}\left|\Psi_n(k)\right\rangle = E_n(k)\left|\Psi_n(k)\right\rangle. \tag{A.1}$$

The Hamiltonian refers to the SSH ring, i.e. we set $\hat{H} \equiv \hat{H}_{\mathsf{SSH,ring}}$. In the SSH case, we need to observe that $|\Psi_n(k)\rangle$ is an element of the tensor product of 2 Hilbert spaces, i.e. $\mathfrak{H}_{ext}$ and $\mathfrak{H}_{int}$ (external and internal part). This is because the Hamiltonian acts on the product of 2 Hilbert spaces (see main text). Therefore, we have

$$\left|\Psi_n(k)\right\rangle \in \mathfrak{H}_{ext} \otimes \mathfrak{H}_{int}, \tag{A.2}$$

$$\left|\Psi_n(k)\right\rangle = \left(\sum_{m=1}^{N} a_m(k)\left|m\right\rangle\right) \otimes \left(\sum_{\alpha\in\{A,B\}} \alpha_n(k)\left|\alpha\right\rangle\right), \tag{A.3}$$

where the coefficients $a_m(k)$ and $\alpha_n(k)$ need to be specified. Let $|\phi\rangle \in \mathfrak{H}_{ext}$ and make use of the completeness relation $\hat{\mathbb{1}} = \sum |m\rangle \langle m|$ of the orthonormal Hilbert basis $\{|m\rangle\}$ by inserting it

$$|\phi\rangle = \sum_{m=1}^{N} \langle m|\phi\rangle \, |m\rangle \, . \tag{A.4}$$

This shows that the expansion coefficients $a_m(\phi)$ of $|\phi\rangle$ obey the equation $a_m(\phi) = \langle m|\phi\rangle$. More information is needed in order to compute the coefficients:

Condition 47 *Let $\hat{T}\colon \big(\{1,\ldots,N\},+\big) \to \mathcal{U}(\mathfrak{H}_{ext})$ be a unitary representation of the translation group (translation symmetry) of the SSH ring, i.e. we must have:*

1. *$\hat{T}$ is unitary,*
2. *$\hat{T}(s+r) = \hat{T}(s)\hat{T}(r)$,*
3. *$[\hat{H}, \hat{T}(s)] = 0, \quad \forall s \in \{1,\ldots,N\}$.*

The eigenvalue equation is $\hat{T}(s)\,|\phi\rangle = \lambda_s \, |\phi\rangle \, , |\phi\rangle \in \mathfrak{H}_{ext}$, where the action of $\hat{T}(s)$ on the basis is given by $\hat{T}(s)\,|m\rangle = |m+s\rangle$.

Remark 48 *The set $\{1,\ldots,N\}$ of unit cells of the SSH ring has a natural additive group structure which can be defined by $i + j \equiv i + j \mod N$. For instance, this implies $[1+N] \equiv [1]$ in terms of equivalence classes.*

This observation leads immediately to the structure of the external symmetry group of the SSH ring.

Corollary 49 *The SSH ring (external) symmetry group is given by the cyclic group $\mathbb{Z}/N\mathbb{Z}$ through the isomorphism*

$$\big(\{1,\ldots,N\},+\big) \cong \mathbb{Z}/N\mathbb{Z}. \tag{A.5}$$

The corollary guarantees the existence of the condition given above: Since we are dealing with a finite group of order N there exist finite–dimensional, unitary representations. The irreducible representations of this cyclic (hence abelian) group are all one-dimensional. Therefore, for the eigenvalues we note that $\lambda_s \in U(1)$,

$$\lambda_s = e^{-iks}, \tag{A.6}$$

with some fixed k in order to fulfil condition (2) of the representation.

Lemma 50 *(discrete Fourier transformation) The eigenvector $|\phi\rangle$ of the translation operator $\hat{T}$ is given by*

$$|\phi\rangle = \frac{1}{\sqrt{N}} \sum_{m=1}^{N} e^{ikm} |m\rangle \tag{A.7}$$

with the additional condition $kN = 2\pi\mathbb{Z}$.

Proof. Since any element $|\phi\rangle \in \mathfrak{H}_{ext}$ can be written in the form $|\phi\rangle = \sum_{m=1}^{N} a_m(\phi) |m\rangle$, we can act with $\hat{T}(1)$ on $|\phi\rangle$ and obtain

$$\hat{T}(1) |\phi\rangle = \lambda_1 |\phi\rangle \tag{A.8}$$

$$\Rightarrow \sum_{m=1}^{N} a_m(\phi) |m+1\rangle = e^{-ik} \sum_{m=1}^{N} a_m(\phi) |m\rangle . \tag{A.9}$$

We note that $|N+1\rangle \equiv |1\rangle$ by group properties and thus $e^{ikN} = 1$ from the eigenvalue equation. This imposes the condition $kN = 2\pi\mathbb{Z}$. Moreover, by comparing the left and right-hand side of the equation we get the recursion formula

$$a_m(\phi) = e^{ik} a_{m-1}(\phi), \tag{A.10}$$

which inductively yields $a_m(\phi) = e^{ikm} a_0$. We arrive at the solution

$$|\phi\rangle = a_0 \sum_{m=1}^{N} e^{ikm} |m\rangle . \tag{A.11}$$

By normalizing $|\phi\rangle$, i.e. $\|\phi\| = 1$, we calculate $a_0 = \frac{1}{\sqrt{N}}$ up to some irrelevant phase factor. All this proves that

$$|\phi\rangle = \frac{1}{\sqrt{N}} \sum_{m=1}^{N} e^{ikm} |m\rangle \tag{A.12}$$

is a solution of the eigenvalue equation for $\hat{T}$. ■

Definition 51 *(Bloch state)*

$$|k\rangle := \frac{1}{\sqrt{N}} \sum_{m=1}^{N} e^{ikm} |m\rangle$$

k takes values in the Brillouin zone ($\mathcal{BZ}$).

Remark 52 *Similar expressions for $|k\rangle$ appear in Bravais lattices with a tight binding (tight–binding–model).*

We can rewrite $|\Psi_n(k)\rangle$ in the form

$$|\Psi_n(k)\rangle = |k\rangle \otimes \underbrace{\left(A_n(k)\,|A\rangle + B_n(k)\,|B\rangle\right)}_{|u_n(k)\rangle}. \tag{A.13}$$

Projecting out the relevant part of the Hamiltonian $\hat{H}(k) := \langle k|\,\hat{H}\,|k\rangle$, we have the following eigenvalue equation

$$\hat{H}(k)\,|u_n(k)\rangle = \langle k|\,\hat{H}\,|k\rangle\,|u_n(k)\rangle = \langle k|\,\hat{H}\,|\Psi_n(k)\rangle = E_n(k)\,|u_n(k)\rangle\,. \tag{A.14}$$

This reduces the diagonalization to a 2×2–matrix problem.

A.2 Momentum space Hamiltonian

For matrix elements of $\hat{H}(k) = \sum_{\alpha,\beta} \langle k,\alpha|\,\hat{H}\,|k,\beta\rangle\,|\alpha\rangle\,\langle\beta|$ we observe

$$\langle k,\alpha|\,\hat{H}\,|k,\beta\rangle = \sum_{i=1}^{N} \left(v\,\langle k,\alpha|i,A\rangle\,\langle i,B|k,\beta\rangle + w\,\langle k,\alpha|i+1,A\rangle\,\langle i,B|k,\beta\rangle + h.c.\right), \tag{A.15}$$

and

$$\langle k,\alpha|m,\gamma\rangle = \langle k|m\rangle\,\langle\alpha|\gamma\rangle = \frac{1}{\sqrt{N}} e^{-ikm}\delta_{\alpha\gamma}. \tag{A.16}$$

From that we compute

$$\langle k,\alpha|\,\hat{H}\,|k,\beta\rangle = \sum_{i=1}^{N} \left(\frac{v}{N}\delta_{\alpha A}\delta_{\beta B} + \frac{w}{N}e^{-ik}\delta_{\alpha A}\delta_{\beta B} + \frac{v}{N}\delta_{\alpha B}\delta_{\beta A} + \frac{w}{N}e^{ik}\delta_{\alpha B}\delta_{\beta A}\right) \tag{A.17}$$

$$= v\delta_{\alpha A}\delta_{\beta B} + v\delta_{\alpha B}\delta_{\beta A} + we^{-ik}\delta_{\alpha A}\delta_{\beta B} + we^{ik}\delta_{\alpha B}\delta_{\beta A} \tag{A.18}$$

Summing over the non–vanishing terms, gives finally

$$\hat{H}(k) = \left(v\,|A\rangle\,\langle B| + h.c.\right) + \left(we^{-ik}\,|A\rangle\,\langle B| + h.c.\right) \tag{A.19}$$

$$= \begin{pmatrix} 0 & v + we^{-ik} \\ v + we^{ik} & 0 \end{pmatrix} \square \tag{A.20}$$

Appendix B

Geometry and Topology

B.1 Gauge field Geometry

B.1.1 Curvature and Wilson loop - A proof

First, we apply the BCH-formula $\exp(A)\exp(B) = \exp(A + B + \frac{1}{2}[A, B] + \dots)$ to

$$
\begin{aligned}
&\mathcal{W}(\mathcal{C}_\square) = \exp(W^\dagger)\exp(Z^\dagger)\exp(Y)\exp(X) \\
&= \exp(W^\dagger + Z^\dagger + \frac{1}{2}[W^\dagger, Z^\dagger] + \dots)\exp(X + Y + \frac{1}{2}[X, Y] + \dots) \\
&= \exp(W^\dagger + Z^\dagger + X + Y + \frac{1}{2}\left([Y, X] + [W^\dagger, Z^\dagger]\right) + \frac{1}{2}[W^\dagger + Z^\dagger, X + Y] + \mathcal{O}(a^3)) \\
&= \exp(W^\dagger + Z^\dagger + X + Y + \frac{1}{2}([Y, X] + [W^\dagger, Z^\dagger] + [W^\dagger, X] + [W^\dagger, Y] + [Z^\dagger, X] + [Z^\dagger, Y]) + \mathcal{O}(a^3))
\end{aligned}
$$

$$X + Z^\dagger = -ia^2\partial_\nu \mathcal{A}_\mu(x) + \mathcal{O}(a^3) \tag{B.1}$$

$$Y + W^\dagger = ia^2\partial_\mu \mathcal{A}_\nu(x) + \mathcal{O}(a^3) \tag{B.2}$$

$$[Y, X] = a^2[\mathcal{A}_\mu, \mathcal{A}_\nu](x) + \mathcal{O}(a^3) \tag{B.3}$$

$$[W^\dagger, Z^\dagger] = a^2[\mathcal{A}_\mu, \mathcal{A}_\nu](x) + \mathcal{O}(a^3) \tag{B.4}$$

$$[W^\dagger, X] = a^2[\mathcal{A}_\nu, \mathcal{A}_\mu](x) + \mathcal{O}(a^3) \tag{B.5}$$

$$[W^\dagger, Y] = a^2[\mathcal{A}_\nu, \mathcal{A}_\nu](x) = 0(+\mathcal{O}(a^3)) \tag{B.6}$$

$$[Z^\dagger, X] = a^2[\mathcal{A}_\mu, \mathcal{A}_\mu](x) = 0(+\mathcal{O}(a^3)) \tag{B.7}$$

$$[Z^\dagger, Y] = -a^2[\mathcal{A}_\nu, \mathcal{A}_\mu](x) + \mathcal{O}(a^3) \tag{B.8}$$

X, Y, Z, W are given in (2.56)-(2.59). Plugging above terms into the exponential expression amounts to

$$\mathcal{W}(\mathcal{C}_\square) = \exp(ia^2(\partial_\mu \mathcal{A}_\nu - \partial_\nu \mathcal{A}_\mu) + a^2[\mathcal{A}_\mu, \mathcal{A}_\mu] + \mathcal{O}(a^3)) \tag{B.9}$$

$$= \exp(ia^2 \mathcal{F}_{\mu\nu} + \mathcal{O}(a^3)), \tag{B.10}$$

where the definition $\mathcal{F}_{\mu\nu} = \partial_\mu \mathcal{A}_\nu - \partial_\nu \mathcal{A}_\mu - i[\mathcal{A}_\mu, \mathcal{A}_\nu]$ has been used. The difference between mathematical (M) and physical (P) nomenclature is

$$\mathcal{A}_\mu^{(P)} = i\mathcal{A}_\mu^{(M)}, \tag{B.11}$$

$$\mathcal{F}_{\mu\nu}^{(P)} = i\mathcal{F}_{\mu\nu}^{(M)}. \tag{B.12}$$

The mathematical convention has a more symmetric structure

$$\mathcal{F}_{\mu\nu}^{(M)} = \partial_\mu \mathcal{A}_\nu^{(M)} - \partial_\nu \mathcal{A}_\mu^{(M)} + [\mathcal{A}_\mu^{(M)}, \mathcal{A}_\nu^{(M)}]. \tag{B.13}$$

B.1.2 Gauge Fields on Manifolds

Let $\{U_i | i \in I\}$ be a collection of charts covering manifold $\mathcal{M}$. A gauge field $\mathcal{A}$ is a $\mathfrak{g}$–valued one-form on $\mathcal{M}$, defined by

$$\mathcal{A}^{(i)} = \mathcal{A}|U_i, \quad \mathcal{A}^{(i)} \in \mathfrak{g} \otimes \Omega^1(U_i). \tag{B.14}$$

The compatibility condition on overlapping charts requires gauge-equivalence ($\sim$):

$$\forall i, j : U_i \cap U_j \neq \emptyset : \mathcal{A}^{(i)} \sim \mathcal{A}^{(j)}, \tag{B.15}$$

$$\mathcal{A}^{(i)}(x) = Ad_{g_{ij}(x)} \mathcal{A}^{(j)}(x) + g_{ij}(x) dg_{ij}^{-1}(x), \quad \forall x \in U_i \cap U_j, \tag{B.16}$$

where $g_{ij} \colon U_i \cap U_j \to G$ and Ad_g is the adjoint map. With reference to specific coordinates we have $\mathcal{A}^{(i)}(x_{(i)})$ on U_i and $\mathcal{A}^{(j)}(x_{(j)})$ on U_j. Now let $x_{(i)} \in U_i \cap U_j$ and express $\mathcal{A}^{(j)}$ in terms of $x_{(i)}$

$$\mathcal{A}_\mu^{(j)}(x_{(i)}) = \frac{\partial x_{(j)}^\nu}{\partial x_{(i)}^\mu} \mathcal{A}_\nu^{(j)}(x_{(j)}). \tag{B.17}$$

This is the usual transformation rule for rank one tensors.

Sphere manifolds $\mathbb{S}^n$

We apply the above results consequently to gauge fields on spheres $\mathbb{S}^n$. A sphere must be covered by (at least) 2 charts, since it is compact. Therefore, one can write $\mathbb{S}^n = U_1 \cup U_2$ and the coordinates of both charts are related by stereographic projection at the intersection

$$\mathbf{r}_{(2)} = \frac{\mathbf{r}_{(1)}}{\left\|\mathbf{r}_{(1)}\right\|^2}. \tag{B.18}$$

Inserting Eq. (B.18) into (B.17) yields ($\mathbf{r}_{(1)} \neq 0$)

$$\mathcal{A}^{(2)}_\mu(\mathbf{r}_{(1)}) = \frac{\partial r^\nu_{(2)}}{\partial r^\mu_{(1)}} \mathcal{A}^{(2)}_\nu(\mathbf{r}_{(2)}) \tag{B.19}$$

$$= \frac{1}{\left\|\mathbf{r}_{(1)}\right\|^2} \left(\delta^\nu_\mu - \frac{2 r^\mu_{(1)} r^\nu_{(1)}}{\left\|\mathbf{r}_{(1)}\right\|^2} \right) \mathcal{A}^{(2)}_\nu \left(\frac{\mathbf{r}_{(1)}}{\left\|\mathbf{r}_{(1)}\right\|^2} \right) \tag{B.20}$$

$$= \frac{1}{\left\|\mathbf{r}_{(1)}\right\|^2} \left(\delta^\nu_\mu - \frac{2 r^\mu_{(1)} r^\nu_{(1)}}{\left\|\mathbf{r}_{(1)}\right\|^2} \right) \left(K_\nu + \mathcal{O}\left(\left\|\mathbf{r}_{(1)}\right\|^{-2} \right) \right), \tag{B.21}$$

with constants $K_\nu \in \mathfrak{g}$ and the expansion has been made for large values $\left\|\mathbf{r}_{(1)}\right\|$. From this we see that $\mathcal{A}^{(2)}_\mu(\mathbf{r}_{(1)}) \to 0$ for $\left\|\mathbf{r}_{(1)}\right\| \to \infty$. Combining this result with Eq. (B.16) implies

$$\mathcal{A}^{(1)}_\mu(\mathbf{r}_{(1)}) \sim \mathcal{A}^{(2)}_\mu(\mathbf{r}_{(1)}) = 0, \quad \left\|\mathbf{r}_{(1)}\right\| \to \infty. \tag{B.22}$$

Hence, $\mathcal{A}(x)$ is gauge–equivalent to a zero-field for $\|x\| \to \infty$ or, equivalently via (B.16)

$$\mathcal{A}(x) = g(x) d g^{-1}(x), \quad \|x\| \to \infty. \tag{B.23}$$

A zero-field has field strength $\mathcal{F} = 0$ (Berry curvature). In particular, $\mathcal{F}(x) \to \mathcal{F}^g(x) = Ad_{g(x)} \mathcal{F}(x) = g(x) \mathcal{F}(x) g^{-1}(x) = 0$ for $\|x\| \to \infty$. Altogether the discussion proves

Claim 53 *A gauge field $\mathcal{A}$ on $\mathbb{S}^n$ can be seen as a gauge field on $\mathbb{R}^n$ which behaves like the zero–field at infinity, i.e.* (B.23) *holds. By compactification $\mathbb{R}^n \cup \{\infty\} = \mathbb{S}^n$ the reverse statement holds. One interprets*

$$\mathcal{A}|\mathbb{S}^n \Leftrightarrow \mathcal{A}|\mathbb{R}^n : \mathcal{A}(x) = g(x) d g^{-1}(x), \quad \|x\| \to \infty.$$

B.2 Results in Algebraic and Differential Topology

This appendix offers a short collection of the ubiquitous topological tools used for this work. We refer the reader to [25, 33, 37, 38, 51] for a more detailed study of the material.

B.2.1 Basics of Homotopy

Let $f, g\colon X \to Y$ be maps of topological spaces X, Y. If there exists a map $H\colon X \times [0,1] \to Y$ such that $H(x,0) = f(x)$ and $H(x,1) = g(x)$, then they are called homotopic maps $f \sim g$. Homotopy of maps $X \to Y$ induces an equivalence relation and we can group homotopic maps in classes - the set of homotopy classes from X into Y is denoted by $\{X, Y\}$. The spaces X, Y are considered homotopic, $X \sim Y$, if there exist maps $f\colon X \to Y$ and $g\colon Y \to X$ such that $f \circ g \sim 1_Y$ and $g \circ f \sim 1_X$. Maps which are homotopic to the constant map are called *null–homotopic*.

Of importance are $\pi_n(X) := \{(\mathbb{S}^n, s), (X, b)\}$ which describe homotopy classes of base point preserving maps $\mathbb{S}^n \to X$, $s \to b$ (b: base point). $\pi_n(X)$ carries a natural group structure, and it is therefore called *homotopy group* for $n \geq 1$. For $n = 0$ the set provides the connected components of X. One fundamental result is frequently used: If two spaces X, Y are homotopic ($X \sim Y$), then their homotopy groups are isomorphic $\pi_n(X) \cong \pi_n(Y)$.

Fibrations, Fibre Bundles. The data structure (E, π, B, F) is a fibration if $\pi\colon E \to B$ is a surjective map (*projection*) and all the fibres $\pi^{-1}(b)$ are homeomorphic to F, i.e. $F \cong \pi^{-1}(b)$. B is the *base space*, E the *total space* and F the *fibre*. If there exist open sets $U_i \subset B$ such that $\pi^{-1}(U_i) \cong U_i \times F$, then it is called a *locally trivial* fibration or fibre bundle. The bundle is *globally trivial* if $E = B \times F$. Most of the fibrations considered in this work turn out to be principal bundles of the type $(X, \pi, X/G, G)$, where fibre F is identical to some Lie group G that acts on a space X.

B.2.2 Homology and Cohomology

We regard $\mathcal{M}$ as a manifold and define (singular) homology and de Rham cohomology (based on differential forms).

Homology

Definition 54 *Let G be an abelian group, i.e. $\mathbb{R}$ or $\mathbb{Z}$, and let $\Delta^k := (v_0, \ldots, v_k)$ represent a k–dimensional simplex. The k–th chain group is given by $C_k(\mathcal{M}) := \left\{\sum_i a_i \sigma_i | \sigma \colon \Delta^k \to \mathcal{M}, a_i \in G\right\}$*

The boundary operator defines a homomorphism $\partial_k \colon C_k(\mathcal{M}) \to C_{k-1}(\mathcal{M})$. This operator acts as $\partial\sigma(v_0, \ldots, v_k) := \sum_i (-1)^i \sigma(v_0, \ldots, \hat{v}_i, \ldots, v_k)$. The cycle group is $Z_k(\mathcal{M}) := \ker \partial_k$ and the boundary group is $B_k(\mathcal{M}) := \mathrm{Im}(\partial_{k+1})$, $B_k(\mathcal{M}) \subset Z_k(\mathcal{M})$. The *homology groups* are defined as quotients $H_k(\mathcal{M}) := Z_k(\mathcal{M})/B_k(\mathcal{M})$. A map $f \colon \mathcal{M} \to \mathcal{N}$ induces a homomorphism $f_\# \colon C_k(\mathcal{M}) \to C_k(\mathcal{N})$, which commutes with the boundary operator, $\partial \circ f_\# = f_\# \circ \partial$. Thus, cycles are mapped into cycles, and boundaries into boundaries. One concludes that there exists a well defined homomorphism $f_* \colon H_k(\mathcal{M}) \to H_k(\mathcal{N})$ given by $f_*[A] := [f_\#(A)]$. A fundamental and frequently used result of the theory is [38]: Homotopic spaces $\mathcal{M} \sim \mathcal{N}$ have isomorphic homology groups, $H_k(\mathcal{M}) \cong H_k(\mathcal{N})$. We consider homology groups over $\mathbb{R}$ for the rest of the discussion.

Cohomology

$\Omega^r(\mathcal{M})$ denotes the vector space of r-forms on $\mathcal{M}$, where the general form of an r-form is given by $\omega = \frac{1}{r!}\omega_{\mu_1 \cdots \mu_r} dx^{\mu_1} \wedge \cdots \wedge dx^{\mu_r}$. Here, we have a map $d_r \colon \Omega^r(\mathcal{M}) \to \Omega^{r+1}(\mathcal{M})$ (exterior derivative): $d\omega = \frac{1}{r!}(\partial_\lambda \omega_{\mu_1 \cdots \mu_r}) dx^\lambda \wedge dx^{\mu_1} \wedge \cdots \wedge dx^{\mu_r}$. $Z^r(\mathcal{M}) := \ker(d_r)$ is the space of closed r-forms, and $B^r(\mathcal{M}) := \mathrm{Im}(d_{r-1})$ is the space of exact r-forms. We have $B^r(\mathcal{M}) \subset Z^r(\mathcal{M})$, since $d \circ d = 0$. *De Rham cohomology groups* are defined by the quotient $H^r(\mathcal{M}) := Z^r(\mathcal{M})/B^r(\mathcal{M})$. It follows from differential geometry that a (smooth) map $f \colon \mathcal{M} \to \mathcal{N}$ between manifolds yields

a pullback map $f^*\colon \Omega^r(\mathcal{N}) \to \Omega^r(\mathcal{M})$ (adjoint linear map) which has the property $d \circ f^* = f^* \circ d$ (see Figure B.1). By a similar reasoning as before, we can assign a well-defined homomorphism $f^*\colon H^r(\mathcal{N}) \to H^r(\mathcal{M})$.

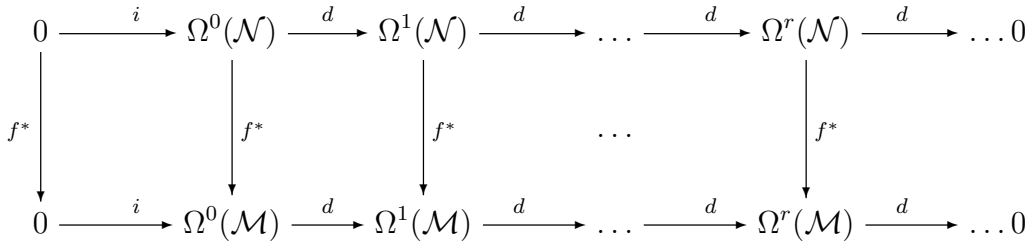

Figure B.1: Cohomology ladder diagram. Sub-diagrams are commutative due to $d \circ f^* = f^* \circ d$

Pairing and De Rham theorem. The connection between homology and (de Rham) cohomology groups is the pairing $(\cdot,\cdot)\colon H^k(\mathcal{M}) \times H_k(\mathcal{M}) \to \mathbb{R}$, defined as an integral $([\omega],[c]) := \int_c \omega$ of the closed k-form ω over a k-cycle c. De Rham's theorem asserts that $H_k(\mathcal{M})$ and $H^k(\mathcal{M})$ are dual to each other for compact manifolds, $H_k(\mathcal{M}) \cong H^k(\mathcal{M})$.

B.3 Berry Curvature - Merging QM and Topology

We derive here the Berry curvature formula for the case of non–degenerate energy eigenstates of the Hamiltonian. The more involved case of a degenerate energy spectrum is discussed to some extent in the main text. If we take $n \equiv n(\mathbf{R})$ for a band state, then it is possible to express the components of the Berry curvature as

$$\mathcal{F}^{(n)}_{\mu\nu}(\mathbf{R}) = i[\langle \nabla_\mu n | \nabla_\nu n\rangle - \langle \nabla_\nu n | \nabla_\mu n\rangle] \tag{B.24}$$

$$= i \sum_m [\langle \nabla_\mu n | m\rangle \langle m | \nabla_\nu n\rangle - \langle \nabla_\nu n | m\rangle \langle m | \nabla_\mu n\rangle] \tag{B.25}$$

Consider the following set of equations, starting from the eigenvalue equation

$$\hat{H}\left|n\right\rangle = E_n\left|n\right\rangle, \tag{B.26}$$

$$(\nabla\hat{H})\left|n\right\rangle + \hat{H}\nabla\left|n\right\rangle = (\nabla E_n)\left|n\right\rangle + E_n\nabla\left|n\right\rangle. \tag{B.27}$$

For states $|m\rangle \neq |n\rangle$ ($\langle m|n\rangle = 0$) we use the scalar product and obtain

$$\left\langle m\right|\nabla\hat{H}\left|n\right\rangle + \underbrace{\left\langle m\right|\hat{H}\nabla\left|n\right\rangle}_{E_m\langle m|\nabla|n\rangle} = E_n\left\langle m|\nabla n\right\rangle \tag{B.28}$$

$$\Rightarrow \left\langle m\right|\nabla\hat{H}\left|n\right\rangle = (E_n - E_m)\left\langle m|\nabla n\right\rangle. \tag{B.29}$$

Thus, the contributions in the sum (B.25) can be written as

$$\left\langle \nabla n|m\right\rangle\left\langle m|\nabla n\right\rangle = \frac{\left\langle n\right|\nabla\hat{H}\left|m\right\rangle\left\langle m\right|\nabla\hat{H}\left|n\right\rangle}{(E_n - E_m)^2}, \quad n \neq m. \tag{B.30}$$

In order to explain why contributions for $n = m$ cancel, observe that $\langle n|n\rangle = 1$ holds. This yields $\nabla(\langle n|n\rangle) = 0$, and consequently $\langle\nabla n|n\rangle + \langle n|\nabla n\rangle = 0$. By inserting Eq. (B.30) into (B.25) we get the celebrated formula for the Berry curvature

$$\mathcal{F}^{(n)}_{\mu\nu}(\mathbf{R}) = i\sum_{m\neq n}\frac{\left\langle n\right|\nabla_\mu\hat{H}\left|m\right\rangle\left\langle m\right|\nabla_\nu\hat{H}\left|n\right\rangle - (\mu\leftrightarrow\nu)}{(E_n - E_m)^2}. \tag{B.31}$$

According to my knowledge, a similar formula appeared for the first time in the work of Thouless et al. [54]. It is an integral part of the so called TKNN invariant for the IQH effect ($\mathbb{Z}$–quantized Hall conductance).

- For band touching points $\mathbf{R}^* \in \mathcal{M}$: $E_n(\mathbf{R}^*) = E_m(\mathbf{R}^*), m \neq n$ the formula (B.31) develops singularities. This is not a surprise since we have derived it with respect to non-degeneracy over a component of the parameter space.

- The sum over all Berry curvatures vanishes identically: $\sum_n \mathcal{F}^{(n)}_{\mu\nu} = 0$. If we integrate this result over some surface $\mathcal{S}$, we obtain for the Chern numbers $\int_{\mathcal{S}}\sum_n \mathcal{F}^{(n)} = 2\pi\sum_n \mathcal{C}^{(n)} = 0$. $\mathcal{F}^{(n)}$ denotes the Berry curvature 2-form for band or level number n.

Appendix C

Symmetries of Hamiltonians

The symmetries discussed here underlie the classification of topological insulators. In particular, our focus will be on their effect on band structures as proposed in the main text. A symmetry of a Hamiltonian $\hat{H}$ is given by a map $\hat{H} \to \hat{S}\hat{H}\hat{S}^\dagger$ where $\hat{S}$ can be either a unitary or anti–unitary operator due to Wigner's theorem (see [40] for a proof). Anti–unitary operators can be always written as a product $\hat{U}K$ where $\hat{U}$ is unitary and K denotes complex conjugation operation.

C.1 Time Reversal Symmetry (TR)

TR is given by the transformation $t \to -t$. If the *real space Hamiltonian* $\hat{H}$ is invariant under TR, then, using the Schrödinger equation one sees immediately that the time–reversal operator must be anti–unitary

$$\hat{\mathcal{T}} = \hat{U}_\mathsf{T} K, \quad \hat{\mathcal{T}}\hat{\mathcal{T}}^\dagger = \hat{\mathbb{1}}, \quad \hat{\mathcal{T}}\hat{H}\hat{\mathcal{T}}^\dagger = \hat{H}. \tag{C.1}$$

We derive some properties. Consecutive operation of $\hat{H}$ and $\hat{\mathcal{T}}$ on an arbitrary state $|\psi\rangle$ yields

$$\hat{\mathcal{T}}\hat{H}|\psi\rangle = \hat{U}_\mathsf{T} K \hat{H}|\psi\rangle = \hat{U}_\mathsf{T}\hat{H}^*|\psi\rangle^* = \hat{U}_\mathsf{T}\hat{H}^*\hat{U}_\mathsf{T}^\dagger\hat{U}_\mathsf{T}K|\psi\rangle = \hat{U}_\mathsf{T}\hat{H}^*\hat{U}_\mathsf{T}^\dagger\hat{\mathcal{T}}|\psi\rangle \tag{C.2}$$

$$\Rightarrow \hat{\mathcal{T}}\hat{H}\hat{\mathcal{T}}^\dagger = \hat{U}_\mathsf{T}\hat{H}^*\hat{U}_\mathsf{T}^\dagger = \hat{H}. \tag{C.3}$$

For the momentum–space Hamiltonian $\hat{H}(\mathbf{k})$ the transformation $t \to -t$ leads to $\mathbf{k} \to -\mathbf{k}$:

$$\hat{\mathcal{T}}\hat{H}(\mathbf{k})\mathcal{T}^{\dagger} = \hat{U}_{\mathsf{T}}\hat{H}^{*}(\mathbf{k})\hat{U}_{\mathsf{T}}^{\dagger} = \hat{H}(-\mathbf{k}). \tag{C.4}$$

Applying the $\hat{\mathcal{T}}$–operator twice to a state must return a physically equivalent state - i.e. $\hat{\mathcal{T}}^2 = e^{i\varphi}$. So, $\hat{U}_{\mathsf{T}}K\hat{U}_{\mathsf{T}}K = \hat{U}_{\mathsf{T}}\hat{U}_{\mathsf{T}}^{*} = e^{i\varphi}$. Thus,

$$\hat{U}_{\mathsf{T}}\underbrace{\hat{U}_{\mathsf{T}}^{*}\hat{U}_{\mathsf{T}}}_{e^{-i\varphi}}\hat{U}_{\mathsf{T}}^{*} = e^{i2\varphi} \Rightarrow e^{-i\varphi}\hat{U}_{\mathsf{T}}\hat{U}_{\mathsf{T}}^{*} = \hat{\mathbb{1}} = e^{i2\varphi}. \tag{C.5}$$

This implies $e^{i\varphi} = \pm 1$ as the only two possibilities or, equivalently $\hat{\mathcal{T}}^2 = \pm\hat{\mathbb{1}}$.

Lemma 55 *(Kramer's degeneracy) Let $\hat{H}\left|\psi\right\rangle = E\left|\psi\right\rangle$ be the eigenvalue equation and $[\hat{H}, \hat{\mathcal{T}}] = 0$ such that $\hat{\mathcal{T}}^2 = -\mathbb{1}$ (fermionic condition) holds. Then the states $\left|\psi\right\rangle$ and $\hat{\mathcal{T}}\left|\psi\right\rangle$ are orthogonal,*

$$\langle\psi|\hat{\mathcal{T}}\psi\rangle = 0. \tag{C.6}$$

Hence, each Hilbert space $\mathfrak{H}_E$ is at (least) double degenerate, $\dim\mathfrak{H}_E \geq 2$.

Proof. $\hat{\mathcal{T}}\left|\psi\right\rangle$ is an eigenstate to E since $[\hat{H}, \hat{\mathcal{T}}] = 0$. We write

$$\langle\psi|\hat{\mathcal{T}}\psi\rangle = \langle\psi|\hat{\mathcal{T}}^{\dagger}\underbrace{\hat{\mathcal{T}}\hat{\mathcal{T}}}_{-\mathbb{1}}\psi\rangle = -\langle\psi|\hat{\mathcal{T}}^{\dagger}\psi\rangle = -\langle\hat{\mathcal{T}}\psi|\psi\rangle^{*} = -\langle\psi|\hat{\mathcal{T}}\psi\rangle,$$

where use has been made of the fact that $\hat{\mathcal{T}}$ is anti-unitary. Hence, $\langle\psi|\hat{\mathcal{T}}\psi\rangle = 0$. ■

C.2 Particle–Hole Symmetry (PH)

PH symmetry stems from the existence of particles (occupied states/sites) and holes (unoccupied states/sites). It is represented by an anti–unitary operator, however, with the difference that it anticommutes with the Hamiltonian due to the fact that unoccupied states carry the opposite energy of the occupied ones.

$$\hat{\mathcal{P}}\hat{H}\hat{\mathcal{P}}^{\dagger} = -\hat{H} \tag{C.7}$$

In the same way as for TR symmetry we get, by setting $\hat{\mathcal{P}} = \hat{U}_{\mathsf{P}}K$,

$$\hat{\mathcal{P}}\hat{H}\hat{\mathcal{P}}^{\dagger} = \hat{U}_{\mathsf{P}}\hat{H}^{*}\hat{U}_{\mathsf{P}}^{\dagger} = -\hat{H}. \tag{C.8}$$

The effect on the Fourier transformed Hamiltonian is

$$\hat{\mathcal{P}}\hat{H}(\mathbf{k})\hat{\mathcal{P}}^{\dagger} = \hat{U}_{\mathsf{P}}\hat{H}^{*}(\mathbf{k})\hat{U}_{\mathsf{P}}^{\dagger} = -\hat{H}(-\mathbf{k}). \tag{C.9}$$

The crucial point is an effect on the energy spectrum or band structure of $\hat{H}(\mathbf{k})$. Assume you have a (positive) band $E^{(+)}(\mathbf{k}) > 0$, then there must exist a (negative) band $E^{(-)}(\mathbf{k})$ such that $E^{(-)}(-\mathbf{k}) = -E^{(+)}(\mathbf{k})$ holds (reflection symmetry with respect to the zero point). This can be used as a check for PH symmetry once the full band structure of the system has been computed or measured.

C.3 Sublattice Symmetry (SL)

SL symmetry is also known, depending on the context, as chiral symmetry. The corresponding, now unitary operator $\hat{\mathcal{S}}$, anticommutes with $\hat{H}$ and the symmetry condition is

$$\hat{\mathcal{S}}\hat{H}\hat{\mathcal{S}}^{\dagger} = -\hat{H}, \tag{C.10}$$

as e.g. in the SSH lattice. Forming the product $\hat{\mathcal{P}} \cdot \hat{\mathcal{T}}$ is one way of constructing such an $\hat{\mathcal{S}}$ operator. This implies that a system with both TR and PH symmetry has also SL symmetry. At the momentum-space level we have

$$\hat{\mathcal{S}}\hat{H}(\mathbf{k})\hat{\mathcal{S}}^{\dagger} = -\hat{H}(\mathbf{k}). \tag{C.11}$$

Let $\hat{\mathcal{S}} = \hat{\mathcal{P}} \cdot \hat{\mathcal{T}} = \hat{U}_{\mathsf{P}}\hat{U}_{\mathsf{T}}^{*}$, then $\hat{\mathcal{S}}\hat{H}(\mathbf{k})\hat{\mathcal{S}}^{\dagger} = \hat{\mathcal{P}}\hat{\mathcal{T}}\hat{H}(\mathbf{k})\hat{\mathcal{T}}^{\dagger}\hat{\mathcal{P}}^{\dagger} = \hat{\mathcal{P}}\hat{H}(-\mathbf{k})\hat{\mathcal{P}}^{\dagger} = -\hat{H}(\mathbf{k})$, which demonstrates that SL symmetry follows from TR and PH symmetry. However, it should be noted that the reverse statement is not true in general - i.e. there can exist systems with SL symmetry but no TR and no PH symmetry. The effect of SL symmetry on $\hat{H}(\mathbf{k})$ is a fully symmetric band structure about $\mathcal{BZ}$. If $E^{(+)}(\mathbf{k}) > 0$ is a positive band, then there exists a negative band $E^{(-)}(\mathbf{k})$ such that $E^{(-)}(\mathbf{k}) = -E^{(+)}(\mathbf{k}), \forall \mathbf{k} \in \mathcal{BZ}$.

C.4 Altland– Zirnbauer classification

TRS	PHS	SLS	Cartan label	Coset space of Hamiltonian
0	0	0	A	$U(n+m)/(U(n)\times U(m)) = \mathbb{G}_{m,n+m}(\mathbb{C})$
1	0	0	AI	$O(n+m)/(O(n)\times O(m)) = \mathbb{G}_{m,n+m}(\mathbb{R})$
-1	0	0	AII	$Sp(n+m)/(Sp(n)\times Sp(m))$
0	0	1	AIII	$(U(n)\times U(n))/U(n)$
1	1	1	BDI	$(O(n)\times O(n))/O(n)$
-1	-1	1	CII	$(Sp(n)\times Sp(n))/Sp(n)$
0	1	0	D	$O(2n)/U(n)$
0	-1	0	C	$Sp(2n)/U(n)$
-1	1	1	DIII	$U(2n)/Sp(2n)$
1	-1	1	CI	$U(n)/O(n)$

Table C.1: "10–fold way". Altland-Zirnbauer table [2, 20, 30] for the ten symmetry classes of Hamiltonians according to time–reversal (TR), particle–hole (PH) and sublattice (SL) symmetry. The numbers $0, \pm 1$ denote absence, presence of the symmetry, respectively. Moreover, ± 1 refers to the properties $\hat{\mathcal{T}}^2 = \pm \mathbb{1}$ and $\hat{\mathcal{P}}^2 = \pm \mathbb{1}$. Note that the cosets are homogeneous spaces, represented as quotients G/H of two Lie groups G and H.

Appendix D

Representation of spin operators

Using the notation $\hat{\mathcal{S}} = (\hat{S}_x, \hat{S}_y, \hat{S}_z) = (\hat{S}_1, \hat{S}_2, \hat{S}_3)$, the spin operators respect the usual commutator relations of the $\mathfrak{su}(2)$ algebra:

$$[\hat{S}_i, \hat{S}_j] = i\epsilon_{ijk}\hat{S}_k. \tag{D.1}$$

To make a connection to a spin j representation it is useful to introduce ladder operators

$$\hat{S}_\pm := \hat{S}_x \pm i\hat{S}_y. \tag{D.2}$$

The inverse transformations are given by

$$\hat{S}_x = \frac{1}{2}(\hat{S}_+ + \hat{S}_-) \tag{D.3}$$

$$\hat{S}_y = \frac{1}{2i}(\hat{S}_+ - \hat{S}_-) \tag{D.4}$$

This transforms the standard Lie algebra basis into a Cartan–Weyl basis which is simpler to deal with

$$[\hat{S}_z, \hat{S}_+] = +\hat{S}_+ \tag{D.5}$$

$$[\hat{S}_z, \hat{S}_-] = -\hat{S}_- \tag{D.6}$$

$$[\hat{S}_+, \hat{S}_-] = 2\hat{S}_z \tag{D.7}$$

Operating on the spin j basis $\{|j, m\rangle\}$ we obtain

$$\hat{S}_\pm |j, m\rangle \propto |j, m \pm 1\rangle \tag{D.8}$$

$$\hat{S}_z |j, m\rangle \propto |j, m\rangle \tag{D.9}$$

More explicitly, we get the following matrix elements for an arbitrary spin j representation

$$\langle j, m'| \hat{S}_+ |j, m\rangle = \sqrt{j(j+1) - mm'}\delta_{m',m+1} \tag{D.10}$$

$$\langle j, m'| \hat{S}_- |j, m\rangle = \sqrt{j(j+1) - mm'}\delta_{m',m-1} \tag{D.11}$$

$$\langle j, m'| \hat{S}_z |j, m\rangle = m\delta_{m',m} \tag{D.12}$$

$$\langle j, m'| \hat{S}_x |j, m\rangle = \frac{1}{2}\sqrt{j(j+1) - mm'}(\delta_{m',m+1} + \delta_{m',m-1}) \tag{D.13}$$

$$\langle j, m'| \hat{S}_y |j, m\rangle = \frac{1}{2i}\sqrt{j(j+1) - mm'}(\delta_{m',m+1} - \delta_{m',m-1}) \tag{D.14}$$

The specific spin 1 matrices for the states $|1, 1\rangle$, $|1, 0\rangle$ and $|1, -1\rangle$ are given below.

D.1 Spin 1 Matrices

We choose $j = 1$ and obtain following matrices for the ladder operators

$$\hat{S}_+ = \sqrt{2}\begin{pmatrix} 0 & 1 & 0 \\ 0 & 0 & 1 \\ 0 & 0 & 0 \end{pmatrix}, \quad \hat{S}_- = \hat{S}_+^\dagger = \sqrt{2}\begin{pmatrix} 0 & 0 & 0 \\ 1 & 0 & 0 \\ 0 & 1 & 0 \end{pmatrix} \tag{D.15}$$

Hence, using the inverse equations we compute

$$\hat{S}_x = \frac{1}{\sqrt{2}}\begin{pmatrix} 0 & 1 & 0 \\ 1 & 0 & 1 \\ 0 & 1 & 0 \end{pmatrix}, \quad \hat{S}_y = \frac{1}{\sqrt{2}i}\begin{pmatrix} 0 & 1 & 0 \\ -1 & 0 & 1 \\ 0 & -1 & 0 \end{pmatrix}, \quad \hat{S}_z = \begin{pmatrix} 1 & 0 & 0 \\ 0 & 0 & 0 \\ 0 & 0 & -1 \end{pmatrix}. \tag{D.16}$$

Bibliography

[1] Aharonov, Y., Anandan, J.: *Phase change during a cyclic quantum evolution*, Phys. Rev. Lett., (58):1593-1596, (1987).

[2] Altland, A., Zirnbauer, M. R.: *Nonstandard symmetry classes in mesoscopic normal–superconducting hybrid structures*, Phys. Rev. B, (55):1142, (1997).

[3] Amo, A., Lefrere, J., Pigeon, S., Adrados, C., Ciuti, C., Carusotto, I. , Houdre, R. , Giacobino, E. , Bramati, A.: *Observation of Superfluidity of Polaritons in Semiconductor Microcavities*, arXiv:0812.2748.

[4] Anderson, M. H., Ensher, J. R., Matthews, M. R., Wieman, C. E., Cornell, E. A.: *Observation of Bose-Einstein Condensation in a Dilute Atomic Vapor*, Science **269** (5221), 198-201, (1995), doi: 10.1126/science.269.5221.198.

[5] Bellissard, J., van Elst, A., Schulz- Baldes, H.: *The noncommutative geometry of the quantum Hall effect*, Journal of Mathematical Physics **35**, 5373, (1994), https://doi.org/10.1063/1.530758.

[6] Berry, M.V.: *Quantal phase factors accompanying adiabatic changes*, Proc. R. Soc. Lond. A **392**, 45-57, (1984).

[7] Berry, M.V.: *The quantum phase, five years after, Geometric phases in Physics*, World Scientific, Singapore, (1989).

[8] Berloff, N. G., Silva, M., Kalinin, K., Askitopoulos, A., Töpfer, J. D., Cilibrizzi, P., Langbein, W., Lagoudakis, P.G.: *Realizing the classical XY Hamiltonian in polariton simulators*, Nature Materials, Vol **16**, (2017), 1120-1126.

[9] Bloch, I.: *Ultracold quantum gases in optical lattices*, Nature Physics **1**, 23–30 (2005), https://doi.org/10.1038/nphys138.

[10] Bukov, M., D'Alessio, L., Polkovnikov, A.: *Universal high-frequency behaviour of periodically driven systems: from dynamical stabilization to Floquet engineering*, Advances in Physics, 64:2, 139-226, (2015), DOI: 10.1080/00018732.2015.1055918.

[11] Callaway, David J. E., Rahman, A.: *Microcanonical Ensemble Formulation of Lattice Gauge Theory*, Physical Review Letters. **49** (9): 613–616 (1982), doi:10.1103/PhysRevLett.49.613.

[12] Callaway, David J. E., Rahman, A.: *Lattice gauge theory in microcanonical ensemble*, Physical Review. D **28** (6): 1506–1514 (1983), doi:10.1103/PhysRevD.28.1506.

[13] Collins, G. P.: *Gaseous Bose–Einstein Condensate Finally Observed*, Physics Today **48**, 8, 17 (1995); https://doi.org/10.1063/1.2808119.

[14] Coxeter, H. S. M.: *Introduction to geometry*, Wiley New York, (1969).

[15] Deng, H., Solomon, G.S., Hey, R., Ploog, K.H., Yamamoto, Y.: *Spatial Coherence of a Polariton Condensate*, Phys. Rev. Lett. **99**, 126403, (2007), https://doi.org/10.1103/PhysRevLett.99.126403.

[16] Dufferwiel, S., Feng, L., Cancellieri, E. et al.: *Spin Textures of Exciton-Polaritons in a Tunable Microcavity with Large TE-TM Splitting*, Phys. Rev. Lett. **115**, 246401, (2017), https://doi.org/10.1103/PhysRevLett.115.246401.

[17] Feynman, R.P.: *Simulating physics with computers*, J. Theor. Phys., (21): 467, (1982).

[18] Fukui, T., Hatsugai, Y., Suzuki, H.: *Chern Numbers in Discretized Brillouin Zone: Efficient Method of Computing (Spin) Hall Conductances*, J. Phys. Soc. Jpn, 74(6):1674–1677, (2005), https://doi.org/10.1143/JPSJ.74.1674.

[19] Guo, H. M., Franz, M.: *Topological insulator on the kagome lattice*, Phys. Rev. B **80**, 113102, (2009), https://doi.org/10.1103/PhysRevB.80.113102.

[20] Heinzner, P., Huckleberry, A., Zirnbauer, M.R.: *Symmetry classes of disordered fermions*, Commun. Math. Phys. 257, 725-771, (2005), doi:10.1007/s00220-005-1330-9.

[21] Hirzebruch, F.: *Topological Methods in Algebraic Geometry*, Springer, Berlin, (1966).

[22] Hopf, H.: *Über die Abbildung der dreidimensionalen Sphäre auf die Kugeloberfläche*, Mathematische Annalen Bd. 104, (1931).

[23] Hu, H. et al.: *Spin-1 topological monopoles in parameter space of ultracold atoms*, arXiv:1802.08222, (2018).

[24] Hu, X., Kargarian, M., Fiete, G.A.: *Topological insulators and fractional quantum Hall effect on the ruby lattice*, Phys. Rev. B **84**, 155116, https://doi.org/10.1103/PhysRevB.84.155116.

[25] Husemoller, D.: *Fibre Bundles*, McGraw-Hill, New York, (1966).

[26] Irvine, W., Bouwmeester, D.: *Linked and knotted beams of light*, Nature Phys **4**, 716–720 (2008). https://doi.org/10.1038/nphys1056.

[27] Janson, S.: *Roots of polynomials of degree 3 and 4*, arXiv:1009.2373v1, (2010).

[28] Jiménez-García, K. et al.: *Peierls substitution in an engineered lattice potential*, Phys. Rev. Lett. **108**, 225303 (2012).

[29] Jotzu, G., Messer, M., Desbuquois, R. et al.: *Experimental realization of the topological Haldane model with ultracold fermions*, Nature **515**, 237–240 (2014), https://doi.org/10.1038/nature13915.

[30] Kitaev, A.: *Periodic Table for Topological Insulators and Superconductors*, AIP Conf. Proc. 1134 , 22, (2009).

[31] Klembt, S. et al.: *Exciton-polariton topological insulator*, arXiv:1808.03179, (2018).

[32] Kolodrubetz, M.: *Measuring the Second Chern Number from Nonadiabatic Effects*, Phys. Rev. Lett. **117**, 015301 (2016), https://doi.org/10.1103/PhysRevLett.117.015301.

[33] Lang, S.: *Differential manifolds*, Addison Wesley, London, (1972).

[34] Lewenstein, M., Sanpera, A., Ahufinger, V.: *Ultracold Atoms in Optical Lattices: Simulating Quantum Many-Body Systems*, 1st edition, Oxford Univ. Press, (2012).

[35] Loring, T. A.: *A Guide to the Bott Index and Localizer Index*, arXiv:1907.11791, (2019).

[36] Loring, T. A.: *Bulk spectrum and K-theory for infinite-area topological quasicrystals*, Journal of Mathematical Physics **60**, 081903 (2019), https://doi.org/10.1063/1.5083051.

[37] Madsen, I., Tornehave, J.: *From calculus to cohomology: de Rham cohomology and characteristic classes*, Cambridge Univ. Press, (1997).

[38] Massey, W. S.: *A basic course in algebraic topology*, Springer New York, (1991).

[39] Milnor, J., Stasheff, J.: *Characteristic Classes*, Annals of Mathematics Studies, 76. Princeton University Press, Princeton, (1974).

[40] Molnar, L.: *An Algebraic Approach to Wigner's Unitary-Antiunitary Theorem*, J. Austral. Math. Soc. (Series A) **65**, 354-369, (1998), https://doi.org/10.1017/S144678870003593X.

[41] Nalitov, A. V., Solnyshkov, D. D., Malpuech, G.: *Polariton $\mathbb{Z}$ Topological Insulator*, arXiv:1409.6564, (2014).

[42] Panzarini, G., Andreani, L.C., Armitage, A., Baxter, D., Skolnick, M. S., Astratov, V. N., Roberts, J. S., Kavokin, A. V., Vladimirova, M. R., Kaliteevski, M. A.: *Exciton–light coupling in single and coupled semiconductor microcavities: Polariton dispersion and polarization splitting*, Physical Review B **59**, 5082 (1999).

[43] Peierls, R.: *Zur Theorie des Diamagnetismus von Leitungselektronen*, Z. Physik **80**, 763–791 (1933). https://doi.org/10.1007/BF01342591

[44] Rañada, A. F.: *Knotted solutions of the Maxwell equations in vacuum*, J. Phys. A **23**, L815–L820, (1990).

[45] Rigolin, G., Ortiz, G.: *Adiabatic Perturbation Theory and Geometric Phases for Degenerate Systems*, Phys. Rev. Lett. **104**, 170406 (2010).

[46] Ruostekoski, J., Javanainen, J., Dunne, G.V.: *Manipulating atoms in an optical lattice: Fractional fermion number and its optical quantum measurement*, Physical Review A **77**, 013603 (2008).

[47] Ruseckas, J., Juzeliūnas, G., Öhberg, P., Fleischhauer, M.: *Non-Abelian Gauge Potentials for Ultracold Atoms with Degenerate Dark States*, Phys. Rev. Lett. **95**, 010404, (2005), https://doi.org/10.1103/PhysRevLett.95.010404.

[48] Sala, V.G., Solnyshkov, D.D., Carusotto, I., Jacqmin, T., Lemaitre, A., Tercas, H., Nalitov, A., Abbarchi, M., Galopin, E., Sagnes, I., Bloch, J., Malpuech, G., Amo, A.: *Spin–Orbit Coupling for Photons and Polaritons in Microstructures*, Phys. Rev. X **5**, 011034, (2015).

[49] Sanvitto D., Kena-Cohen S.: *The road towards polaritonic devices*, Nature Materials, Vol **15**, (2016), 1061-1073.

[50] Schumacher, B.: *Quantum coding*, Physical Review A **51** (4): 2738–2747 (1995), doi:10.1103/PhysRevA.51.2738.

[51] Steenrod, N.: *The Topology of Fibre Bundles*, Princeton Unversity Press, Princeton, (1951).

[52] Suchomel, H. Klembt, S., Harder, T. H., Klaas, M., Egorov, O. A., Winkler, K., Emmerling, M., Thomale, R., Höfling, S., Schneider, C.: *Platform for Electrically Pumped Polariton Simulators and Topological Lasers*, Phys. Rev. Lett. **121**, 257402, (2018), https://doi.org/10.1103/PhysRevLett.121.257402.

[53] Sugawa, S., Salces-Carcoba, F., Perry, A. R., Yue, Y., Spielman, I. B.: *Observation of a non-Abelian Yang monopole: from new Chern numbers to a topological transition*, arXiv:1610.06228.

[54] Thouless D.J., Kohmoto M., Nightingale M.P. and M. den Nijs: *Quantized Hall Conductance in a 2D Periodic Potential*, Phys. Rev. Lett. **49**, 405 (1982).

[55] Toniolo, D.: *On the equivalence of the Bott index and the Chern number on a torus, and the quantization of the Hall conductivity with a real space Kubo formula*, arXiv:1708.05912v2, (2017).

[56] Urvoy, A., Vendeiro, Z., Ramette, J., Adiyatullin, A., Vuletić, V.: *Direct Laser Cooling to Bose-Einstein Condensation in a Dipole Trap*, Phys. Rev. Lett. **122**, 203202, (2019), https://doi.org/10.1103/PhysRevLett.122.203202.

[57] Weeks, C., Franz, M.: *Topological Insulators on the Lieb and Perovskite Lattices*, Phys. Rev. B **82**, 085310, (2010), https://doi.org/10.1103/PhysRevB.82.085310.

[58] Weinberg, S.: *The Quantum Theory of Fields*, Volume 1: Foundations, Cambridge University Press, Chap. 3 and Appendix A, (2005).

[59] Whitehead, G.W.: *Elements of Homotopy Theory*, Springer, (1978).

[60] Wilczek, F., Zee, A.: *Appearance of Gauge Structure in Simple Dynamical Systems*, Phys. Rev. Lett. **52**, 2111 (1984).

[61] Wilson, K.: *Confinement of quarks*, Physical Review D. **10** (8): 2445, (1974), doi:10.1103/PhysRevD.10.2445.

[62] Yugui Yao, Fei Ye, Xiao-Liang Qi, Shou-Cheng Zhang, and Zhong Fang: *Spin-orbit gap of graphene: First-principles calculations*, Phys. Rev. B **75**, 041401(R), (2007).